Yvonne Maria Mos was born on April 17th, 1985 in Weesp, The Netherlands. After finishing her athenaeum at the St. Ludger College in Doetinchem, she moved to Deventer to study Environmental Technology at Saxion University of Applied Science. At the end of these four years, she was eager to increase her theoretical background and continued her studies at Utrecht University to obtain an MSc degree in Geochemistry in 2010.

After a six-month holiday in South America followed by a year-long consultancy project, she realized that she missed doing research. This led her to the department of Environmental Technology at Wageningen University, where she started the temporary position of research assistant within the PlantPower project. This was followed by a short but successful research project for Paqell. In July 2014, she started her PhD research on the topic of magnetite (bio)crystallization at the department of Environmental Technology of Wageningen University.

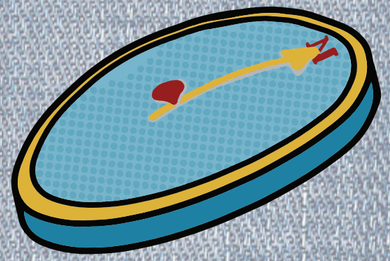

Gonna rise up

Find my direction magnetically

(Rise, Eddie Vedder)

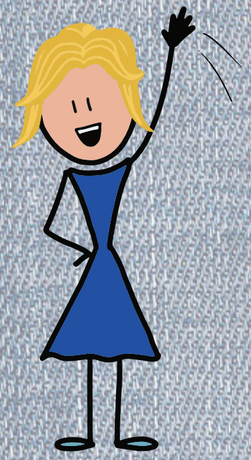

Magnetite crystallization through oxidation and bioreduction. Yvonne M. Mos. 2018

Magnetite crystallization through oxidation and bioreduction

Processes for iron recovery from groundwater

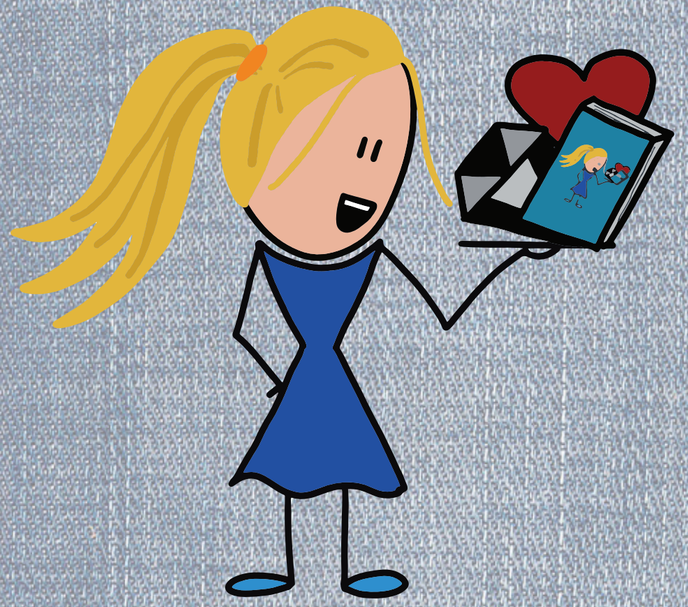

Yvonne M. Mos

Propositions

1. The indication that magnetite crystallization by oxidation as well as by bioreduction proceeds through a green rust precursor phase offers the opportunity to combine both processes.
(this thesis)

2. The type of iron phase that is crystallized through partial oxidation or partial reduction depends on the relative rates of oxidation/reduction and precipitation.
(this thesis)

3. The knowledge that our brains are hardwired for prejudice cannot justify the discrimination of people on any basis, but rather makes it inexcusable (Amodio, 2014, Nat Rev Neurosci).

4. Next to scientific capability, creativity and perseverance, the ability to *'fake it 'till you make it'* is very helpful for the completion of a PhD (Starek and Keating, 1991, Basic Appl Soc Psych).

5. The fact that approximately 90% of the candidates take longer than four years to complete their PhD creates a positive feedback loop leading to continuously increasing expectations and a consequential increase of the aforementioned percentage (VSNU, 2016).

6. The tendency of universities to employ their own students for PhD and Post-Doc positions limits scientific progress.

7. Since many people specialized in environmental technology do not know how to correctly separate their waste, one cannot expect the general public to do so.

8. Crocheting and knitting benefit health, society and the environment (Wiseman, 2007, British Council; Sarah Corbett, 2013, A little book of craftivism).

Propositions belonging to the thesis, entitled
"Magnetite crystallization through oxidation and bioreduction: Processes for iron recovery from groundwater"

Yvonne M. Mos
Wageningen, 19 October 2018

Magnetite crystallization through oxidation and bioreduction

Processes for iron recovery from groundwater

Yvonne M. Mos

Thesis committee

Promotor

Prof. Dr C.J.N. Buisman

Professor of Biological Recovery and Reuse Technology

Wageningen University & Research

Co-promotor

Dr J. Weijma

Assistant Professor, Sub-department of Environmental Technology

Wageningen University & Research

Other members

Prof. Dr A.J.M. Stams, Wageningen University & Research

Prof. Dr N.A.J.M. Sommerdijk, Eindhoven University of Technology, the Netherlands

Prof. Dr J.A. Puhakka, Tampere University of Technology, Finland

Dr J.H. Bruins, WLN, Glimmen, the Netherlands

This research was conducted under the auspices of the Graduate School for Socio-Economic and Natural Sciences of the Environment (SENSE).

Magnetite crystallization through oxidation and bioreduction

Processes for iron recovery from groundwater

Yvonne M. Mos

Thesis
submitted in fulfilment of the requirements for the degree of doctor
at **Wageningen University**
by the authority of the Rector Magnificus
Prof. Dr A.P.J. Mol
in the presence of the
Thesis Committee appointed by the Academic Board
to be defended in public
on Friday 19 October 2018
at 1:30 p.m. in the Aula

Yvonne M. Mos

Magnetite crystallization through oxidation and bioreduction: Processes for iron recovery from groundwater, 148 pages.

PhD thesis, Wageningen University, Wageningen, the Netherlands (2018).

With references, with summaries in English and Dutch.

ISBN: 978-94-6343-465-2
DOI: https://doi.org/10.18174/454865

Table of contents

Chapter 1

General introduction

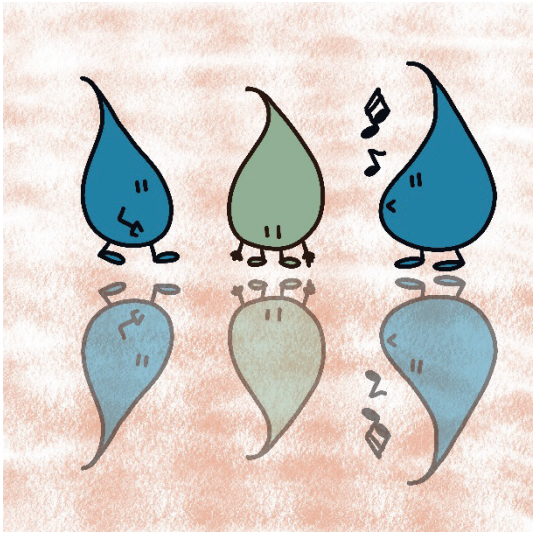

More than 50% of the drinking water worldwide is produced from groundwater [1]. Groundwater contains up to 0.9 mM (50 mg L^{-1}) of iron, which can affect the taste of drinking water, cause staining of laundry and clogging of pipes. Therefore, iron removal is part of the purification process. The World Health Organization (WHO) recommends a maximum iron concentration of 5.10^{-3} mM (0.3 mg L^{-1}) [2]. In this thesis, we propose to combine the iron removal with the production of magnetite: a compact ferrous-ferric iron oxide with strong magnetic properties and therefore multiple high-end applications [3,4].

1.1 Current iron removal practice and product applications

Iron is present as ferrous iron (Fe^{2+}) in anaerobic groundwater. The most common method of removal is uncontrolled aeration, which leads to the oxidation of ferrous to ferric (Fe^{3+}) iron that will form iron hydroxide precipitates, followed by rapid sand filtration (RSF) [5]. Iron oxidation during RSF can be divided in three categories; chemical homogeneous, chemical heterogeneous and biological oxidation. Chemical homogeneous iron oxidation is characterized by the oxidation of Fe^{2+} in solution with dissolved oxygen and leads to sludge consisting of small flocs of low density. In chemical heterogeneous iron oxidation, dissolved Fe^{2+} adsorbs to hydrous ferric oxide (HFO), followed by oxidation and hydrolysis. This pathway does not yield sludge, but leads to growth of the filter bed particles. Lastly, the biological oxidation takes place at the interface of the dissolved Fe^{2+} and oxygen and leads to high density sludge. This higher density is attributed to bonding of the iron oxyhydroxide by exopolymers [6]. The ratio between these processes depends on the oxygen content, flow, temperature and pH [5–7]. Since the chemical oxidation of Fe^{2+} by oxygen is very rapid, the oxygen content of the stream must be relatively low (around 1 mg L^{-1}) for the biological process to play a significant role [6,8].

Instead of sand filtration, membrane filtration can be applied to remove the iron hydroxide precipitates formed by the oxidation of Fe^{2+} [9–11]. Iron removal through this method is sufficient to meet the standard set by WHO in both artificial as well as natural groundwater [9]. An expected advantage of membrane filtration is that the treatment unit can be reduced in size compared to sand filtration units [9]. However, membrane fouling will likely reduce the efficiency of the system over time [12].

While both aforementioned methods are effective, both produce up to 10 000 ton of sludge per day worldwide [13,14]. The estimated cost for the transport and disposal of the iron sludge for the Netherlands alone was estimated to be €1.2 million [15].

In the Netherlands, the sludge is mainly used for sulfur removal from biogas reactors [15]. Another application is the production of bricks or use in other building materials like concrete [13,16]. However, the composition of the sludge can vary over time and across locations, impacting shrinkage percentages and product strength. Therefore, it is difficult to design a standard process for such an application [13]. The sludge can also be applied to soils, enhancing their stability and plant growth. However, while the sludge contains trace elements beneficial for plant growth, these benefits are not comparable to those of fertilizer. Moreover, repeated addition of the sludge will lead to an accumulation of iron and possibly other metals such as copper that are toxic to the

environment at elevated levels [13]. Finally, iron sludge can be used as a coagulation agent for phosphate removal in waste water treatment and agricultural soils and run-off [13]. While this is a useful application for the sludge, it will not remove the sludge from the overall waste stream.

Lodestone

In geology, magnetite is known as lodestone, literally meaning 'leading stone' in Middle English. This name stems from the use of this mineral for early versions of the compass [116].

1.2 Magnetite: magnetic iron mineral

Magnetite (Fe_3O_4) is a crystalline, black iron oxide that contains both ferrous and ferric iron ions at a ratio of 1 to 2, resulting in strong magnetic properties [3]. Magnetite occurs naturally and is the cause for the remanent magnetization of the earth's crust and can be used as a key marker of geological history [17,18]. Magnetite is present in organisms ranging from bacteria to large mammals like dolphins, enabling them to 'sense' the earth's magnetic field, thereby aiding orientation and navigation [19,20]. The occurrence and synthesis of this biogenic magnetite has been researched mainly in bacteria. These so-called magnetotactic bacteria synthesize a predetermined amount of magnetite inside a their cell [21]. The crystals are formed in chains of well-defined particles of a uniform shape and size [22].

The particle size and shape determines the strength of the magnetic properties of magnetite. Particles smaller than 30 nm exhibit superparamagnetic behavior, meaning that particles only show magnetic properties when placed in a magnetic field. Particles larger than 80 nm have multiple magnetic domains that can partially cancel each other out, thereby decreasing the strength of the overall magnetic strength. Magnetite particles in the size range of 30 to 80 nm have a single magnetic domain and are therefore exhibiting the strongest magnetic properties [23]. The shape of the crystals influences the magnetic properties by determining the number of axes in the crystal lattice, which is where the magnetism is strongest [3]. Spherical magnetite particles therefore have weaker magnetic properties than octahedral shaped particles [3].

1.3 Magnetite applications: from steel manufacturing to site-specific chemotherapy

The possible applications of magnetite depend greatly on its magnetic properties. 'Low grade' magnetite consists of particles of a non-specific size. These particles do however contain a high percentage of iron (72%), making them a good resource for the production of analytical grade iron salts and steel [24]. Moreover, low grade magnetite can be used as a catalyst (e.g. for the synthesis of NH_3), polishing agent and pigment for paints and cosmetics [3]. Magnetite particles that possess a permanent magnetic field can be used in magnets, but also in agricultural supplements and magnetic inks [3].

Superparamagnetic magnetite particles are the most versatile. They can be used for in situ remediation of soils. Toxic heavy metal ions like Cr(VI), Ni(II), Hg(II), Cd(II) and Pb(II) can be removed

through sorption onto magnetite. Moreover, magnetite has been shown to promote the dehalogenation of organic contaminants like trichloroethane (TCE) and perchloroethylene (PCE) [25]. Superparamagnetic particles that have a high purity and uniform size and shape are suitable for high-tech in vivo applications. These particles can be used in for instance MRI contrast fluid, tissue repair, bioseparation, biosensing, immunoassays and site-specific chemotherapy [4,26].

1.4 Magnetite synthesis

Since natural magnetite contains many impurities, there is a need for engineered magnetite particles [27]. To obtain magnetite particles of high purity and in a certain size range, numerous chemical methods can be employed. These methods, like the hydrolysis or thermal decomposition of precursors, sonochemical reactions, sol-gel synthesis, micro-emulsions, hydrothermal precipitation and electrospray synthesis [4,28] require high temperatures [3,29,30], high pressure and/or the addition of chemicals (e.g. solvents) [4,20,31,32]. This renders these methods environmentally unfriendly and expensive. The co-precipitation, partial oxidation and partial reduction methods on the other hand, offer chances for magnetite production under mild and therefore more environmentally friendly conditions.

1.4.1 Iron oxides and their transformation pathways

Since magnetite contains both Fe^{2+} and Fe^{3+}, the synthesis requires the presence of both ions. Obtaining the correct ratio between both is crucial. This can be achieved by simply supplying both ions in the desired ratio, or starting from either ferrous or ferric iron followed by partial oxidation and reduction, respectively.

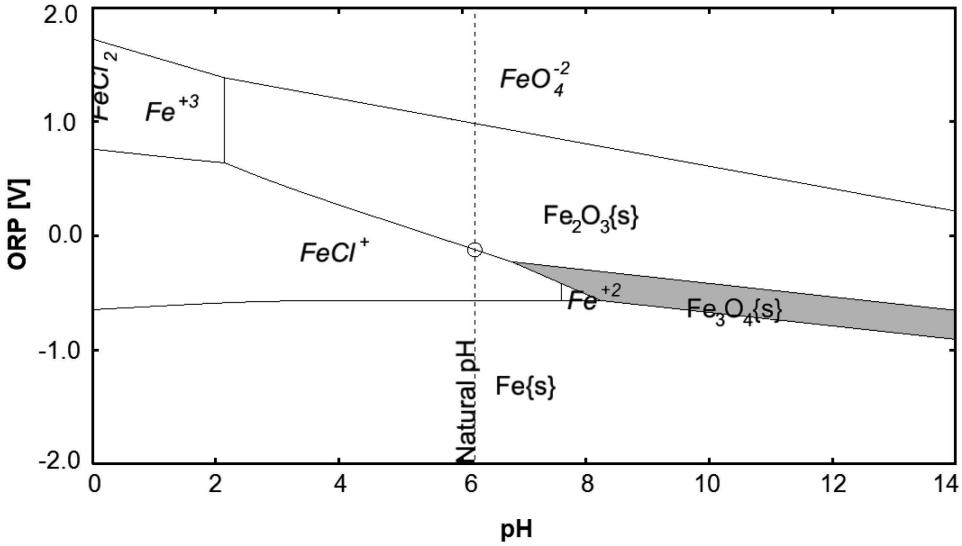

Figure 1.1 Pourbaix diagram for 1 mM iron chloride as modeled with OLI studio 9.2.

Magnetite formation requires an alkaline pH as shown in the Pourbaix diagram (Fig. 1.1). Since the solubility of both iron ions at pH > 4 is very poor [17], magnetite synthesis often involves a dissolution-reprecipitation mechanism [33,34]. Figure 1.2 shows relevant chemical transformations between iron ions, oxides and hydroxides that can occur under the influence of pH and redox potential (ORP).

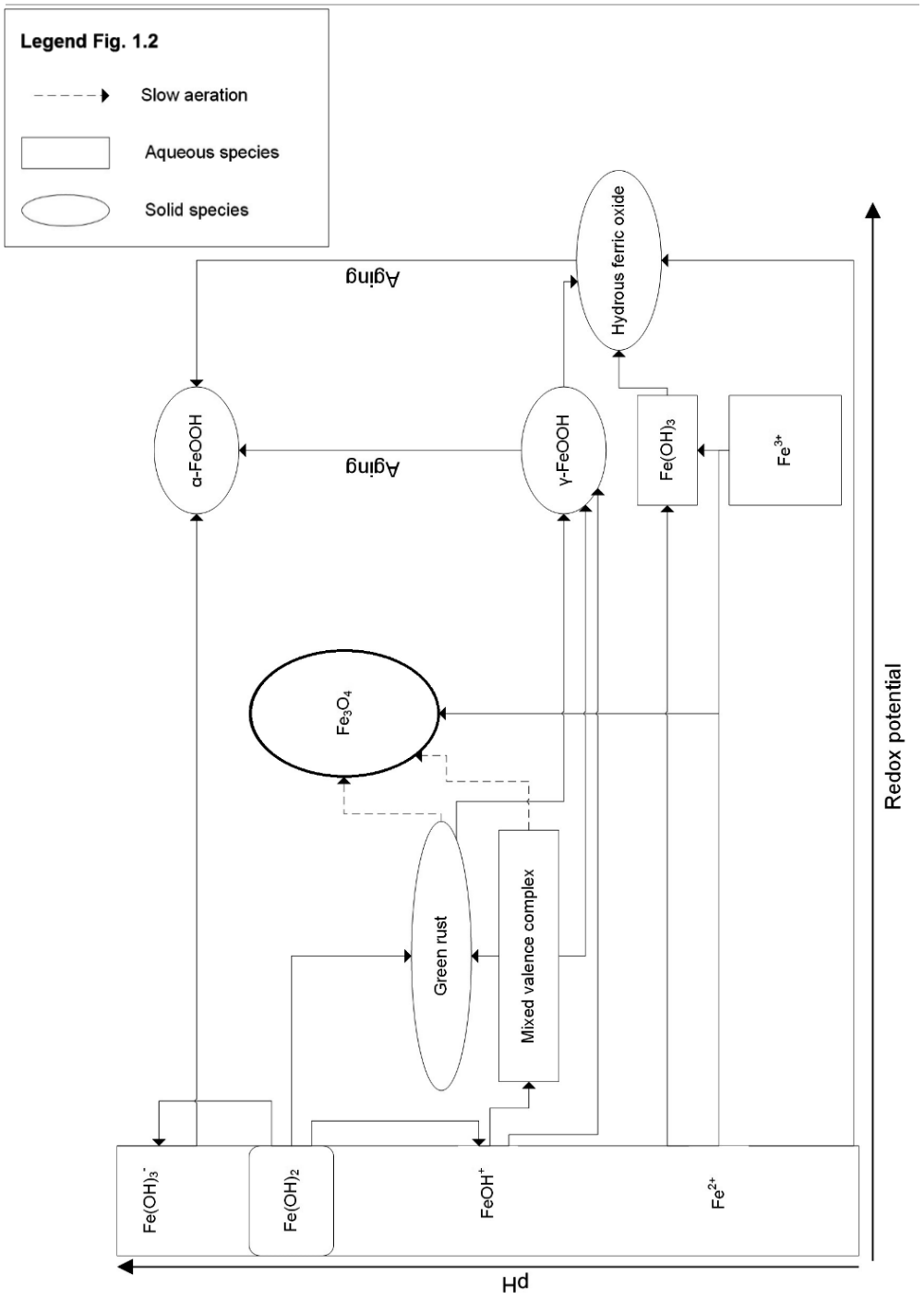

Figure 1.2 Iron transformations as a function of pH and redox potential. Adjusted from [35].

As seen in Figure 1.2, aqueous mixed valence iron complexes and green rust are common precursors for magnetite. Like magnetite, these contain both Fe^{2+} and Fe^{3+} ions. However, the precursors are only stable in anoxic environments and rapidly transform into a different iron mineral when brought in contact with an oxidant. The resulting mineral phase depends on the oxidation rate. When exposed to ambient air, the oxidation will be so rapid that all iron ions oxidize and lepidocrocite (γ-FeOOH) or goethite (α-FeOOH) is formed. However, when the oxidant is limiting or the oxidation rate is sufficiently slow for the right Fe^{2+} to Fe^{3+} ratio to occur, magnetite will be formed.

Magnetite is prone to oxidation under weathering conditions, causing a transformation into maghemite [36]. While some researchers consider this transformation to take place in more sheltered environments as well [4], this is a very slow process [3] and magnetite is generally considered to be a stable iron mineral phase under ambient temperature and pressure [3,37].

Iron oxides and hydroxides [3]

Ferric minerals:

α-FeOOH	Goethite
β-FeOOH	Akaganéite
γ-FeOOH	Lepidocrocite
α-Fe_2O_3	Hematite
γ-Fe_2O_3	Maghemite
$Fe_5HO_8.4\ H_2O$	Ferrihydrite

Mixed valence minerals:

Fe_3O_4	Magnetite
$Fe_x^{III}Fe_y^{II}(OH)_{3x+2y-z}(A^-)_z$, with A = Cl^- or $\frac{1}{2}SO_4^{2-}$	Green rust (GR)

Ferrous minerals:

$FeCO_3$	Siderite
$Fe_3(PO_4)_2$	Vivianite

1.4.2 The co-precipitation method

The simplest and most efficient chemical method for magnetite formation is the co-precipitation method [4]. Here, ferrous and ferric iron are supplied in the stoichiometric ratio for magnetite formation (i.e. 1 : 2). This is a well-known chemical process that can yield very defined particles [4,38]. However, it requires the addition of chemicals and is often performed at an elevated temperature [28,38].

It is known that bacteria can catalyze particle formation by serving as a nucleation site [39]. Their cell membrane has a negative surface charge, leading to binding of cations, stabilization of mineral surfaces and a decrease in the free energy barrier for nucleation [40,41]. Therefore, it was attempted to reach the same results of magnetite synthesis in a more environmentally friendly process with the use of microorganisms. Vali et al. [42] discovered that magnetite can be formed from ferric citrate and $FeCl_2$ at 30°C in the presence of the iron reducer *Geobacter metallireducens*. Bharde et al. [43] found that *Actinobacter* spp. can instigate the formation of magnetite in aerobic conditions from a ferricyanide/ferrocyanide solution at pH 6.6 by the excretion of two ferrisiderophore reductase proteins. Later research by the same group shows that two species of fungi, *Fusarium oxysporum* and *Verticillium* sp., are capable of excreting proteins aiding magnetite formation in a similar way [44].

Hansel et al. [45] found that the presence of bicarbonate also influences the formation of magnetite. The starting materials were quartz sand coated with ferrihydrite and $FeCl_2$ or $FeSO_4$. The experiments were conducted with either PIPES buffer (N_2 headspace) or 10 mM bicarbonate buffer (90% N_2 / 10% CO_2 headspace) at pH 7.2. Magnetite was formed in the system containing PIPES buffer when 20 mM Fe^{2+} was added to 1.35 g of the ferrihydrite-coated sand. Magnetite did not form in the presence of bicarbonate. The authors suggest that this is due to either complexation of the aqueous Fe^{2+} with (bi)carbonate species or by decreased accessibility of the surface sites on the solid precursor phase by (bi)carbonate species.

1.4.3 The partial oxidation method

When ferrous iron in solution with a pH higher than 4 is brought in contact with ambient air, it is rapidly chemically oxidized. This chemical oxidation adheres to a first order kinetic rate law with respect to ferrous iron [8]:

$$-\frac{d[Fe^{II}]}{dt} = k_1 * [Fe^{II}] \quad (1.1)$$

With:

$$k_1 = k(OH^-)^2 * pO_2 \quad (1.2)$$

And:

$[Fe^{II}]$ = concentration of Fe^{2+} (M)
t = time (days)
OH^- = concentration of OH^- (M)
pO_2 = partial pressure of O_2 (bar)

From this rate law, it follows that 1 M of Fe^{2+} at pH 7.5 and ambient air and pressure is completely oxidized in 10 minutes. This shows the significance of a controlled supply of oxidant when one wants to obtain the right ratio for magnetite formation from ferrous iron.

A defined method for magnetite formation from ferrous iron was originally developed by Sugimoto and Matijević [46]. In their partial oxidation method, the pH of an $FeCl_2$, $FeSO_4$ or $Fe(NH_4)_2(SO_4)_2$ solution was elevated from approximately 5.8 to 7.0 to form a ferrous hydroxide solid phase. The addition of KNO_3 to the batch system led to magnetite formation within four hours at 90 °C. The final pH of the experiments was approximately 13.

In the partial oxidation method, NO_3^- is used to partially oxidize Fe^{2+} (leading to NO_2^- and eventually NH_4^+ formation). This leads to the formation of GR, followed by the transformation to magnetite. Alternatively, O_2 can be used as oxidant, resulting in the same iron precipitation pathway [20,47–49]. The (simplified) reactions involved are:

$$2\,Fe^{2+} + NO_3^- + 2\,H^+ \rightarrow 2\,Fe^{3+} + NO_2^- + H_2O \quad (1.3)$$

$$8\,Fe^{2+} + NO_3^- + 10\,H^+ \rightarrow 8\,Fe^{3+} + NH_4^+ + 3\,H_2O \quad (1.4)$$

Or:

$$4\,Fe^{2+} + O_2 + 4\,H^+ \rightarrow 4\,Fe^{3+} + 2\,H_2O \quad (1.5)$$

Followed by:

$$Fe^{2+},\ Fe^{3+},\ H_2O \rightarrow GR \quad (1.6)$$

$$Fe^{2+}, GR \rightarrow Fe_3O_4,\ H_2O \quad (1.7)$$

Sugimoto and Matijević [46] found that a batch incubated without a deoxygenation step yielded not only magnetite, but also goethite.

Tamaura et al. [33] elucidated the process further by synthesizing magnetite through co-precipitation of the solid ferric iron phase lepidocrocite and aqueous Fe^{2+}. Based on their kinetic experiments and the change in particle shape, they conclude that the Fe^{2+} first adsorbs to the surface of the lepidocrocite, after which it is transformed into magnetite via a dissolution-reprecipitation mechanism. Experiments were started at pH 5, after which the pH was increased to a 'reaction pH' ranging up to pH 9. Magnetite formation was only observed at pH 7.3 and higher, causing the researchers to conclude that adsorption of Fe^{2+} onto the lepidocrocite surface does not take place at a pH lower than 7.3. The experiments were conducted at 25 °C and for a duration of 60 hours. Following the same experimental procedure using goethite instead of lepidocrocite did not yield magnetite.

Couling et al. [50] synthesized magnetite at 100 °C from 0.5 M $FeCl_2$ through the partial oxidation method with KNO_3. Their experiments focused on the influence of phosphate on the formation of magnetite. Results show that a low concentration of inorganic phosphate (0.025 to 0.05 M) led to magnetite crystals with a well-defined and uniform shape compared to crystals formed in the absence of phosphate. A higher concentration (0.1 or 0.15 M) of phosphate however, completely prevented magnetite formation. The researchers hypothesized that the presence of phosphate stabilizes the GR precursor phase by binding PO_4^{3-} to its surface, thereby preventing the transition to magnetite.

As mentioned in paragraph 1.4.2, bacteria can play various roles in crystallization processes. There is a broad diversity of bacteria that can gain energy from the oxidation of iron coupled to the reduction of, for example, nitrate or low concentrations of oxygen [17], thereby creating a mixture of Fe^{2+} and Fe^{3+} ions. However, chemical oxidation is fast and therefore a fierce competition for this biological pathway above pH 4. There is only limited literature on the influence of microorganisms on magnetite formation through partial oxidation of ferrous iron and the overall role(s) of microorganisms is often not clear.

Chaudhuri et al. [51] was the first to evaluate the influence of a bacterial species on the partial oxidation method. They found that *Dechlorosoma suillum* can facilitate the formation of GR from $FeCl_2$ with NO_3^- as electron acceptor. The following transformation into magnetite is hypothesized to be a chemical process. The formation of magnetite was achieved in a medium containing 30 mM bicarbonate, which has not been found in research without microorganisms present [45,52]. The synthesis yielded several other iron mineral by-products, but no siderite ($FeCO_3$) was formed. Other research shows that the addition of bacteria can accelerate the formation process and thereby influence the particle size [53]. The presence of a protein associated with magnetite formation in a magnetotactic bacterium led to uniform shaped particles in a narrow size range, which was not achieved without the protein present [29].

1.4.4 The partial reduction method

Magnetite can also be formed starting from a ferric iron phase. This requires the partial reduction of ferric iron, which is a process that needs a catalyst under standard conditions (room temperature, atmospheric pressure). This can be in the form of a chemical reductant, but a more environmentally friendly manner is to use bacteria [20].

Dissimilatory iron reducing bacteria (DIRB) gain energy by converting Fe^{3+} into Fe^{2+} [17]. In this way, their metabolism can create suitable conditions (i.e. Fe^{2+}/Fe^{3+} mixture, pH, ORP) for the chemical crystallization of magnetite to take place:

$$Fe^{III}O_x \rightarrow Fe^{III}O_x + Fe^{2+} \quad \textit{(biological)} \tag{1.8}$$

$$Fe^{III}O_x + Fe^{2+} \rightarrow Fe_3O_4 \quad \textit{(chemical)} \tag{1.9}$$

This induced biological crystallization of magnetite from ferric iron was first reported in literature in 1987 [54,55]. Lovley et al. [55] isolated *Geobacter metallireducens* and discovered that it was capable of reducing HFO with acetate to form magnetite. In the same year, Bell et al. [54] achieved magnetite formation through the same pathway using a mixed culture isolated from creek sediment.

While Bell et al. showed that isolates from their mixed culture could not induce magnetite formation [54], researchers since then have worked solely with pure cultures. Magnetite formation has been achieved with pure cultures of *Geobacter metallireducens* [56,57], *Thermoanaerobacter ethanolicus* [39,58], *Shewanella putrefaciens* [41,59,60], *S. oneidensis* [61], *S. alga* [58], *S. pealeana* [58] and *S. piezotolerans* [62]. Substrates provided in the aforementioned literature are acetate, lactate, glucose, formate and H_2.

As mentioned in paragraph 1.4.2, bacteria can catalyze particle formation by serving as a nucleation site. However, Behrends and Van Cappellen [60] showed that these catalytic properties are not essential for magnetite formation by separating the reduction reaction from the nucleation by a membrane. Here, hematite was partially reduced in one compartment, after which the resulting Fe^{2+} crossed a membrane into a second compartment, where it reacted with hematite to form magnetite.

Bell et al. [54] concluded that the type of iron mineral that is formed depends greatly on pH and ORP, as is also evident from Figures 1.1 and 1.2. However, experimental data in literature considering ORP is obscure. Publications that do mention measured ORP after magnetite formation from a ferric iron phase report a wide range of values between -200 and -450 mV [39,54,57,58,63]. Data on pH values is more often provided. Bell et al. [54] reported that in their magnetite-yielding experiments with HFO, acetate, yeast extract and H_2, the pH increased from 7.4 to 8.5. In experiments where glucose was added to the medium however, no magnetite was formed, the pH dropped from 7.4 to 5.5 and more Fe^{2+} was present in the medium than in the experiments without glucose. Behrends and Van Cappellen [60] controlled the pH of their experiments by the addition of HCl or NaOH and formed magnetite at pH 7.5±0.4. Other researchers do not control their pH and magnetite formation is reported at a final pH ranging from 7.1 [59] to 8.5 [58]. Zhang et al. [39] monitored the pH over time. They found a sharp drop from pH 8.5 to 7.9, which was attributed to the fast growth of the bacteria at that time interval, producing organic acids and CO_2 through their metabolism. This pH drop coincides with the first observation of magnetite. It is followed by a rise to 8.4, after which the pH slowly decreased again, but not below 7.9.

In all literature mentioned above, a buffered medium is used. While PIPES [59] and HEPES [41,61,62] have been used, most experiments are buffered by bicarbonate [54,56–58,60,61]. While Behrends and Van Cappellen [60] state that carbonate can promote magnetite formation by aiding the dissolution of, in this case, hematite, it is often considered to hinder magnetite formation in favor of siderite formation [54,58,59,64]. Siderite is mainly formed when the ration of Fe^{2+}/Fe^{3+} is high [56,58,59]. Under the same circumstances and in the presence of phosphate, vivianite formation is favored over the formation of magnetite [59]. In the scale-up research of Byrne et al. [57], siderite was produced in the larger experiment vessels of 1 and 10L, whereas it was absent in experiments conducted in 10 and 100 mL vessel volumes. Fredrickson et al. [59] state that in their experiments, it cannot be excluded that siderite and vivianite are formed through the reduction of magnetite. Lovley et al. [55] however, concluded that *Geobacter metallireducens* is not capable of reducing the Fe^{3+} present in magnetite under similar circumstances.

1.5 Magnetite formation from the drinking water production process

Recovery of iron from groundwater in the form of magnetite leads to a potentially high-value product. The process for drinking water production presents opportunities for both the partial oxidation and the partial reduction process described in paragraphs 1.4.3 and 1.4.4.

When groundwater is extracted from the soil under anaerobic conditions, the iron will be present as aqueous Fe^{2+}. The partial oxidation method for magnetite production could be applied to this stream or a concentrate thereof to produce magnetite. However, the presence of other ions, such as carbonates, could impede magnetite formation.

The partial reduction method can be applied to the sludge that is formed in RSF. This is a concentrated stream with relatively high iron concentrations. However, other (metal) ions are often

present in elevated concentrations, with unknown effects on magnetite formation and possibly contaminating the product [3,13].

1.6 Thesis objective and outline

While several pathways for magnetite formation under mild conditions are known, data on the effects of control parameters such as pH and ORP, as well as the effect of iron concentrations is scattered and often poorly comparable due to dissimilar experimental methods. Moreover, magnetite formation reported in literature so far is achieved in batch experiments. Since drinking water production involves a large and continuous flow of water, treatment processes should operate continuously in order to be feasible. The objectives of this thesis are therefore to identify control parameters and process boundaries for magnetite formation as well as to develop a continuous process with this purpose. Two opposite approaches are explored; the chemical partial oxidation of ferrous iron and the biological partial reduction of ferric iron. A graphical abstract of this thesis can be found inside the back cover.

This research, and research involving crystals in general, depends heavily on X-Ray Diffraction for phase identification. **Chapter 2** elaborates on that analytical technique and discloses how the choice of radiation type for the analysis of iron minerals influences the quality of the obtained results.

Chapter 3 focusses on magnetite synthesis through the partial oxidation method with $FeCl_2$ and either nitrate or oxygen as oxidizing agent in a continuous stirred tank reactor. Magnetite crystallization was achieved in a two-step process that required a forced pH elevation. Alternatively, additional magnetite was formed at a constant pH when previously formed magnetite was supplied as seed material. Experiments were conducted in 50% tap water as intermediate step towards a groundwater matrix.

In **Chapter 4**, a similar reactor system as in the previous chapter is described. Here, it was placed in a glovebox under N_2 atmosphere to exclude the influence of ambient air. Experiments were conducted in Milli-Q water, diluted tap water or growth medium and partial oxidation was realized by the controlled addition of air to the headspace. The effect of iron load, hydraulic retention time, medium complexity and the presence of a mixed microbial culture on the efficiency of magnetite crystallization are evaluated.

Chapter 5 focusses on the partial reduction of HFO by a mixed microbial culture, followed by magnetite formation. Batch experiments were conducted with electron donors acetate, glucose, lactate and ethanol. The relation between pH, ORP and the formed precipitate is discussed and a defined pH/ORP window for the formation of magnetite is revealed.

Chapter 6 presents a continuous stirred tank reactor for the partial reduction of HFO. Continuous reactor experiments yielded GR. When the reactor containing GR was spiked with aqueous $FeCl_3$, the two iron phases reacted to form magnetite.

Finally, **Chapter 7** summarizes and discusses the results. The two pathways of partial oxidation and partial reduction are evaluated. Furthermore, discrepancies in the results are identified and discussed. Finally, a two-reactor setup for the application of the pathways to drinking water production is proposed.

Chapter 2

X-ray diffraction of iron containing samples: The importance of a suitable configuration

Yvonne M. Mos[a], Arnold C. Vermeulen[b], Cees J.N. Buisman[a], Jan Weijma[a]

[a] Sub-Department of Environmental Technology, Wageningen University & Research, P.O. Box 17, 6700 AA Wageningen, the Netherlands
[b] Malvern Panalytical, Lelyweg 1, 7602 AE Almelo, The Netherlands

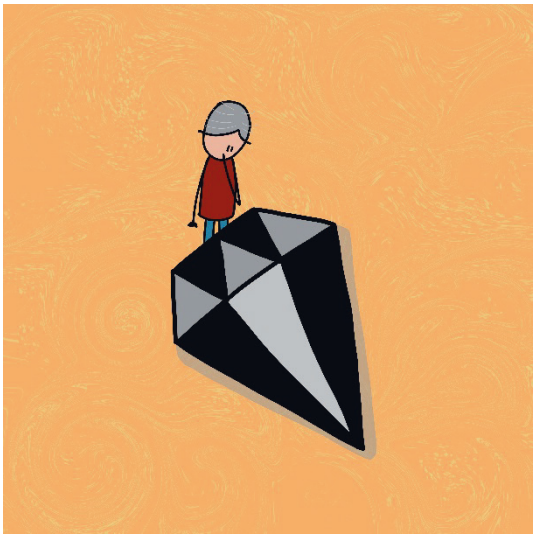

This chapter is published as:

Y.M. Mos, A.C. Vermeulen, C.J.N. Buisman, J. Weijma, X-Ray Diffraction of Iron Containing Samples: The Importance of a Suitable Configuration, Geomicrobiol. J. (2018). doi:10.1080/01490451.2017.1401183

Abstract

In X-ray diffraction, a good combination of configuration and sample is essential. Copper radiation for iron containing materials leads to a high background. Although this has been recognized, many researchers still use this combination. To clearly show the unsuitability of copper radiation for iron oxides, magnetite, goethite, maghemite, and hematite were analyzed in different configurations using copper or cobalt radiation. Results show effects of fluorescence repressing measures and different radiation sources. Copper radiation diffractograms make phase identification contestable. Studies using copper radiation for iron oxides must therefore be carefully evaluated. Cobalt radiation yielded high quality diffractograms, making phase identification unambiguous.

Key words: X-ray diffraction; radiation type; fluorescence; iron

2.1 Introduction

The iron redox cycle is important in the field of geomicrobiology. Ferric and ferrous iron are abundant in nature and are can be reduced or oxidized, depending on the redox conditions. Both chemical and biological oxidation/reduction reactions can occur. These reactions often lead to dissolution and formation of iron minerals, of which there are many. To understand the role of iron in biogeochemistry, numerous studies have focused on assessing the effect of environmental parameters on the redox conversion and mineral dissolution/precipitation. Although advancements have been made, there is still a large potential for future research. Comprehension of iron speciation and conversions lead to insights in the effects of, for example, acid mine drainage and availability of nutrients (e.g. [41,60,62,65,66]). Furthermore, the biological formation of minerals like magnetite is a topic of high interest (e.g. [43,44,57,67,68]).

Iron mineral phase identification is crucial for understanding the role of iron in natural and engineered environments. Recently we started research on iron mineral formation from ferrous iron solutions, aiming to develop a new microbiological method for iron removal from groundwater. In literature concerning microbiological iron conversions, X-ray diffraction (XRD) is a commonly used method for the phase identification of crystalline solids. In many papers, also in the last decade, the most commonly applied configuration for XRD uses a copper radiation source (e.g. [41,43,44,60,62,66–68]). By using copper radiation when analyzing iron minerals however, it is often overlooked that the choice of radiation should be compatible to the sample composition in order to obtain a diffractogram of good quality. A mismatch therein can lead to a high background signal that, especially in combination with a low peak intensity, makes interpretation more difficult and can even lead to incorrect phase identification. The most striking example thereof is when dealing with magnetite and/or maghemite. Diffractograms of these two minerals are only distinguishable by a few low intensity peaks. Both can form in similar environments and be converted into one another, in the case of magnetite to maghemite simply by exposure to ambient air [69].

The mismatch between copper radiation and iron is well-known in the iron and steel industry, where cobalt radiation is used [70], but is it not common knowledge in other fields of research, while there is an increasing interest in the biomineralization of iron oxides. This issue is even more important in this field, where samples often do not only contain crystalline, but also amorphous minerals and microorganisms, which will increase the background signal further. Despite indications in literature that it is unfavorable, copper radiation is often used in XRD analysis of iron oxides and interpretation of the results is not always sufficiently careful. An example is found in Adams et al. [65]. The diffractograms in Figure 6 and the interpretation thereof show that some peaks that are used for identification are of equal height as the background noise. Other peaks are excluded from identification for no apparent reason. A similar case is present in Byrne et al.[57], Figures 1c and 4b, where peaks are hardly distinguishable from the background and the identification of siderite is based on the presence of only one peak. These diffractograms of mixtures of iron oxides were obtained with a copper radiation source and are open to multiple interpretations. Drawing firm conclusions from this data is therefore inadvisable. Many other

researchers draw conclusions based on diffractograms of iron oxides obtained with copper radiation that are vulnerable for incorrect interpretation (e.g. [41,43,44,60,68]). Others strengthen their conclusions with TEM analysis [62,67] or Mössbauer spectroscopy [66]. While this can confirm the conclusions that are based on the XRD results, time, costs and effort can be saved by obtaining a good quality diffractogram in the first place.

The incompatibility of copper radiation and iron oxides has been indicated by, amongst others, Cullity [69], Fransen [71] and Klug and Alexander [70]. While these authors give a well-founded theoretical explanation for this, examples and a visuals to illustrate this are not presented. In the current paper, we visualize the advantages of cobalt radiation for the analysis of iron oxides as well as giving some other possible measures that can be taken to decrease fluorescence.

In this paper, we demonstrate that the use of Cu radiation for XRD analysis of iron oxides, as still applied in recent literature, can result in incorrect and/or incomplete phase identification. We will illustrate this by analyzing four iron oxides which are commonly investigated in biomineralization research (magnetite, goethite, maghemite and hematite) with various equipment configurations using both copper and cobalt radiation. The results of the various scans are compared to show the effects of the different configurations and radiation sources.

2.2 Theoretical background

The information in XRD analysis is provided by the interaction between X-rays and the sample material. The different types of interaction and their effects are discussed in this section, which is primarily based on the works of Cullity [69].

When an X-ray hits an electron, as is the case in XRD imaging, it will be scattered. The diffraction of the X-ray takes place in all directions. Since in XRD a beam of X-rays (the incident beam) hits a crystal lattice, many atoms are hit simultaneously. The diffracted X-rays can either interact constructively or destructively. This can be understood when one considers X-rays to be waves; when in antiphase, the sum of the two waves is zero. When the waves are in phase, they will reinforce each other maximally, giving a high intensity peak in the diffractogram.

X-rays have properties of both waves and particles (photons). Moreover, X-rays are electromagnetic, meaning that at any point in a beam, there is a varying electric field. Scattering can happen in two ways; elastic or inelastic. In elastic scattering, the X-ray is diffracted by the electron it hits. Since the electron is hit by a photon with an alternating electric field, it will start to oscillate around its mean position. This causes the electron to emit an electromagnetic wave of its own. This wave has the same wavelength as the incident beam and therefore contributes to the diffractogram.

In inelastic scattering, the X-ray is also diffracted by the electron it hits. However, in this case, the X-ray knocks one of the electrons out of the inner shell of an atom, emitting a characteristic fluorescent radiation. While this is the basis of the technique of XRF (X-ray fluorescence), this is an unwanted phenomenon in XRD. Since a relatively large part of the energy of the incident beam is absorbed in this process, the intensity of the beam reaching the detector (the diffracted beam),

and therefore the peak in the diffractogram, will be lower. Also, the fluorescent radiation will be detected, causing a high background. These two effects combined can cause peaks to become invisible, making it difficult to analyze the diffractogram.

Inelastic scattering and therefore fluorescence always takes place during XRD. However, the amount of inelastic scattering that occurs, depends on the combination of the type of X-rays and the material that is analyzed. X-rays have a characteristic radiation with peaks at different wavelengths, depending on the source material. The wavelength of these peaks determines the extent to which it will penetrate, absorb and scatter. To ensure sufficient scattering, the wavelength of the so called Kα radiation peak used should be longer than the so called K absorption edge of the sample material. The K adsorption edge of iron is 1.743 Å, which, in principle, would exclude copper (as well as molybdenum) as suitable radiations for analysis (Table 2.1). However, some physical measures can be taken to decrease the background signal in the diffractogram. The first is setting a sensitivity window for the detector. This window would typically be set for energies of the Kα ± 50% keV (Table 2.1). This solves the problem for iron analysis with molybdenum radiation, but not for copper radiation [69,71]. Furthermore, one can use monochromators, both in the incident beam as well as in the diffracted beam [71]. A monochromator is a crystal like germanium or graphite. By allowing the beam to be diffracted by the crystal, the radiation of wavelengths other than Kα will be eliminated. In this way the radiation hitting the sample as well as the radiation reaching the detector can be 'cleaned up'.

Radiation	Wavelength of Kα peak [Å]	Characteristic energy [keV]
Molybdenum	0.711	17.44
Copper	1.542	8.039
Cobalt	1.790	6.926
Iron	1.937	6.400
Manganese	2.103	5.895
Chromium	2.291	5.411

Table 2.1 Wavelengths and characteristic energies of the Kα peak of different radiations used in XRD.

Applying a suitable type of radiation or using monochromators are both good options to avoid fluorescence [69–71]. However, as mentioned before, when a poorly suitable type of radiation is used, a relatively large part of this will be absorbed by the sample. This means that 1) besides causing a lower background signal, it results in a lower peak intensity as well, and 2) it causes a smaller penetration depth of the sample, implying that the volume of the sample that is analyzed in a scan is reduced, possibly leading to a less representative result. Calculated penetration depths of different radiation types for magnetite are shown in Figure 2.1.

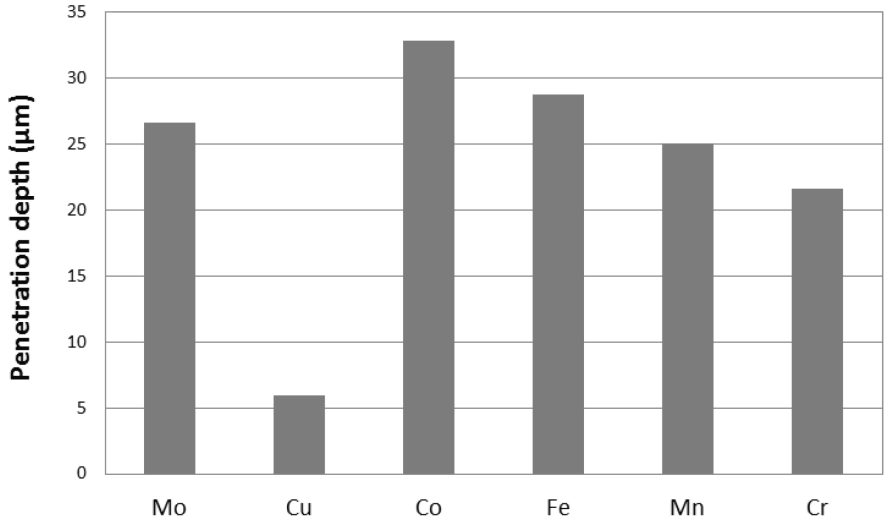

Figure 2.1 Calculated penetration depths of various types of radiation for magnetite.

2.3 Materials and methods

Four different iron oxides were purchased from chemical suppliers. Indicated purity and particle size is according to supplier information. The used magnetite (Fe_3O_4, Sigma Aldrich, the Netherlands) is ≥ 97% pure, with a particle size ranging from 50 to 100 nm. Goethite (α-FeOOH, Santa Cruz Biotechnology, USA) with a purity of ≥ 98% was used (particle size not indicated). The maghemite (γ-Fe_2O_3) was obtained from US Research Nanomaterials, Inc. and is ≥ 99% pure, with nanoscale particle sizes ranging from 20 to 40 nm. Lastly, the hematite (α-Fe_2O_3) (Cofermin Chemicals GmbH & Co. KG, Germany) is ≥ 96% pure with a particle size of ~700 nm.

The iron oxide powders were analyzed with a PANalytical Empyrean diffractometer system equipped with a sample spinner and PreFIX (Pre-aligned Fast Interchangeable X-ray) modules. The Bragg-Brentano diffraction geometry was used in all cases. X-ray tubes with Cu and Co anode materials were utilized as radiation sources. Two different incident beam modules have been applied. First the traditional incident beam slits (PDS, programmable divergence slits) and secondly the novel Bragg-Brentano^{HD} module (BBHD), which produces a monochromatized divergent incident beam. The samples were spun with 1 rev s^{-1}. As detector the PIXcel^{3D} is used in linear (1D) scanning mode with adjustable energy sensitivity (PHD, pulse height distribution) settings. The standard PHD settings used are set to a range of 25-80%, where the typical Kα energy of the radiation source is defined at 50%. To suppress the fluorescence radiation from Fe the lower level PHD setting was increased. For the Cu radiation source the optimum peak-to-noise ratio was found with a PHD range of 50-80%. For Co radiation increasing the lower level PHD setting did not

further improve the peak-to-noise ratio. Finally the effectiveness to remove fluorescence of a diffracted beam monochromator was tested.

Scans were made over a 2θ range of 10 – 110 with a total exposure time of 15.5 min. For the regular powders a step size of 0.0263 and a counting time of 56.9 s step^{-1} were used. For the nanocrystalline powder the step size and counting time were adapted to 0.105 and 227 s step^{-1}, respectively.

2.4 Results and discussion

2.4.1 Phase purity powder samples

The diffractograms gave insight into the phase purity of the samples. Both the magnetite and maghemite samples had a phase purity close to 100% based on the obtained diffractograms. The goethite and hematite samples however, contained various mineral phases. The goethite sample consisted of goethite with both a cubic and an orthorhombic configuration. Next to this, it contained about 40 to 50% hematite and 1 to 2% quartz. The hematite sample contained about 10% maghemite and a trace (1 – 2%) of quartz.

2.4.2 Qualifying the diffractogram

The peak to background ratio is commonly used for a comparison of diffractograms. This ratio is defined by the net peak height of the highest peak divided by the background level below that same peak:

$$P/B = \frac{I_{net\ peak}}{I_{background}} \tag{2.1}$$

A higher value for P/B indicates a better quality of the diffractogram. This is a quick and easy evaluation of the quality. However, this method does not take peak intensity loss into account that is caused by physical measures taken to prevent fluorescence (e.g. monochromators).

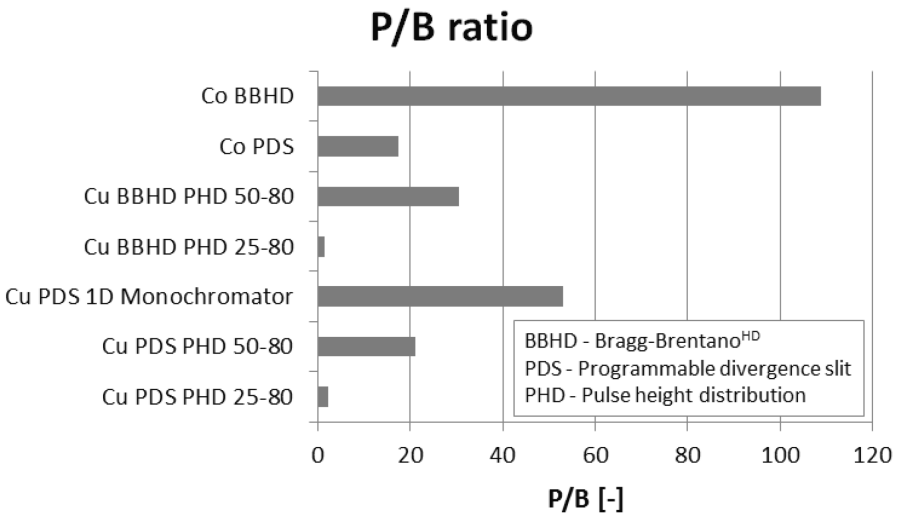

Figure 2.2 Peak to background ratios of all tested configurations.

Considering the P/B ratio of the diffractograms of the magnetite sample for all tested configurations (Fig. 2.2), the combination of Cu radiation with a diffracted beam monochromator yields a good quality diffractogram. However, due to the loss of efficiency, the net peak intensity is rather low. To counteract this, the exposure time must be increased significantly (order of magnitude 10 times) for small peaks to be visible. Hence, the P/B ratio is not full proof as quality parameter in practice.

A different approach to qualify a diffractogram is looking at the peak to noise ratio. Here, the net peak height of the highest peak is divided by the noise of the background level. A common simplified formula for this ratio is obtained by replacing the latter by the square root of the number of counts of the background level below that same peak:

$$P/N = \frac{I_{net\,peak}}{\sigma(I_{background})} = \frac{I_{net\,peak}}{\sqrt{I_{background}}}. \qquad (2.2)$$

With the P/N ratio, the loss of intensity is considered, making it a more suitable parameter for comparison of diffractograms in different configurations (Fig. 2.3, magnetite sample). This is illustrated by the lower score of the setup with Cu radiation and the diffracted beam monochromator. Therefore, we conclude that the P/N ratio is an excellent measure to judge the quality of a measurement.

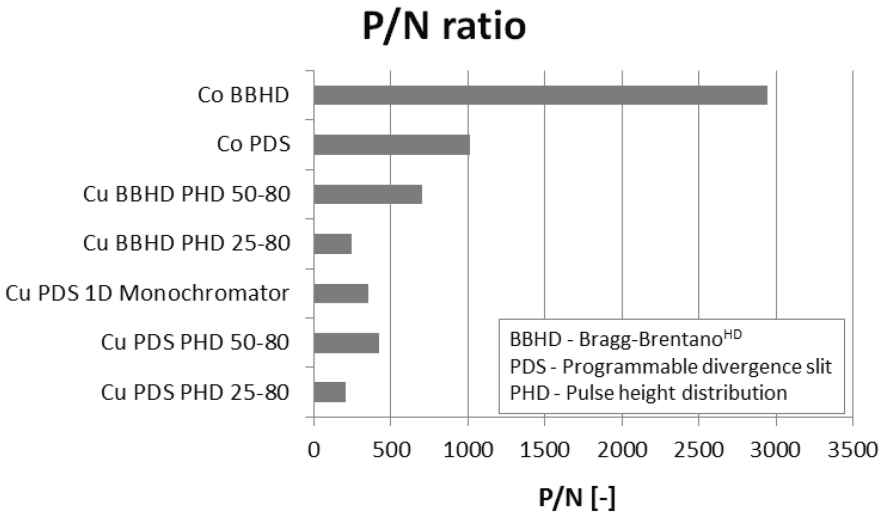

Figure 2.3 Peak to noise ratios of all tested configurations.

Further improvement of the P/N ratio can be achieved by increasing the exposure time. For example, to improve the P/N ratio with a factor of 5, exposure time needs to be 25 times longer. Or alternatively, a measurement can be done in a shorter time when a lower P/N ratio is considered as sufficient. A commonly used rule of thumb is that the P/N ratio has to be > 3 to identify trace peaks and > 10 for an accurate phase quantification.

Comparison of the diffractograms of maghemite measured with PDS for the two radiation types shows that cobalt radiation gives both a lower background and a higher peak intensity (Fig. 2.4a and b). Comparison of the Cu and Co results of the same sample with the highest P/N ratio however, shows a background for the Cu radiation that is about 2.5 times lower (Fig. 2.4c and d). However, due to the induced fluorescence and the use of a BBHD, the intensity of the peaks is 5 times lower. While the main peaks are visible in all diffractograms, the peaks with lower intensity (at larger d-spacing) are not detected in the diffractograms obtained with Cu radiation (Fig. 2.4a and c). The P/N ratio is therefore better in the scan with cobalt radiation.

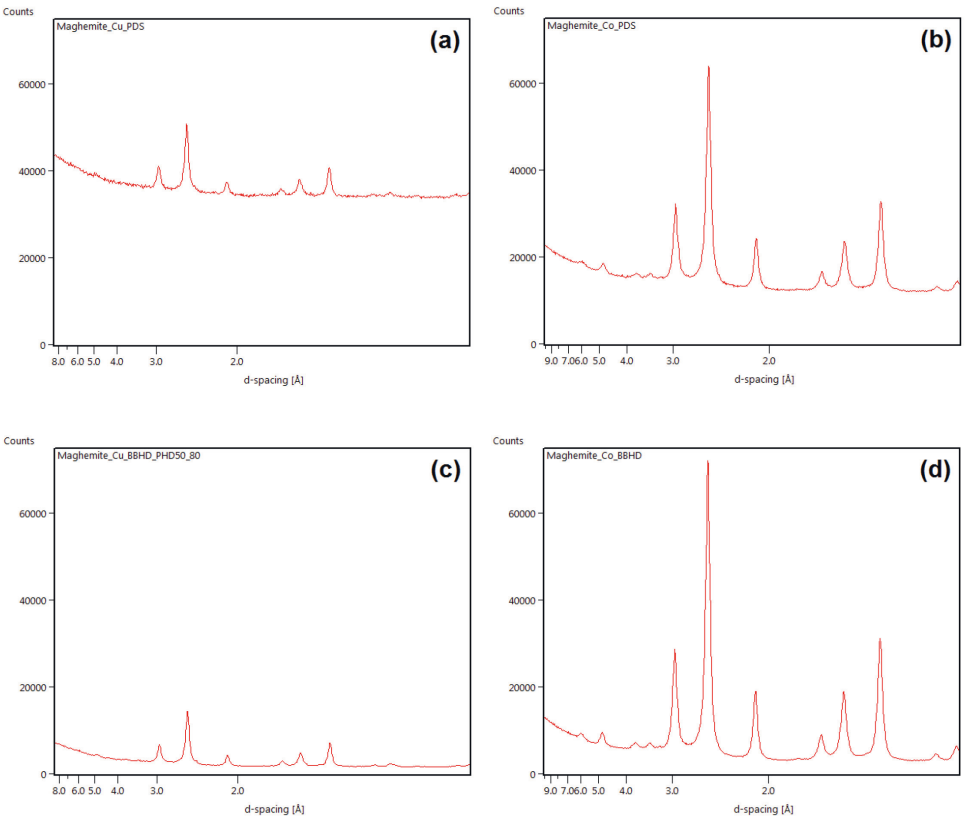

Figure 2.4 Diffractograms of the maghemite samples measured in the configurations a) Cu radiation with PDS; b) Co radiation with PDS; c) Cu radiation, BBHD and PHD 50 – 80; and d) Co radiation with BBHD.

The penetration depth of the radiation into the sample is important for a representative result. This is especially true for (inhomogeneous) multiphase samples or samples containing impurities. The penetration depth or analysis volume is not directly included in the P/N ratio. However, the X-ray intensity yield is proportional to the analyzed sample volume and therefore it is indirectly represented in the net peak intensity. Consequently, we see no need to explore this further in this paper. Nevertheless, when the occasion arises that one has to choose between options with Cu or Co radiation with similar P/N ratios, it is preferable to take the penetration depth of the radiation type into account (Fig. 2.1).

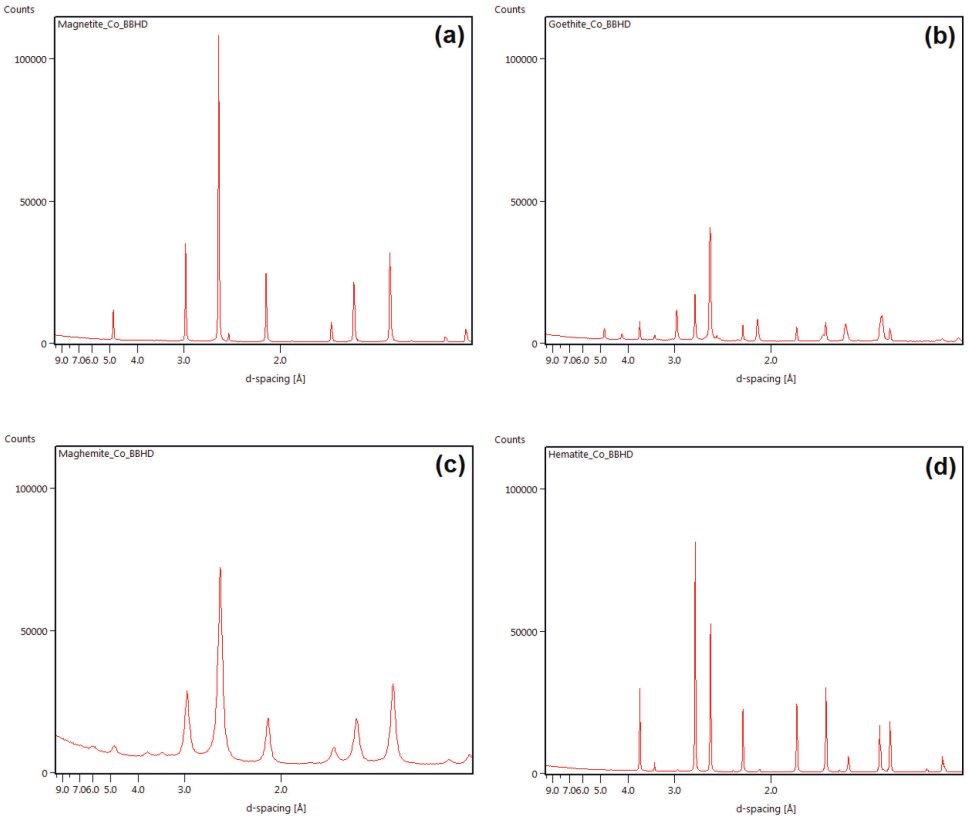

Figure 2.5 Diffractograms of a) magnetite; b) goethite; c) maghemite; and d) hematite as measured with the Co – BBHD configuration.

2.4.3 Implications for iron mineral identification

As the measurements with the Co – BBHD setup have the best P/N ratio, these are used to provide an overview of the different samples. Figure 2.5 shows the diffractograms of a) magnetite, b) goethite, c) maghemite, and d) hematite. The diffractograms of magnetite and maghemite in particular show a great resemblance, as is highlighted in Figure 2.6. A striking difference is the width of the peaks in case of the maghemite. This is caused by the nanoscale particle size and is independent of the type of iron oxide and is therefore not regarded as a relevant parameter in this comparison. It is clearly visible that both materials share many peaks at the same d-spacing. The distinguishing peaks, specifically at high d-spacing (left side of X-axis), are small. In the scan with Co – BBHD, there are clearly distinguishable peaks present for the maghemite sample in this range, while in the Cu – BBHD – PHD50-80 scan, these are obscured by the background (see frame). Moreover, the latter shows a shoulder for the highest intensity peak. This could be mistaken for one of the signature peaks of magnetite that occurs around the same d-spacing.

When considering a single type of sample of either mineral with this configuration therefore, the identification becomes inconclusive. When a sample is measured with a shorter exposure time, the smaller peaks will become even less distinguishable. With only the larger intensity peaks visible, a maghemite sample can easily be identified as magnetite. Moreover, these analysis have been performed on high grade chemical iron oxides, many samples in research are of a lower grade and/or are mixtures of several phases, complicating analysis further. A good quality diffractogram is therefore vital for correct phase identification.

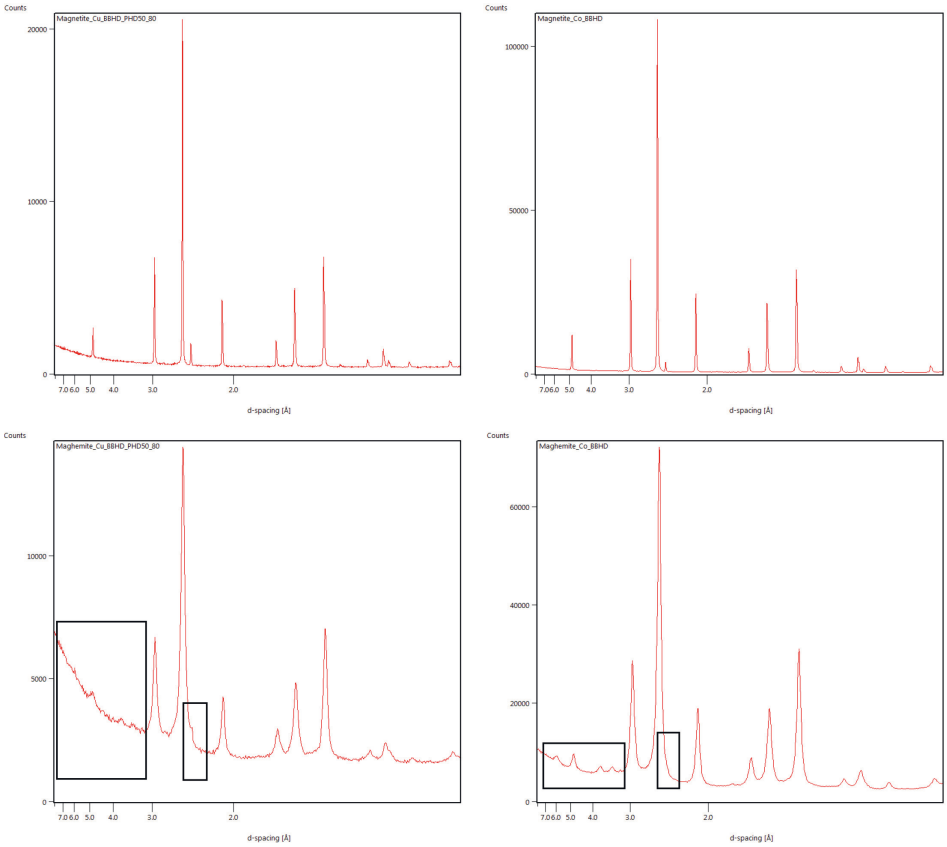

Figure 2.6 Comparison of diffractograms of the magnetite and maghemite samples as measured with on the left Co – BBHD; and on the right Cu – BHHD – PHD50-80 configurations. Frames highlight the distinguishing peaks.

2.5 Conclusion

Analyzing an iron containing sample with copper radiation yields a high background level due to fluorescence. This can lead to incorrect phase identification, especially when dealing with magnetite, maghemite or mixtures. Multiple measures can be applied to suppress fluorescence (e.g. monochromators). However, these also have disadvantages, like loss of peak intensity and low penetration depth, leading to diffractograms that yield inconclusive identification. This is avoided by applying cobalt radiation. The lower fluorescence leads to a superior peak to noise ratio and therefore an unambiguous phase identification. We recommend that for the XRD analysis of iron oxides, cobalt radiation is used to avoid misinterpretations. In addition, research reported in the past that made use of copper radiation for this type of samples without special measures, should be interpreted cautiously.

Chapter 3

Magnetite synthesis from ferrous iron solution at pH 6.8 in a continuous stirred tank reactor

Yvonne M. Mos, Karin Bertens Zorzano, Cees J.N. Buisman, Jan Weijma

Sub-Department of Environmental Technology, Wageningen University & Research, P.O. Box 17, 6700 AA Wageningen, the Netherlands

This chapter is published as:

Y.M. Mos, K. Bertens Zorzano, C.J.N. Buisman, J. Weijma, Magnetite synthesis from ferrous iron solution at pH 6.8 in a continuous stirred tank reactor, Water Science and Technology (2018). doi:10.2166/wst.2018.062

Abstract

Partial oxidation of defined Fe^{2+} solutions is a well-known method for magnetite synthesis in batch systems. The partial oxidation method could serve as basis for an iron removal process in drinking water production, yielding magnetite (Fe_3O_4) as compact and valuable product. As a first step toward such a process, a series of experiments was carried out, in which magnetite was synthesized from an Fe^{2+} solution in a 2 L continuous stirred tank reactor at atmospheric pressure and 32 °C. In four experiments, elevating the pH from a start value of 5.5 or 6.0 to a final pH between 6.8, 7.0 or 7.5 caused green rust to form, eventually leading to magnetite. Formation of NH_4^+ in the reactor indicated that NO_3^- and subsequently NO_2^- served as oxidant. However, mass flow analysis revealed an influx of O_2 to the reactor. In a subsequent experiment, magnetite formation was achieved in the absence of added nitrate. In another experiment, seeding with magnetite particles led to additional magnetite precipitation without the need for a pH elevation step. Our results show, for the first time, that continuous magnetite formation from an Fe^{2+} solution is possible under mild conditions, without the need for extensive addition of chemicals.

Key words: CSTR, groundwater, iron removal, magnetite, nitrate, oxygen

3.1 Introduction

Groundwater is an often used source for drinking water and can contain up to 50 mg L^{-1} of ferrous iron. Iron removal is a necessary step in the production of drinking water, since the World Health Organization recommends an iron level of less than 0.3 mg L^{-1} [2]. Currently, ferrous iron is usually removed by aeration, which leads to uncontrolled chemical precipitation of the resulting ferric iron, followed by sand filtration to remove the precipitates [5]. This produces a poorly dewaterable sludge of low value [14]. Alternatively, groundwater is treated by membrane filtration, resulting in a concentrate with an elevated iron concentration [9] or by a chemical-biological process that operates at a slightly acidic pH and yields a compact iron residue [5].

Better controlled iron precipitation could result in more valuable and compact iron minerals like magnetite and reduce water losses in drinking water production. Magnetite (Fe_3O_4) is a black ferrous-ferric iron oxide with strong magnetic properties at particle sizes above 20 nm [3]. These properties make magnetite particles of high purity and uniform size and shape useful in high-tech applications such as data storage, MRI techniques and site-specific chemotherapy [4].

Conventional chemical methods to produce magnetite for such applications require high temperatures [3,29,30], high pressure and/or the addition of chemicals (e.g. for pH adjustment) [4,20,31,32], rendering these methods environmentally unfriendly, expensive and incompatible with drinking water production.

Several chemical methods for the synthesis of magnetite in water under mild conditions are known, but do not start from ferrous iron. For example, Tamaura et al. [33] reported magnetite formation from γ-FeOOH at a minimum pH of 7.3 and 25 °C and Hansel et al. [45] produced magnetite from ferrihydrite at pH 7 in ultra-pure water.

Here we study the partial oxidation method, originally developed by Sugimoto and Matijević [46], for synthesis of magnetite under groundwater-like conditions in a continuous reactor. Our ultimate aim is to develop a continuous iron removal process for ferruginous groundwater treatment yielding magnetite as a more compact and valuable iron product. Although the partial oxidation method has been studied by several research groups to elucidate the magnetite formation mechanism, these studies were not directed at using the method as basis for a groundwater treatment process. In the partial oxidation method, Fe^{2+} is partially oxidized to form green rust (GR) and subsequently, magnetite. NO_3^- is commonly used as oxidant, leading to NO_2^- and eventually NH_4^+ [47–49]. Alternatively, Fe^{2+} can be oxidized by O_2, resulting in the same iron precipitation pathway [20]. The (simplified) reactions involved are:

$$2\,Fe^{2+} + NO_3^- + 2\,H^+ \rightarrow 2\,Fe^{3+} + NO_2^- + H_2O \quad (3.1)$$

$$8\,Fe^{2+} + NO_3^- + 10\,H^+ \rightarrow 8\,Fe^{3+} + NH_4^+ + 3\,H_2O \quad (3.2)$$

Or:

$$4\,Fe^{2+} + O_2 + 4\,H^+ \rightarrow 4\,Fe^{3+} + 2\,H_2O \quad (3.3)$$

Followed by:

$$Fe^{2+},\ Fe^{3+},\ H_2O \rightarrow GR \quad (3.4)$$

$$Fe^{2+}, GR \rightarrow Fe_3O_4, H_2O \quad (3.5)$$

The formation of magnetite by this method occurs within 50 minutes to 9 hours, depending on the initial pH and Fe^{2+} concentration (1.1 to 28 g L^{-1}) [46,50,72,73]. Initial pH values range from 6 at 100C to 8 or 9 at room temperature [50,73]. Since drinking water production involves large and continuous volumes of water, any treatment process should operate continuously, under mild conditions and with little use of chemicals.

In this paper we report continuous magnetite synthesis from dissolved $FeCl_2$ at pH 6.8 in a lab scale CSTR (2 L). Initially, the CSTR was fed with 50% tap water with added nitrate as intended oxidant and 50% Milli-Q water containing 570 mg L^{-1} $FeCl_2$, as intermediate step towards levels more typical for groundwater. In later experiments, nitrate was omitted from the tap water.

3.2 Materials and methods

3.2.1 Chemicals and analysis

All chemicals used were analytical grade. $FeCl_2$ (Alfa Aesar) was 99.5% pure, anhydrous and the container was only opened in an anaerobic hood to prevent exposure to O_2. Nitrate was used in the form of KNO_3. $FeCl_2$ solutions were prepared in an anaerobic hood. All solutions were prepared using water that was purged with 99.999% pure N_2 gas (5.0 N_2, O_2 < 5 ppmv, Linde Gas Benelux B.V., the Netherlands) for at least 40 min L^{-1} prior to use.

Soluble iron and dissolved nitrite, nitrate, and ammonium concentrations in the reactor and reactor effluent were determined with Hach Lange kits (LCK 320, LCK 339, LCK 341, LCK 305) and a DR3900 spectrophotometer (Hach Lange). The nitrate concentration in tap water was analyzed by ion chromatography (Dionex ICS 2100, Dionex IonPac AS17, 4 x 2505 mm).

The precipitates were separated by settling and then air-dried at room temperature. This method will lead to the oxidation of any unstable Fe^{2+} present in the sample. However, magnetite is stable over a period of years and no additional magnetite can be formed in this way [3]. The precipitate samples were analyzed by X-Ray Diffraction (XRD) with a Bruker D2 Phaser equipped with Co radiation (300 W). A Lynxeye 1D detector was used with an incident beam slit of 1.0 mm, a diffracted beam slit of 3.0 mm and a knife at 2.0 mm above the sample holder. The sample was spun at a speed of 5.0 rpm to ensure statistically optimal results. The scanning range was 10 to 90 2θ, the step size was 0.04 and the counting time per step was 2 s.

3.2.2 CSTR experiments

Table 3.1 lists the conducted experiments. The CSTR had a working volume of 2 L. Before the start of each experiment, the reactor was filled with 1 L Milli-Q water and 1 L local tap water from Wageningen, the Netherlands (see Table 3.2 for composition). A 570 mg L^{-1} $FeCl_2$ (251 mg L^{-1} Fe^{2+}) solution was prepared in Milli-Q water and an 81 mg L^{-1} KNO_3 solution was prepared in tap water.

Initially, the CSTR was fed with tap water with added KNO_3 as intended oxidant and Milli-Q water containing 570 mg L^{-1} $FeCl_2$ at 0.028 L h^{-1} (0.67 L d^{-1}) for both, giving a hydraulic retention time (HRT) of 36 h. In later experiments, no nitrate was added to the tap water. Mixing was accomplished with a stainless steel rotor with a diameter of 4 cm and at 60 rpm in the center of the water column and magnetic stirring at approximately the same speed with a 4-cm magnetic bead placed centrally on the reactor bottom. Each experiment was conducted in a cabinet that was kept at 32 °C. The reactor was connected to a pH sensor (QP156X, QIS) and controller, which dispensed HCl (0.25 M) or NaOH (0.25 M) when the deviation from the pH set point value became greater than 0.1. Reactor, feed solutions, effluent, acid and base stocks were constantly flushed with N_2 gas.

Experiment	Inflow 1 (in MQ)	Inflow 2	Initial pH	Final pH	Comment
a	570 mg L^{-1} $FeCl_2$	81 mg L^{-1} KNO_3 in TW	5.5	7.5	
b	570 mg L^{-1} $FeCl_2$	81 mg L^{-1} KNO_3 in TW	5.5	7.0	
c	570 mg L^{-1} $FeCl_2$	81 mg L^{-1} KNO_3 in TW	5.5	6.8	initial pH elevation to 6.5
d	570 mg L^{-1} $FeCl_2$	81 mg L^{-1} KNO_3 in TW	6.0	7.5	
e	570 mg L^{-1} $FeCl_2$	TW	5.5	7.5	
f	127 mg L^{-1} $FeCl_2$	MQ	6.0	6.0	quantification O_2 influx
g	570 mg L^{-1} $FeCl_2$	TW	7.0	7.0	seed crystals added at t_0
h	570 mg L^{-1} $FeCl_2$	TW	5.5	7.0	step-wise procedure

Table 3.1 Overview of experiments. TW = tap water, MQ = Milli-Q water.

Ion	Unit	Concentration
Ammonium	mg NH_4^+ L^{-1}	<0.005
Nitrite	mg NO_2^- L^{-1}	<0.012
Nitrate	mg NO_3^- L^{-1}	0.17
Ferrous iron	mg Fe^{2+} L^{-1}	<0.2
Ferric iron	mg Fe^{3+} L^{-1}	<0

Table 3.2 Concentrations of ions of interest in the tap water; most concentrations were below the detection limit.

We assessed the possibility of O_2 entering the system through the N_2 sparging gas (3.6 L h^{-1} in reactor and 7.2 L h^{-1} in $FeCl_2$ feed solution). The O_2 concentration in the sparging gas was less than 5 ppmv, so the molar mass flow into the reactor equaled no more than $3.14.10^{-8}$ mol O_2 h^{-1}. This would account for a maximum oxidation of $7.85.10^{-9}$ mol Fe^{2+} h^{-1} or $8.09.10^{-7}$ mol (0.01% of total Fe^{2+} load) during an entire experiment.

3.2.3 Calculations and modeling

The oxidation/reduction potential (ORP) of the reactor can be calculated based on the concentrations of Fe^{2+} and Fe^{3+}, using a standard potential of 0.771 V and the Nernst equation, as follows:

$$E = E^0 + \frac{RT}{nF}\ln\left(\frac{[ox]^i}{[red]^i}\right) \quad (3.6)$$

Modeling was done with OLI Studio 9.2 (OLI Systems, Inc.).

3.3 Results and discussion

3.3.1 Initial tests

The reported procedure for magnetite formation with the partial oxidation method involves a pH increase (see e.g. [72,74]). In trial tests (data not shown), a starting pH of around 5.5 followed by a pH elevation to 11 induced the formation of a black precipitate, which contained magnetite and no substantial amount of other mineral phases, as determined with XRD. Operating the reactor at a constant pH of either 5.5 or 7.5 did not yield magnetite precipitation.

3.3.2 pH limits of magnetite formation by partial oxidation in CSTR

Since our aim is to develop a process for drinking water production, the addition of pH-correcting chemicals should be kept to a minimum. We therefore conducted four CSTR experiments (see Table 3.1) for the following selections of start pH and final pH: (a) pH 5.5 to 7.5, (b) pH 5.5 to 7.0, (c) pH 5.5 to 6.8, and (d) pH 6.0 to 7.5. Each experiment lasted approximately four days (103 hours). KNO_3 was supplied as oxidizing agent. We increased the pH after approximately 24 hours. The color changes in the reactor content followed the same trend in experiments (a), (b) and (d). The color of the suspension in the reactor was slightly orange at the initial pH. Following the pH increase on day 1, the suspension became dark green/brown and increasingly turbid and black during days 2 and 3. In experiment (c), however, the solution became more turbid after we increased the pH to 6.5, but the suspension remained orange. We increased the pH further to 6.8 on day 3, after which the color changed to black. We conclude that the minimum pH for magnetite formation under the applied conditions lies between pH 6.5 and 6.8. Experiment (d) had an initial pH of 6.0 and a final pH of 7.5. This procedure resulted in magnetite formation following the same trend as experiments (a) and (b), which had an initial pH of 5.5. These results demonstrate that

the pH only needs a slight adjustment around circumneutral values to induce magnetite formation. The formation of magnetite was confirmed by XRD analysis for all four experiments.

3.3.3 Pourbaix diagram

Fig. 3.1 shows a Pourbaix diagram for the iron phases in the CSTR. We calculated the ORP in the reactor based on the measured concentrations of dissolved Fe^{2+}, Fe^{3+} and NO_3^- (experiment (b)) and the calculated O_2 concentration (experiment (f)) in the reactor. Based on nitrate reduction, the ORP was 0.677 V (against standard hydrogen electrode (SHE)), which is far outside the magnetite range (indicated with an asterisk in the Pourbaix diagram). However, based on O_2 reduction, the ORP was -0.496 V (vs. SHE). At pH 6.8, this is just outside of the narrow range in which magnetite is the dominant form of iron (indicated with a plus sign). Since iron conversions other than the oxidation of Fe^{2+} also took place and the concentrations in the reactor increased over time, the actual ORP in the reactor would deviate slightly from the calculated value, allowing magnetite formation under the reactor conditions. The observed pH limit for magnetite formation in the CSTR experiments therefore correspond well with thermodynamic calculations. Although we cannot exclude the possibility that part of the ferrous iron was biologically oxidized, we consider it unlikely that this was a substantial fraction due to the low numbers of bacteria in tap water, the lack of carbon source due to CO_2 stripping, and the relatively short run time of the experiment.

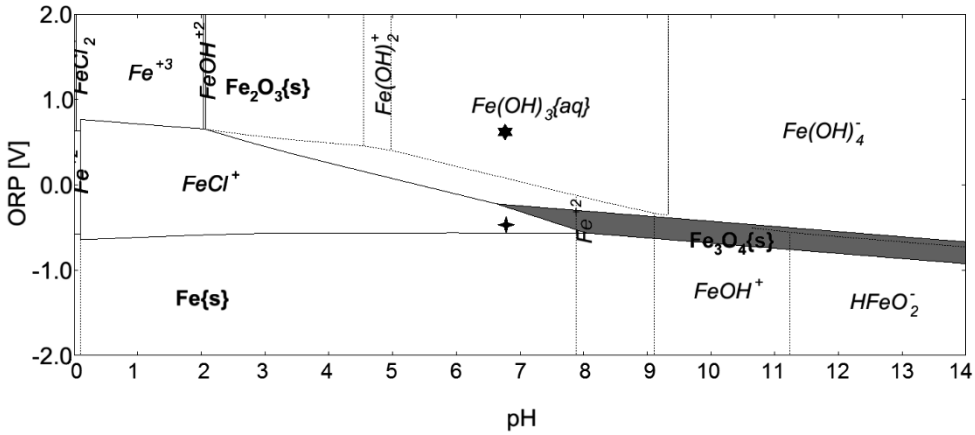

Figure 3.1. Pourbaix diagram created with OLI Studio 9.2 for the iron system; 1 mM Fe2+ (i.e. 55.85 mg L^{-1}, based on measurements in the reactor) and 32° C. The magnetite range is the highlighted area, * represents the reaction with NO_3^- and + represents the reaction with O_2.

3.3.4 Mass flow analysis of iron

We carried out a mass flow analysis for iron for the end state of the experiments. Calculations were based on the Fe^{2+} load, iron concentrations in the solution and precipitate concentration in both the reactor and the effluent collection vessel at the end of the experiments, assuming the

precipitates to be 100% magnetite (Appendix eq. S3.1 and S3.2). These calculations reveal a deviation of 2 to 8% in the iron balance, which we consider acceptable for a continuous process (data in Appendix).

3.3.5 Efficiency and rate of Fe^{2+} precipitation

The decrease in aqueous Fe^{2+} concentrations in the CSTR at the end of the experiments (day 4) was (a) 49%, (b) 42%, and (c) 29%, relative to the influent. Although the final pH of 7.5 in experiment (d) was the same as that of experiment (a), a higher fraction of iron precipitated (81%), corresponding to a rate of Fe^{2+} removal of 5.7 mg h^{-1}. The higher initial pH of 6.0 in experiment (d), compared to a pH of 5.5 for the other three experiments, apparently strongly affected the precipitation. Both the initial and the final pH therefore appear relevant for the efficiency of precipitation.

3.3.6 Fe^{2+}-oxidizing agents

Occurrence of reactions 3.1 and 3.2 was confirmed by the presence of nitrite and ammonium (Fig. 3.2, showing experiment (b)). Since NH_4^+ is the end product of nitrate reduction with ferrous iron [47,48,75] and green rust [49], nitrite represents a mere intermediate. The standard deviation of the analytical methods was $1.5.10^{-3}$ mg NO_2^--N L^{-1} and $11.6.10^{-3}$ mg NH_4^+-N L^{-1}. Because of the higher standard deviation of the analytical method ($42.9.10^{-3}$ mg L^{-1} for NO_3–N) and small fluctuations over time, we were unable to quantify nitrate depletion (Appendix, Table S3.6). Moreover, formation of other intermediate nitrogen compounds such as N_2O, as suggested by Etique et al. [49], or the formation of N_2 cannot be excluded.

To determine to what extent nitrate reduction to nitrite and ammonium accounted for all Fe^{2+} oxidized, an electron balance was calculated for experiment (b) at day 4 (Appendix eq. S3.3). The amount of iron that was oxidized was calculated based on the Fe^{2+} load, the weight of precipitates in both the reactor and the effluent per liter of total inflow and the measured Fe^{2+} in the reactor. Next to this, the amount of iron oxidation by NO_3^- reduction was calculated based of the measured concentrations of NO_2^- and NH_4^+ in the reactor according to reactions 3.1 and 3.2.

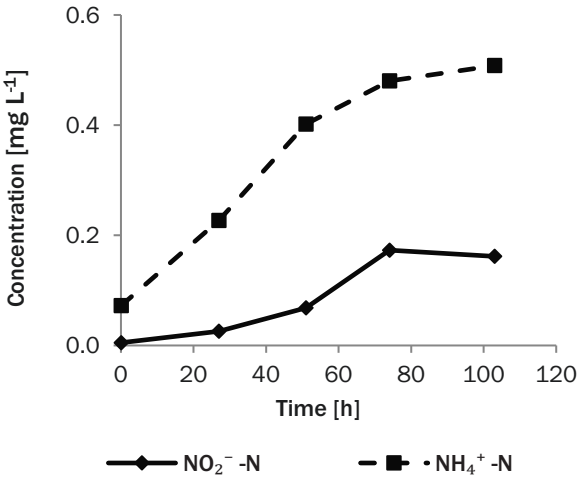

Figure 3.2 Formation of nitrite and ammonium (mg L^{-1}) over time in the reactor in experiment (b).

As Fig. 3.3 shows, reduction of nitrate to nitrite and ammonium cannot account for all Fe^{2+} oxidization, indicating the presence of another oxidant in the reactor system, which can only have been O_2. The N_2 sparging gas was a source of O_2 (see Section 3.2.2), but this could only account for the oxidation of up to $2.32.10^{-10}$ mg Fe^{2+}, which is only 0.1% of the total of $3.32.10^{-7}$ mg Fe^{2+} (experiment (b)). Hence, we suspected diffusion of O_2 into the reactor setup, e.g. through the Teflon tubing. To confirm this, we carried out experiment (e), in which the NO_3^- feed solution was replaced with tap water without added nitrate (see Table 3.2 for composition). Initial (5.5) and final pH (7.5) were the same as in experiment (a). Experiment (e) yielded magnetite in a similar manner as the experiments with NO_3^-. So, although a fraction of the added nitrate is reduced, the addition of nitrate is not essential for magnetite formation. Since O_2 is more reactive with Fe^{2+}, some accumulation of nitrite is visible in the reactor. The iron precipitation was 59%, which is fairly similar to that of experiment (a) (49%) (Appendix).

We quantified the O_2 influx into the system in experiment (f), in which the reactor was run at a constant pH of 6 with inflow solutions of 56 mg L^{-1} Fe^{2+} in Milli-Q water and pure Milli-Q water. No magnetite or other precipitate formed. We measured the Fe^{2+} concentration in the reactor over the course of six days. By acidifying the reactor samples to pH 3.3±0.2, we assured that all present Fe^{2+} was in solution before analysis. In steady state, the rate of iron oxidation was $4.88.10^{-11}$ mg Fe^{2+} h^{-1} (s.d. $2.29.10^{-12}$). This is a significant contribution (32% Fe^{2+} removal); as is clearly visible in Fig. 3.3. The sum of the percentages of the different Fe^{2+}-removing processes adds up to an acceptable 87%.

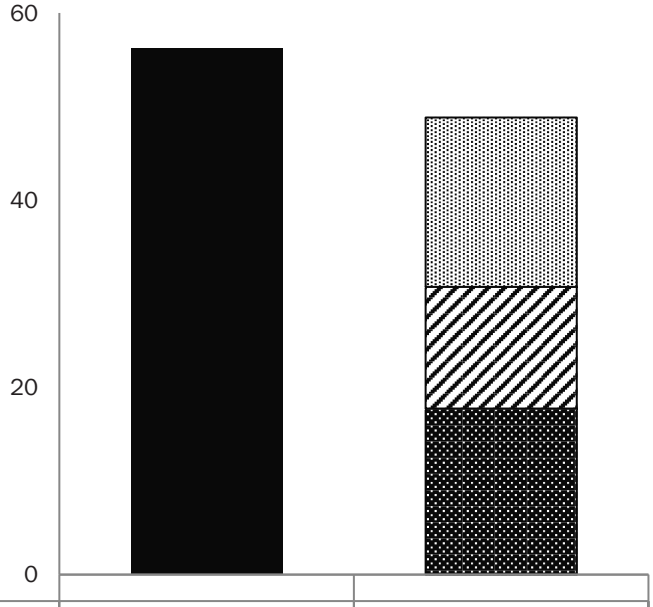

Fe^{2+} presumably oxidized by O_2 diffused into reactor [mg L^{-1}]		18.1
Fe^{2+} oxidized based on formation of NO_2^- and NH_4^+ in the reactor [mg L^{-1}]		13.0
Fe^{2+} in Fe_3O_4 in reactor and effluent per liter of total inflow [mg L^{-1}]		17.8
Fe^{2+} oxidized based on measured Fe^{2+} concentration in the reactor [mg L^{-1}]	56.2	

Figure 3.3 Calculated contributions of different processes to the decrease in Fe^{2+} concentration relative to the decrease as measured directly in the reactor at the end of experiment (b). Values were calculated based on the weight of the formed precipitates per liter of total inflow and the measurements of nitrite and ammonium at the end of experiment (b) and by O_2 diffusion as measured in experiment (f).

3.3.7 Precipitate analysis

As stated before, magnetite formed in all experiments, except in experiment (f). However, in experiments (a) and (d), lepidocrocite (γ-FeOOH) was also present in the precipitate samples from both the reactor and the effluent (see Table 3.3). According to Cornell and Schwertmann [3],

lepidocrocite formation is favored at a higher oxidation rate and lower Fe^{2+} concentration compared to magnetite formation. The higher final pH and lower Fe^{2+} concentrations of experiments (a) and (d) (44.4 mg L^{-1} and 24.8 mg L^{-1} respectively) therefore led to lepidocrocite formation.

Experiment	pH range	Precipitates found in reactor (XRD)	Precipitates found in effluent (XRD)
a	5.5 – 7.5	magnetite + lepidocrocite	magnetite + lepidocrocite
b	5.5 – 7.0	magnetite	magnetite
c	5.5 – 6.8	magnetite	magnetite
d	6.0 – 7.5	magnetite + lepidocrocite	magnetite + lepidocrocite

Table 3.3 Overview of precipitates formed in experiments a, b, c and d.

3.3.8 Precipitation pathway

Although the experiments were not directly aimed at researching the pathway of magnetite precipitation under the applied conditions, several observations and comparisons with other studies allow some insight. The color and turbidity changes of the reactor content after increasing the pH indicate that magnetite formed from a solid phase precursor that visually resembles GR, which is in agreement with what is described in the literature [3,76–78]. The Fe^{2+} concentration increased over time due to the constant supply of 570 mg L^{-1} $FeCl_2$. However, the constant influx of NO_3^- and/or O_2 caused a fraction of the Fe^{2+} to precipitate immediately as is evident from the development of the concentration of dissolved Fe^{2+} (Fig. 3.4). When we elevated the pH, the rate of increase in Fe^{2+} concentration became lower, indicating faster precipitation, which stems directly from the iron solubility at the different pH values.

To explore the mechanism of magnetite formation further, we carried out a follow-up experiment (h) with a slightly modified procedure. After a day of inflow of $FeCl_2$ and tap water at pH 5.5 in the reactor, we raised the pH to 7.0 and simultaneously stopped the inflows. The reactor content remained translucent green throughout this phase. On day 2, we switched the inflow pumps back on. Within an hour, dark green precipitates were visible. Less than 21 hours later, the reactor had a turbid dark green to black color, becoming entirely black over time. XRD analysis confirmed magnetite formation. The green color of the reactor content points to GR having formed as the precursor for magnetite. From the well supported dissolution-reprecipitation theory, it is known that Fe^{2+} in solution reacts with NO_3^- or O_2 on the surface of GR to from magnetite [20]. In experiment (h), Fe^{2+} was available in the reactor, even without inflow. However, the simultaneous

presence of both an unstable green precursor as well as an inflow of Fe^{2+} ions are necessary to initiate formation of magnetite.

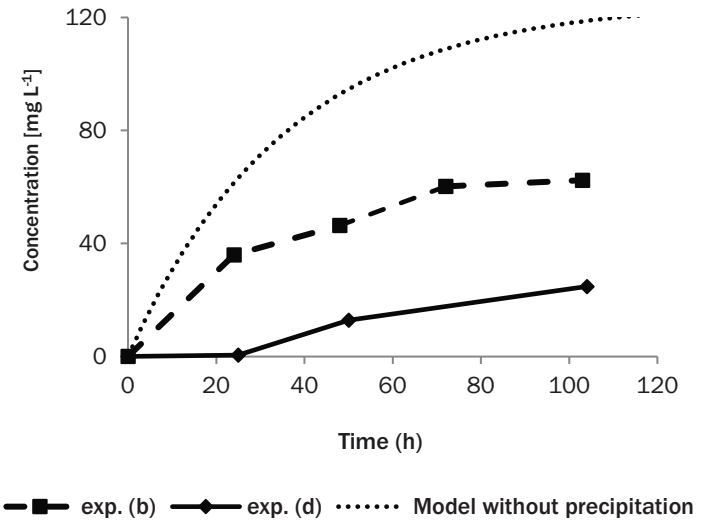

Figure 3.4 Concentration of Fe^{2+} over time as calculated based on the feed and measured in experiments (b) and (d)

3.3.9 Magnetite synthesis from seed crystals without pH elevation

As we found during our initial tests, a lower initial pH was necessary to initiate magnetite precipitation. During this phase, precipitates formed that were unstable once exposed to air, as was evident by the change in color from dark green to orange. This GR precursor appears to be essential, since no magnetite precipitated in its absence, i.e. when the reactor was run at a constant pH of 7.5. However, once the pH was raised from a lower initial value and magnetite had formed, the crystallization of magnetite continued for the three remaining days of the experiment at a constant pH of 6.8, 7.0 or 7.5.

One can hypothesize that the GR precursor that forms at the lower pH has been consumed and that the presence of already crystallized magnetite instigates further formation through the availability of surface sites [3]. To test this hypothesis, a reactor experiment (g) was conducted at a constant pH of 7; 27.7 mg L^{-1} magnetite from a previous experiment was added at the start of the experiment. No KNO_3 was supplied. Further procedures were the same as in experiments (a) through (d). This led to additional black particle formation within 24 hours. Weighing of the precipitates and XRD analysis at the end of the 4-day experiment showed that additional magnetite had formed. Thus, the process can be started up without pH elevation. We cannot exclude that in this experiment, GR also acted as precursor for magnetite formation, although the presence of this

intermediate could not be observed due to the presence of the seeding crystals. The mechanism of magnetite formation in the presence of magnetite seeds without elevating the pH requires further attention in future work.

3.3.10 Implications for application

The results presented in this paper show that magnetite formation from an aqueous Fe^{2+} solution is possible in a continuous process operated at circumneutral pH and without addition of chemicals. Both aspects are important for any process intended for implementation in drinking water production. We regard this result as a first step toward application of this partial oxidation method for iron removal in drinking water production. In order to assess its application potential, numerous aspects require further research. For example, our experiments were conducted at 32 °C, whereas groundwater temperature in most areas is lower and heating is not economically feasible. Further research will have to show the possible influence of temperature on the process. We conducted our experiments in 50% diluted tap water, showing that small concentrations of other ions did not inhibit the formation of magnetite in the process. However, groundwater is a more complex medium than tap water, containing different ions at often higher concentrations. Based on our research, the presence of nitrate at concentrations typical for groundwater will not disturb the process. However, phosphate and carbonate for example are known to cause precipitation of vivianite and siderite respectively, rather than magnetite [3]. Further research into the effects of ions typically present in groundwater and corresponding concentrations is therefore necessary to evaluate the suitability of this process for application in drinking water production. Moreover, the process will have to be tested with the lower iron concentrations typical for groundwater. Alternatively, this process could be applied in a concentrated stream, e.g. after membrane filtration. In addition, the effect of the presence of microorganisms in a reactor will have to be evaluated. We did not consider the presence of microorganisms in our short-term experiments, but growth of microorganisms into a full-scale reactor cannot be avoided in an environmentally friendly and cost-effective manner and may be either beneficiary to the process or inhibit it. Furthermore, increasing the rate and efficiency of the process is necessary to make this a viable iron removal process. The possibilities for the application of this process are not limited to the treatment of groundwater. In the metallurgical industry, iron-rich streams are produced that result in large volumes of solid waste. Treatment of these streams with the magnetite crystallization process might result in an additional valuable product for this industry.

3.4 Conclusions

In this paper, we have reported on the formation of magnetite in a continuous reactor from a medium based on 50% tap water and 50% Milli-Q water, at a slightly elevated temperature (32 °C), atmospheric pressure and circumneutral pH.

A series of short experiments was conducted, from which can be concluded that O_2 caused the partial Fe^{2+} oxidation that led to the formation of magnetite. The formation of magnetite was instigated by a pH elevation from between 5.5 and 6.0 to between 6.8 and 7.5. Using a starting

pH of 5.5 or slightly higher and a final pH of 7.0 (or slightly higher) suffices and may also prevent the simultaneous formation of lepidocrocite. Also, an experiment was conducted with seed crystals, revealing that seeding with magnetite particles allowed magnetite to form at a constant pH of 7, i.e. without requiring a pH change.

Since this method requires very limited addition of chemicals, this could yield a promising process for environmentally friendly iron removal in drinking water production. Further work is ongoing to explore its potential.

3.6 Appendix to Chapter 3

S3.1 Iron mass balance equations

S3.2 Electron balance equation

S3.3 Iron mass balances

Table S3.1 Iron mass balance experiment (a)

Table S3.2 Iron mass balance experiment (b)

Table S3.3 Iron mass balance experiment (c)

Table S3.4 Iron mass balance experiment (d)

Table S3.5 Iron mass balance experiment (e)

S3.4 Measured concentrations of nitrogen species over time in experiment (b), compared to the modeled NO_3^--N concentration

Table S3.6

S3.1 Iron mass balance equations

$$Fe_{in} = Q_{FeCl_2} * C_{Fe} * t_{exp} \quad \text{(S3.1)}$$

$$Fe_{out} = V_R * \left([Fe^{2+}] + [Fe^{3+}] + \frac{167.5}{231.5} * Fe_3O_4\right)_R + V_E * \left([Fe^{2+}] + [Fe^{3+}] + \frac{167.5}{231.5} * Fe_3O_4\right)_E \quad \text{(S3.2)}$$

In these equations:

Fe_{in} = iron mass fed to CSTR during experiment (mg Fe)
Q_{FeCl_2} = flow iron feed solution (L h^{-1})
C_{Fe} = concentration of Fe in feed solution (mg Fe L^{-1})
t_{exp} = duration of experiment (h)
Fe_{out} = sum of iron mass in CSTR and effluent vessel at t=t_{end} (mg Fe)
V_R = volume of CSTR (L)
V_E = liquid volume in effluent container (L)
$([Fe^{2+}] + [Fe^{3+}] + \frac{167.5}{231.5} * Fe_3O_4)$ = sum of dissolved and solid iron concentrations in CSTR (R) or effluent (E) at t=t_{end} (mg Fe L^{-1})

S3.2 Electron balance equation

$$\frac{[Fe^{2+}]_{mod} - [Fe^{2+}]_R - \frac{1}{3} * \frac{167.5}{231.5} * Fe_3O_4}{55.845} = 8 * \frac{[NH_4^+]}{18.0385} + 2 * \frac{[NO_2^-]}{46.0055} + 4 * \frac{[O_2]}{31.9988} \quad \text{(S3.3)}$$

In this equation:

$[Fe^{2+}]_{mod}$ = modeled concentration of Fe^{2+} in the CSTR for an inert system (mg L^{-1})
$[Fe^{2+}]_R$ = measured concentration of aqueous Fe^{2+} in the CSTR (mg L^{-1})
$\frac{1}{3} * \frac{167.5}{231.5} * Fe_3O_4$ = concentration of Fe^{2+} present in the precipitate per liter inflow (mg L^{-1})
$[NH_4^+]$ = measured concentration of NH_4 in the CSTR (mg L^{-1})
$[NO_2^-]$ = measured concentration of NO_2^- in the CSTR (mg L^{-1})
$[O_2]$ = calculated diffusion of O_2 into the reactor (mg L^{-1})

S3.3 Iron mass balances

Total Fe^{2+} inflow	**[mg]**	**723.90**	
Meas. Fe reactor (total)	[mg]	92.96	
Meas. Fe effluent (total)	[mg]	224.1	
Fe in precipitate*	[mg]	354.55	*Assuming 100% magnetite
Difference Fe	[mg]	52.28	
Difference Fe	[%]	7.22	
Decrease Fe^{2+} (aq)	[%]	49.0	
Fe removal rate	mg h^{-1}	3.44	

Table S3.1 Iron mass balance experiment (a).

Total Fe^{2+} inflow	**[mg]**	**723.90**	
Meas. Fe reactor (total)	[mg]	128.96	
Meas. Fe effluent (total)	[mg]	276.2	
Fe in precipitate*	[mg]	307.23	*Assuming 100% magnetite
Difference Fe	[mg]	11.51	
Difference Fe	[%]	1.59	
Decrease Fe^{2+} (aq)	[%]	42.4	
Fe removal rate	mg h^{-1}	2.98	

Table S3.2 Iron mass balance experiment (b).

Total Fe^{2+} inflow	**[mg]**	**730.93**	
Meas. Fe reactor (total)	[mg]	148.96	
Meas. Fe effluent (total)	[mg]	328.9	
Fe in precipitate*	[mg]	211.28	*Assuming 100% magnetite
Difference Fe	[mg]	41.78	
Difference Fe	[%]	5.72	
Decrease Fe^{2+} (aq)	[%]	28.9	
Fe removal rate	mg h^{-1}	2.05	

Table S3.3 Iron mass balance experiment (c).

Total Fe^{2+} inflow	**[mg]**	**737.95**	
Meas. Fe reactor (total)	[mg]	52.04	
Meas. Fe effluent (total)	[mg]	57.8	
Fe in precipitate*	[mg]	592.46	*Assuming 100% magnetite
Difference Fe	[mg]	35.67	
Difference Fe	[%]	4.83	
Decrease Fe^{2+} (aq)	[%]	80.3	
Fe removal rate	mg h^{-1}	5.70	

Table S3.4 Iron mass balance experiment (d).

Total Fe^{2+} inflow	**[mg]**	**730.93**	
Meas. Fe reactor (total)	[mg]	65.84	
Meas. Fe effluent (total)	[mg]	179.9	
Fe in precipitate*	[mg]	425.96	*Assuming 100% magnetite
Difference Fe	[mg]	59.26	
Difference Fe	[%]	8.11	
Decrease Fe^{2+} (aq)	[%]	58.3	
Fe removal rate	mg h^{-1}	4.14	

Table S3.5 Iron mass balance experiment (e).

S3.4 Measures concentrations of nitrogen species over time in experiment (b), compared to the modeled NO_3^--N concentration

time t	**NO_3^--N**	**Modeled [NO_3^--N] in reactor without NO_3^- reduction**	**Difference modeled and measured NO_3^--N**	**NO_2^--N**	**NH_4^+-N**	**Sum NO_2^--N + NH_4^+-N**	**Total N**
[hours]	[mg/L]	[mg/L]	[mg/L]	[mg/L]	[mg/L]	[mg/L]	[mg/L]
0	0.08	0	0*	<0.004	<0.004	0	0.08
24	2.72	2.74	0.02*	0.026	0.227	0.253	2.97
48	3.90	4.14	0.24	0.068	0.402	0.470	4.37
72	4.91	4.85	-0.06*	0.173	0.480	0.653	5.56
103	5.40	5.29	-0.11	0.162	0.508	0.670	6.07

Table S3.6 Measured concentrations of nitrogen species over time in experiment (b), compared to the modeled NO_3^--N concentration (assuming no denitrification). *value smaller than the standard deviation of NO_3^- (see paragraph 3.2.1).

Chapter 4

Magnetite crystallization by partial oxidation of aqueous ferrous iron in a continuous stirred tank reactor with controlled air supply

Yvonne M. Mos, Cees J.N. Buisman, Jan Weijma

Sub-Department of Environmental Technology, Wageningen University & Research, P.O. Box 17, 6700 AA Wageningen, the Netherlands.

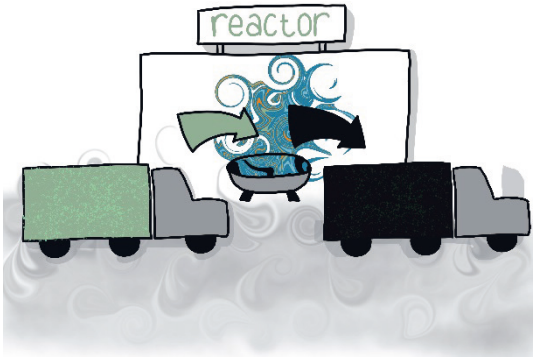

A modified version of this chapter is submitted as:

Y.M. Mos, C.J.N. Buisman, J. Weijma, Magnetite crystallization by partial oxidation of aqueous ferrous iron in a continuous stirred tank reactor with controlled air supply.

Abstract

Magnetite was crystallized through partial oxidation of aqueous ferrous iron with O_2 from air supplied to the headspace of a 2 L continuous stirred tank reactor which was operated under mild conditions (pH 7.5, ambient temperature). Experiments were carried out in a glovebox under a N_2 atmosphere to prevent uncontrolled diffusion of O_2 from the surrounding environment into the reactor. Effects of the ferrous iron feed concentration (2.25 to 0.25 mM Fe^{2+}) and hydraulic retention time (8 to 69 h) on the precipitated solid phases were evaluated to assess the applicability of this process for groundwater treatment. Magnetite was formed in experiments with iron feed concentrations of 1 and 2.25 mM Fe^{2+}, but not a lower feed concentrations. The main factor determining the iron phase formation was the concentration of aqueous Fe^{2+} in the reactor, with an optimum for magnetite crystallization around 1 mM. These results indicate that ferrous iron from groundwater used for drinking water production could be removed as the mineral magnetite. In order to implement magnetite crystallization to practice however, magnetite crystallization needs to take place in a more complex medium. Therefore, additional experiments were conducted in diluted tap water and growth medium with and without the addition of a mixed microbial culture. Experiments with tap water yielded maghemite and goethite. Experiments in growth medium without microorganisms led to lepidocrocite and goethite formation. When a mixed microbial culture was added to the medium, vivianite and goethite were formed.

Keywords: crystallization; CSTR; ferrous iron; groundwater; magnetite; mixed microbial culture

4.1 Introduction

At least 50% of the drinking water worldwide is produced from groundwater [1]. Anaerobic groundwater contains up to 0.9 mM ferrous iron while the World Health Organization recommends a maximum concentration of 5.10^{-3} mM (0.3 mg L^{-1}) to avoid effect on flavor and appearance [2]. Currently, the most widely used method for ferrous iron removal is uncontrolled oxidation using O_2 from air and precipitation of the resulting ferric iron oxides, followed by sand filtration to remove these solids [5]. This is an effective but not optimal method, since it produces a bulky and poorly dewaterable sludge [14]. Moreover, use of the iron residue is limited to low-value applications such as the production of bricks and sulfur removal from biogas reactors [15,16]. We propose to precipitate the ferrous iron in groundwater as magnetite (Fe_3O_4), aiming to yield a more compact and potentially valuable product.

Applications of magnetite range from the demobilization of pollutants and magnetic data storage to several high-end medical applications, like contrast fluid for MRI, cell separation and site-specific chemotherapy [29,79]. The application potential of magnetite depends strongly on the product characteristics, especially particle size, morphology and purity.

Numerous methods for chemical synthesis of magnetite exist, like thermal decomposition of iron pentacarbonyl, microemulsion, hydrothermal precipitation and co-precipitation [4,28]. However, these methods require high temperatures and/or pressures and often addition of chemicals in order to produce magnetite particles with a narrow particle size range, rendering them environmentally unfriendly and expensive [4].

In previous research, we have shown that synthesis of magnetite from aqueous ferrous iron in a continuous reactor (CSTR) operated at circumneutral pH, ambient temperature and without extensive addition of chemicals is feasible (Ch. 3). Magnetite was synthesized through the partial oxidation method with either nitrate or O_2 as oxidizing agent, feeding the CSTR with a 2.25 mM Fe^{2+} solution. However, O_2 diffused into the reactor set-up and therefore its addition was uncontrolled. In the current research, we placed the CSTR in a glovebox under an N_2 atmosphere and continuously added a controlled flow of air to the headspace. The partial ferrous iron oxidation and magnetite crystallization involves the following reactions [20]:

$$4\,Fe^{2+} + O_2 + 4\,H^+ \rightarrow 4\,Fe^{3+} + 2\,H_2O \quad (4.1)$$

Followed by:

$$Fe^{2+},\ Fe^{3+},\ H_2O \rightarrow GR \quad (4.2)$$

$$Fe^{2+}, GR \rightarrow Fe_3O_4, H_2O \quad (4.3)$$

Medium complexity can influence precipitate formation. The presence of carbonate can prevent magnetite precipitation by formation of the ferrous mineral siderite ($FeCO_3$) from Fe^{2+} before oxidation can take place (10 mM carbonate buffer, [45]). Likewise, the presence of phosphates can lead to vivianite ($Fe_3(PO4)_2$) formation (≥ 0.1 M PO_4^{3-}, [50]). Moreover, several cations like copper and manganese can be incorporated into the magnetite structure [3,27]. Since groundwater can contain these and other ions, it is important for our aimed field of application to evaluate the influence thereof.

Microbiological magnetite synthesis has been a topic of research for years [54,55]. In the process of magnetite formation from ferrous iron, iron oxidizing bacteria could contribute to the realization of the desired Fe^{2+} to Fe^{3+} ratio [17]. Moreover, bacteria can catalyze crystallization by providing a nucleation site. While microbiological synthesis of magnetite is possible both intracellularly and extracellularly, so far this was shown only in small scale batch experiments and is not ready for large scale application yet (e.g. [21,40–42,44,53,57,60]).

We conducted experiments with different iron concentrations to assess the technological feasibility of the process for the treatment of groundwater. Additionally, we did experiments varying the hydraulic retention time (HRT) of the reactor. Economically, a short HRT is preferred to minimize reactor volume. Additionally, we conducted experiments in diluted tap water to research magnetite crystallization in more complex media. Experiments in growth medium with and without microorganisms present were conducted to evaluate the possible influence of bacteria on precipitate formation.

4.2 Materials and methods

4.2.1 Chemicals and analysis

All chemicals used were analytical grade. $FeCl_2$ (Alfa Aesar) was 99.5% pure, anhydrous and the container was only opened in an anaerobic hood to minimize exposure to O_2. $FeCl_2$ solutions were prepared in an anaerobic glovebox. All solutions were prepared using Milli-Q water that was purged with 99.999% pure N_2 gas (5.0 N_2, O_2 < 5 ppmv, Linde Gas Benelux B.V., the Netherlands) for at least 40 minutes per liter prior to use.

The soluble Fe^{2+} and Fe^{3+} concentrations in the reactor were determined with a cuvette kit (LCK 320) and a DR3900 spectrophotometer (Hach). Sampling, dilution of the sample and addition thereof to the cuvette took place in the same glovebox that was used for reactor experiments. The concentration of O_2 in the glovebox was measured by means of an O_2-sensitive spot, with a detection limit of 294 ppmv (Presens).

At the end of the experiment, precipitates from the reactor and the accumulated effluent were separated by settling and then air-dried at room temperature. Precipitates from experiments [Fe]-A, [Fe]-B, BB and BIO (Table 4.1) were washed with Milli-Q water before drying to remove dissolved salts that could impede interpretation of the diffractogram. This preparation step was not necessary for the precipitate samples of the other experiments, since those were conducted in Milli-Q water and iron concentrations therein were higher. Any oxidation of Fe^{2+} present in the

sample is not affecting the magnetite content since magnetite is stable over a period of years under ambient conditions and no additional magnetite can be formed in this way [3] as was also confirmed by reanalyzing older samples. The precipitate samples were analyzed by X-Ray Diffraction (XRD) with a Bruker D8 Advance equipped with Cu radiation (1600 W). A Lynxeye XE-T detector was used with a fixed sample illumination of 10 mm, position sensitive detection window set at 2.91°, and an air scatter knife at 1.0 mm above the sample holder. The sample was spun at a speed of 5.0 rpm to ensure statistically optimal results. The scanning range was 10° to 80° 2θ, the step size was 0.02° and the counting time per step was 0.5 – 5 s. The percentages of the different solid phases present in the precipitates were calculated from the XRD data with Diffrac.EVA software (Bruker).

4.2.2 CSTR experiments

A CSTR with a working volume of 2 L plus 1 L headspace was placed inside a glovebox at ambient temperature with a N_2 atmosphere at approximately 20 mbar above atmospheric pressure. The O_2 concentration inside the glovebox remained below $6.3.10^3$ ppmv during experiments. Parameters varied were the iron concentration and the HRT.

The CSTR was simultaneously fed with 1) Milli-Q water containing 4.5 mM $FeCl_2$ and 2) Milli-Q water without any addition, tap water or growth medium (Watson Marlow pumps). A validation experiment with an HRT of 50 h showed that no precipitation took place in the CSTR when no air was supplied to the headspace, indicating that no significant O_2 diffusion to the reactor took place. The pH in this experiment was set at 5.5 for the first 24 h and was increased to pH 7.0 for the period of 24 h to 72 h.

Before starting an experiment, the CSTR was filled with 2 L of the desired medium. The pH was set at 5.5 for the first 24 h, after which it was increased to 7.5 since a forced pH raise is essential to instigate the process (Ch. 3). During the experiments, the flows were set according to desired Fe^{2+} feed concentration and HRT. Table 4.1 presents an overview of the varied parameters (Fe^{2+} feed concentration and HRT) in the CSTR experiments. Compressed air was supplied to the headspace (1 L) of the reactor with a mass flow controller (Bronkhorst). The headspace of the reactor was circulated by a compressor (KNF) to ensure mixing of the gas phase and connected to a water lock to release overpressure. Mixing of the liquid phase was accomplished with magnetic stirring at approximately 90 rpm with a 4-cm magnetic bead placed centrally on the reactor bottom. The reactor was connected to a pH electrode (QIS) and controller, which dispensed HCl (0.25 M) or NaOH (0.25 M) when the absolute deviation from the pH set point value (5.5 or 7.5) became more than 0.1. Oxidation/reduction potential (ORP) was monitored with an electrode (QIS). Both the pH and ORP were continuously logged by a multi-parameter analyzer (Consort).

Experiment	$FeCl_2$ feed concentration [mM]	$FeCl_2$ load [mmol.h^{-1}]	Air supply [NmL.h^{-1}]	HRT [h]	Medium composition
Blank	2.25	13.10^{-2}	-	50	100% MQ
BE	2.25	13.10^{-2}	7.0	34	100% MQ
[Fe]-A	0.5	3.9.10^{-2}	1.6	34	100% MQ
[Fe]-B	0.25	1.0.10^{-2}	0.8	34	100% MQ
HRT-A	2.25	6.8.10^{-2}	3.5	69	100% MQ
HRT-B	2.25	58.10^{-2}	30.3	8	100% MQ
TW-A	2.25	13.10^{-2}	7.0	34	50% MQ, 50% TW
TW-B	2.25	13.10^{-2}	7.0	34	10% MQ 90% TW
BB	2.25	13.10^{-2}	7.0	34	GM
BIO	2.25	13.10^{-2}	7.0	34	GM + MMC

Table 4.1 Overview of experiments. pH in all experiments was controlled 5.5±0.1 for the first 24 h, after which the pH was raised to 7.5±0.1 for the remainder of the experiment. MQ = Milli-Q water, TW = tap water, GM = growth medium, MMC = mixed microbial culture.

4.2.3 Tap water and growth medium composition

The used tap water was obtained from Wageningen, the Netherlands (see Table 4.2 for composition). Since all water is sparged with N_2 for 40 min L^{-1}, we assume that the hydrogen carbonate concentration is lower than listed.

Compound	Average concentration	Unit
Hydrogen carbonate	1.6	mM
Chloride	0.2	mM
Sulphate	0.07	mM
Sodium	0.26	mM
Potassium	0.02	mM
Silicate	0.08	mM
Calcium	0.73	mM
Magnesium	0.10	mM
Ortho-phosphate	0.63	µM PO_4 L^{-1}
Iron (after acidification)	0.45	µM
Arsenic (after acidification)	0.04	µM
Barium (after acidification)	0.03	µM
Copper (after acidification)	0.12	µM

Table 4.2 Concentrations of ions of interest in Wageningen tap water [80]

The composition of the growth medium is shown in Table 4.3. Vitamin and trace element solutions are according to DSMZ [81]. The medium was prepared with Milli-Q water. O_2 was supplied by means of a gas cylinder containing a gas mixture consisting of 59% N_2, 21% O_2 and 20% CO_2 pressurized at 5 bar. A custom gas mixture was used to ensure sufficient availability of carbon for the microorganisms. During the experiment BIO, the tank was refilled after 336 hours, resulting in 15 min without gas flow to the CSTR headspace.

Compound	Unit	Concentration
NH_4Cl	mM	2.8
$NaH_2PO_4.H_2O$	mM	$7.3.10^{-3}$
KCl	mM	1.3
Vitamin solution	mL L^{-1}	10
Trace element solution	mL L^{-1}	10

Table 4.3 Medium composition. Additionally, vitamin and trace element solutions were added.

4.2.4 *Mixed microbial culture*

Experiment BIO was inoculated with a mixed culture of microorganisms that originated from activated anaerobic sludge from the waste water treatment plant in Ede, the Netherlands. The sludge was washed 3 times with medium (Table 4.2) and diluted with medium to obtain a suspension with a dry weight of 20 g L^{-1}. A volume of 200 mL was added to the reactor immediately after the pH raise at t = 24 h. Moreover, an additional inoculation of the reactor, following the same procedure, at t = 480 h.

4.2.5 *Calculations and modeling*

Scaling tendencies were calculated using OLI Studio 9.2 (OLI Systems, Inc.). Input for the model were the measured aqueous Fe^{2+} and Fe^{3+} concentrations and the set pH value.

The concentration of total Fe in the reactor was modeled with:

$$C_{Fe_R} = (1 - \exp\left(-\frac{Q_l}{V_R} * t\right)) * C_{Fe} \quad (4.4)$$

In this equation:

C_{Fe_R} = modeled concentration of iron present in reactor (M)
Q_l = flow of liquid phase (L h^{-1})
V_R = volume of reactor (L)
t = elapsed time (h)
C_{Fe} = concentration of Fe in feed (M)

4.3 Results

4.3.1 *Effect of ferrous iron concentration in the feed*

To assess magnetite formation in the process at Fe^{2+} concentrations in the groundwater range (up to 0.9 mM [2]), experiments were conducted with feed concentrations of 2.25, 1.0, and 0.5 mM Fe^{2+} (BE, [Fe]-A and [Fe]-B respectively). The molar O_2 : Fe supply ratio was kept at 0.46 by adjusting the air flow to the reactor. However, air flow during the first 24 h of experiment [Fe]-A was higher using a ratio of 1.0 during that interval.

A lower feed concentration led to a higher percentage of iron precipitation. In experiment [Fe]-B, 72% of the iron precipitated at t = 96 h, while this was only 36% in experiment BE (eq. 4.4).

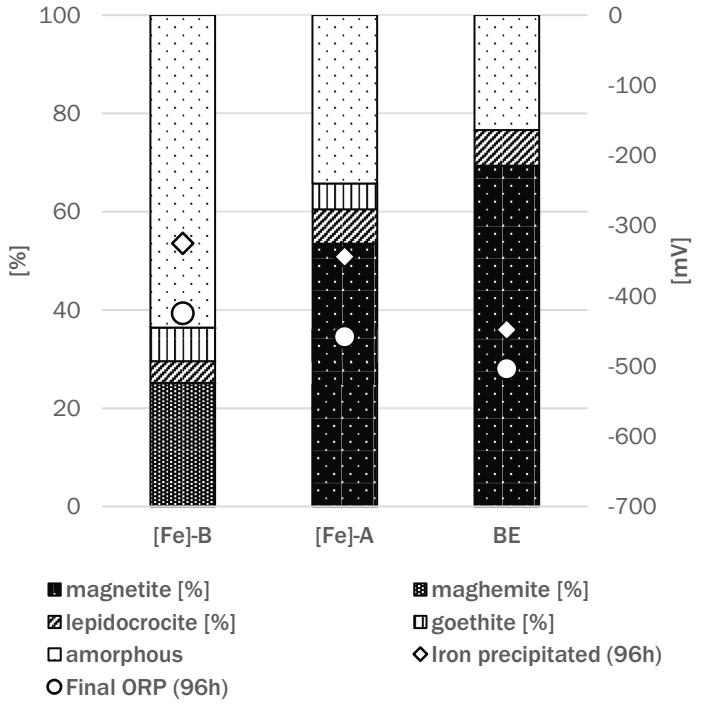

Figure 4.1 Composition of precipitates collected from the reactor at t = 96 h, fraction of precipitated iron and final ORP of the experiments with different iron feed concentrations. [Fe]-B: 0.50 mM; [Fe]-A: 1.00 mM; BE: 2.25 mM. HRT 34 h.

Figure 4.1 shows the composition of the precipitates from the reactor at the end of the experiments. Magnetite was identified at 1 and 2.25 mM Fe^{2+} in the feed (experiments BE and [Fe]-A), where it accounted for 69% and 54% of the precipitates respectively. Magnetite was also present in the collected effluent in these experiments, indicating continuous formation thereof. However, magnetite was not formed at the lower feed concentration of 0.5 mM Fe^{2+} (experiment [Fe]-B). Apparently, under the applied conditions, the minimum Fe^{2+} concentration in the feed for magnetite formation lies between 0.5 and 1 mM.

Maghemite (γ-Fe_2O_3) was the dominant crystalline precipitate in experiment [Fe]-B. Lepidocrocite (γ-FeOOH) is a known side product in the partial oxidation method for magnetite formation (Ch. 3, [53]) and was found in all experiments (4% to 7%). Goethite (α-FeOOH) was formed in experiments [Fe]-A (5%) and [Fe]-B (7%).

4.3.2 Effect of hydraulic retention time

The effect of the HRT on the precipitated solid phases was assessed in three experiments with HRTs of 8, 34 and 69 h (experiments HRT-B, BE and HRT-A respectively). A short HRT has a

preference for application, since it reduces reactor volume. However, because the selectivity for magnetite formation was not optimal at 8 and 34 h, prolonging the HRT was evaluated as well. The concentration of ferrous iron in the feed was 2.25 mM at all HRTs, corresponding to loads of 58.10^{-2} (8 h), 13.10^{-2} (34 h) and $6.8.10^{-2}$ (69 h) mmol Fe h^{-1}. The air supply was adjusted to keep a constant O_2 to iron molar load ratio.

Figure 4.2 shows that a HRT of 8 h led to a lower magnetite (18%) and much higher lepidocrocite (43%) content of the precipitate compared to the experiments at HRTs of 34 h (magnetite 69%, lepidocrocite 7%) and 69 h (magnetite 60%, lepidocrocite 7%). Additionally, a small fraction (3%) of goethite was formed at the lower HRT, while this was not present at an HRT > 8 h. The type of solid phases did not differ between the experiment at HRTs of 34 and 69 h, with only a fairly small difference in the fraction of magnetite in the precipitate (69% vs. 60% at 34 and 69 h, respectively).

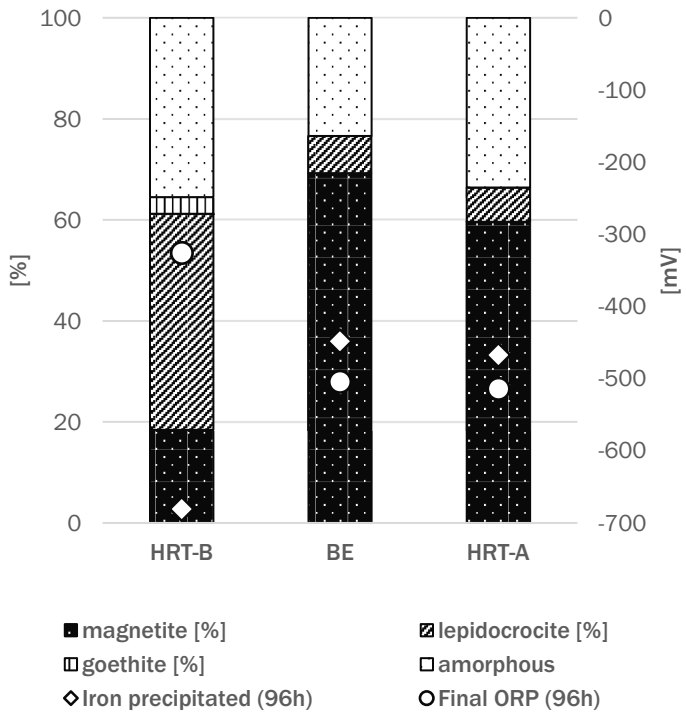

Figure 4.2 Composition of precipitates collected from the reactor at t = 96 h, fraction of precipitated iron and final ORP of the experiments with different HRT (iron feed concentration 2.25 mM) and, consequently, different iron load. HRT-B: 8 h, $58.0.10^{-2}$ mmol h^{-1}; BE: 34 h, $13.0.10^{-2}$ mmol.h^{-1}; HRT-A: 69 h, $6.8.10^{-2}$

4.4 Discussion

4.4.1 Scaling tendencies

OLI defines the scaling tendency as 'the ratio of the real-solution solubility product to the thermodynamic limit based on the thermodynamic equilibrium constant' [82]. Therefore the scaling tendency for a precipitate lies between 0 and 1. Modeling of the scaling tendencies showed that magnetite is the thermodynamically most stable phase t = 24 h onwards for all experiments (Fig. 4.3). Both siderite and magnetite reach a scaling tendency of 1 in experiment HRT-B. While the ratio of Fe^{2+} and CO_2 in the feeds are kept equal throughout the experiments, the higher iron concentration in HRT-B leads to an increased overall scaling tendency and consequently to an increased scaling tendency for siderite. The lack of formation of siderite in the experiments was probably due to the addition of the air to the headspace, depending on diffusion for the formation of carbonates in the liquid phase, while the model assumed vigorous mixing of the liquid and gas phase. The concentration of carbonates in solution is therefore expected to be significantly lower than the model predicts. According to the model, hematite is the thermodynamically most stable phase in the first 24 h. However, hematite is not mentioned as a possible product of (partial) oxidation of ferrous oxides by Cornell and Schwertmann [3]. Input parameters for the model were the concentrations of Fe^{2+} and Fe^{3+} at the time of measurement. In the practical experiments however, Fe^{3+} is formed through oxidation of Fe^{2+} causing a gradual increase in concentration. This likely favors the formation of mixed valence complexes like green rusts and magnetite.

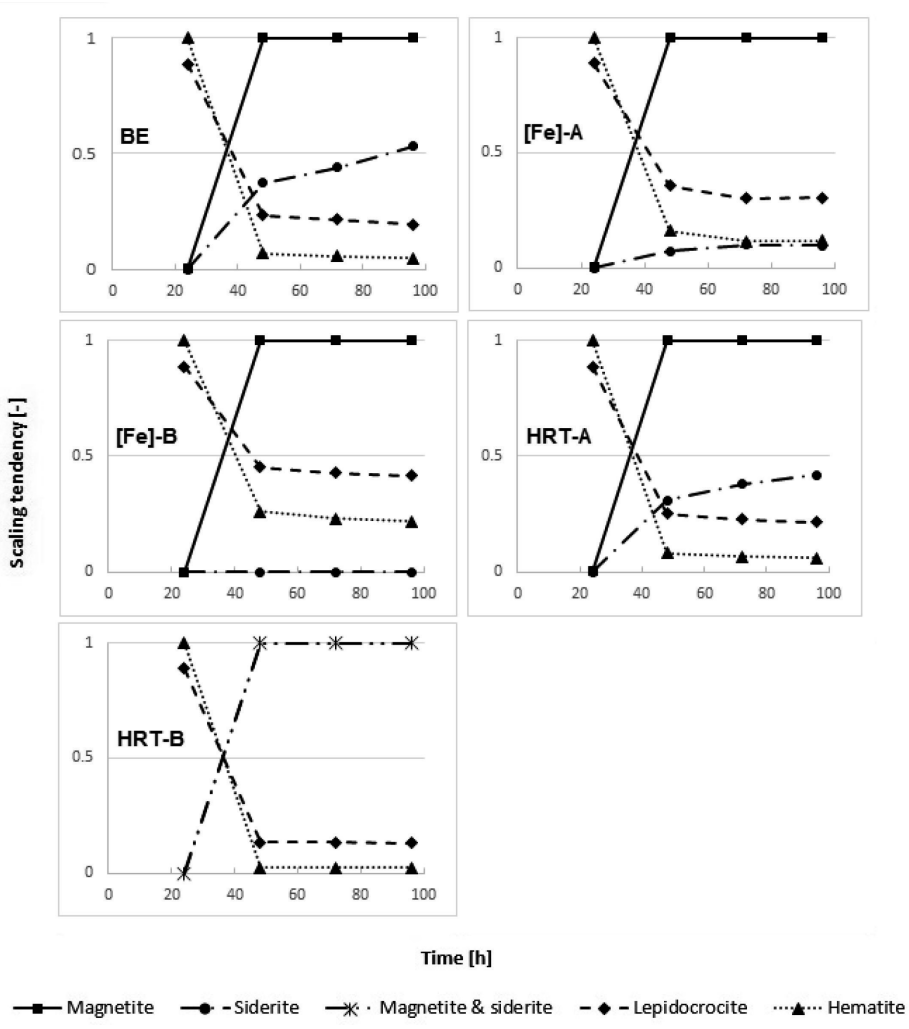

Figure 4.3 Scaling tendencies over time for the different experiments as modeled in OLI.

4.4.2 ORP vs. precipitated solid phases

The pH and ORP determine the stable thermodynamic solid iron phase [3]. Figure 4.4 shows the ORP over time in the experiments. The fluctuations in the ORP are related to fluctuations in pH that was allowed to deviate ±0.1 unit. The ORP only partially relates to the composition of precipitated solid phases in the experiments. Experiments BE, HRT-A and [Fe]-A, that yielded the highest percentages of magnetite (69%, 60% and 54% respectively, Fig. 4.1 and 4.2), all have an ORP that reached below -450 mV (Fig. 4.4). However, an increasingly higher final ORP cannot be

related to a decreasingly lower percentage of magnetite as shown by HRT-B (34% magnetite, ORP -326 mV) and the absence of magnetite in the precipitates collected from the reactor in [Fe]-B (Fig. 4.1).

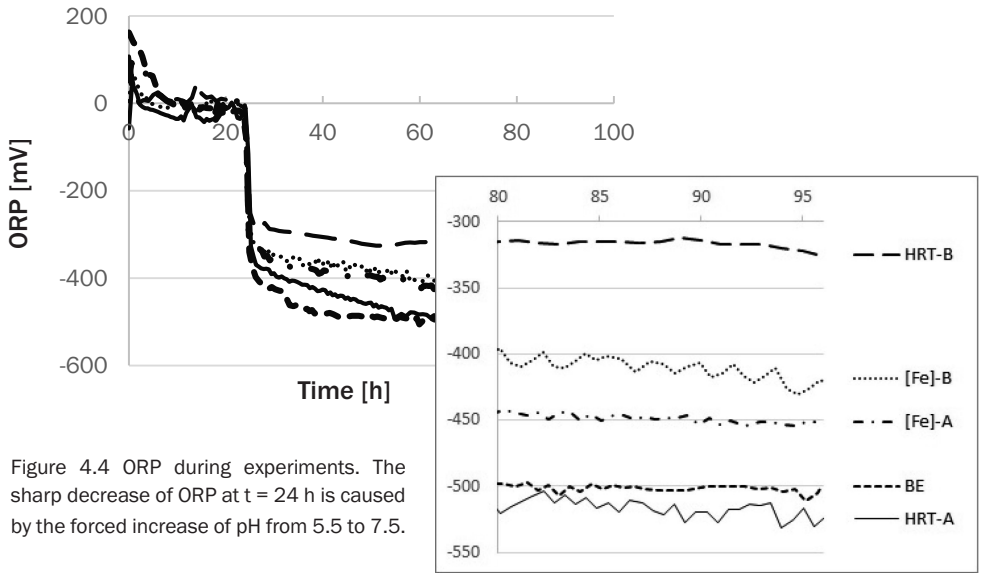

Figure 4.4 ORP during experiments. The sharp decrease of ORP at t = 24 h is caused by the forced increase of pH from 5.5 to 7.5.

4.4.3 Aqueous Fe^{2+} concentration vs. formed precipitates in reactor

In the partial oxidation method, aqueous Fe^{2+} reacts with GR complexes to form magnetite [20,28], suggesting that the Fe^{2+} concentration in solution plays a key role. Figure 4.5 shows the percentages of the various solid phases in the precipitates collected from the reactor at t = 96 h plotted versus the concentration of Fe^{2+} in the reactor. Magnetite was not formed below 0.36 mM Fe^{2+} (aq) (Fig. 4.5a), which apparently represents a threshold value under the applied conditions.

The fraction of lepidocrocite ranges between 4% and 7% for an aqueous Fe^{2+} concentration of 1 mM or lower (Fig. 4.5c). At 2.1 mM Fe^{2+} (aq), the fraction of lepidocrocite increases to 43%. Lepidocrocite is formed through oxidation of chloride-GR when this is exposed to ambient air [3,35]. While GR is an unstable iron phase, its stability in an aqueous environment is increased at a higher aqueous Fe^{2+} concentration [59,83]. We therefore hypothesize that lepidocrocite is formed after the end of the experiments, during the sample preparation for XRD analysis. This hypothesis is strengthened by the results of experiments BE and HRT-B, where the sum of magnetite and lepidocrocite fractions is fairly constant (61% - 76%, Fig. 4.2), suggesting a competition for reactants between the pathways for their formation. Similarly, the small fractions of goethite are likely formed through the oxidation of carbonate-GR by ambient air during sample preparation for XRD analysis [3,84].

Maghemite is only formed in experiment [Fe]-B, which has the lowest Fe^{2+} concentration and no magnetite was found (Fig. 4.5a and b). A known pathway for the formation of maghemite is through the oxidation of magnetite [4,36]. However, magnetite formed in these experiments has been proven to be stable over a period of weeks (data not shown). The formation of maghemite in this experiment is therefore not well understood.

The amorphous fraction formed at an aqueous Fe^{2+} concentration of 0.2 mM is 64% (Fig. 4.5e) and it decreases to 23 – 36% at higher aqueous Fe^{2+} concentrations. This coincides with a higher percentage of precipitated iron.

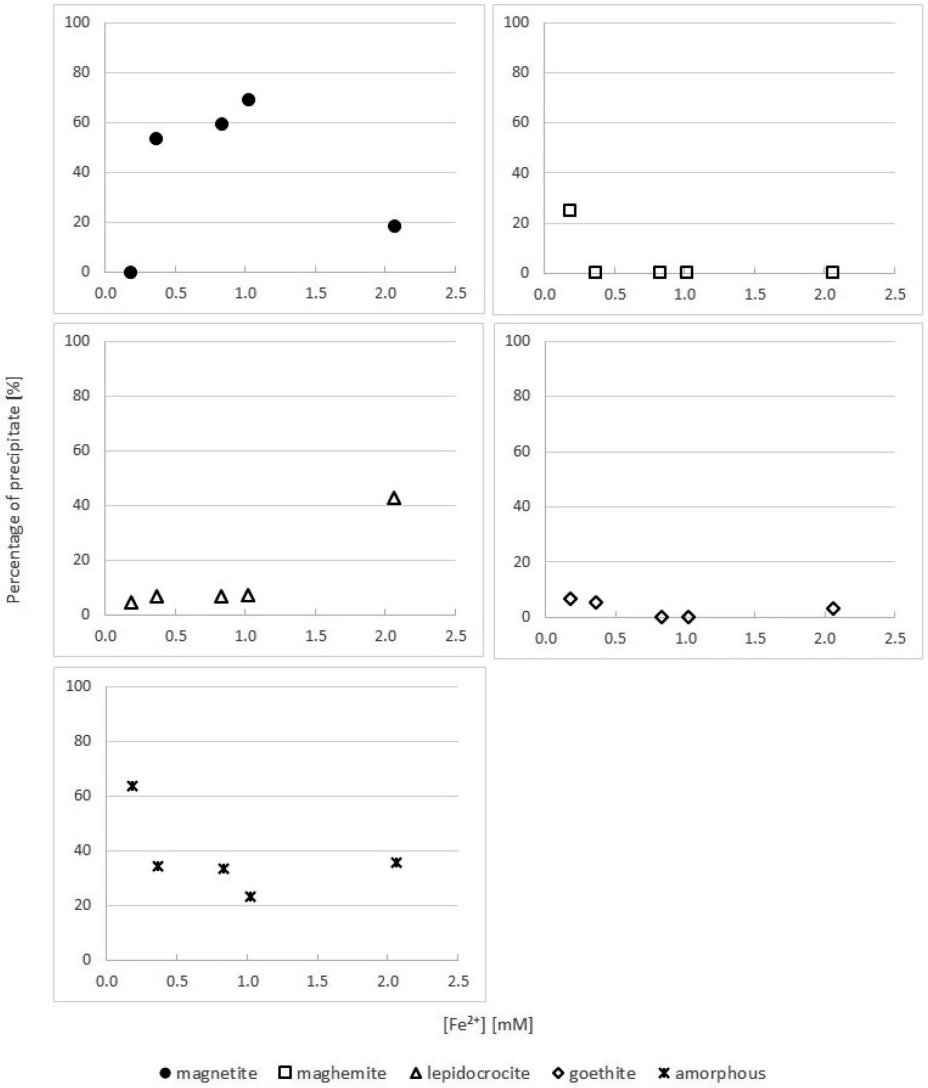

Figure 4.5 Percentages of formed precipitates collected from the reactor versus the concentration of aqueous Fe^{2+} in the reactor at t = 96 h.

4.4.4 Iron oxide formation in diluted tap water

In previous experiments described in Chapter 3, magnetite formation was demonstrated in 50% tap water and 50% Milli-Q water. To assess the effect of the tap water on the formation of iron precipitates, experiments were conducted in the new reactor setup in 50% (TW-A) and 90% (TW-B) tap water (and 50% and 10% Milli-Q water, respectively). HRT was 34 h. Figure 4.6 shows the precipitates formed in the reactor during experiments BE, TW-A and TW-B. Contrary to findings described in chapter 2, magnetite formation did not take place in the experiments with diluted tap water. The main precipitates were maghemite (TW-A, 36%) or goethite (TW-B, 35%).

Figure 4.6 shows that the presence of tap water enhances goethite formation (61% in experiment TW-B). This is likely the influence of the carbonates still present in the tap water, which could lead to the formation of carbonate-GR (instead of chloride-GR), that is known to oxidize to goethite when brought in contact with ambient air [3]. This indicates that goethite is formed after the end of the experiments, during sample preparation for XRD analysis.

The concentration of aqueous Fe^{2+} in the reactor at the end of experiments TW-A (1.0 mM) and TW-B (0.8 mM) are equal to the concentrations in experiments BE and HRT-A respectively (Fig. 4.5). The formed precipitates however, do not correspond. Apparently, the components in tap water have a larger influence than the aqueous Fe^{2+} concentration.

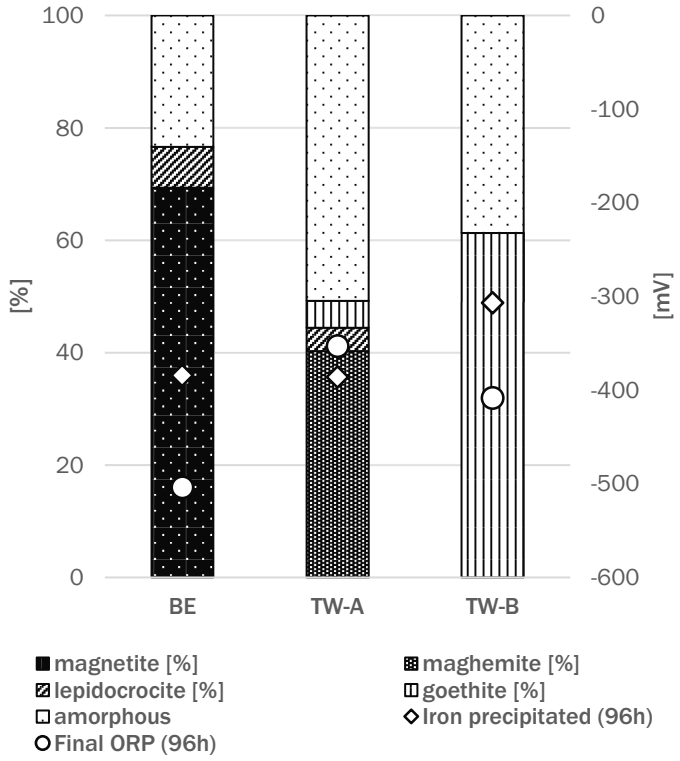

Figure 4.6 Composition of precipitates collected from the reactor at t = 96 h, fraction of precipitated iron and final ORP of experiments BE (100% Milli-Q water), TW-A (50% tap water, 50% Milli-Q water) and TW-B (90% tap water, 10% Milli-Q water).

4.4.5 The effect of addition of a mixed microbial culture

Since microorganisms are known to influence precipitation reactions, two experiments were conducted in growth medium; (1) without the addition of a mixed microbial culture (BB) and (2) with the addition of a mixed microbial culture after the pH increase at t = 24 h (BIO). Figure 4.7 shows the precipitates collected from the reactor at the end of the experiments. The experiment in growth medium yielded lepidocrocite (55%) and goethite (11%). Similar to experiments tap water, the presence of medium inhibited magnetite formation. The large fraction of lepidocrocite in BB indicates the formation of chloride-GR that oxidized to lepidocrocite during sample preparation for XRD analysis. The addition of microbial inoculum to the reactor led to the formation of the ferrous iron phosphate mineral vivianite ($Fe_3(PO_4)_2$, 28%). This could be due to elevation of the phosphate concentration or seeding with vivianite through inoculation, since both can be present in activated anaerobic sludge [85]. Additionally, minor fractions of lepidocrocite (4%) and goethite (9%) were formed.

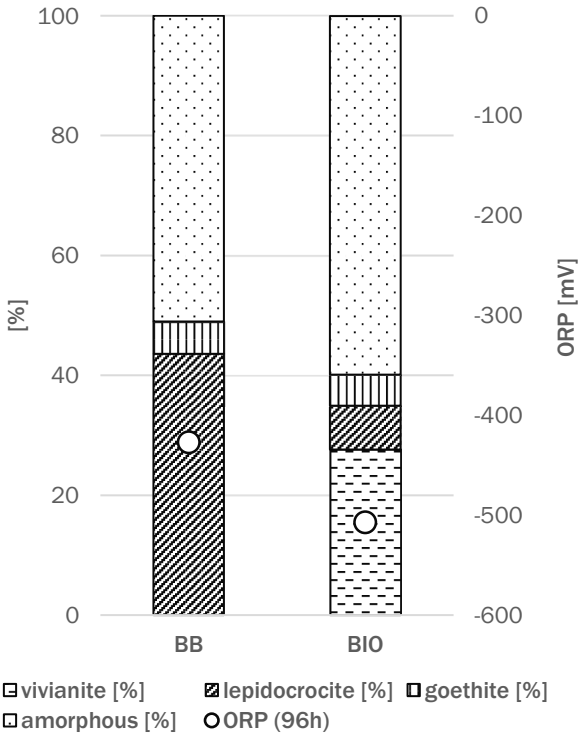

Figure 4.7 Composition of the precipitates collected from the reactor at t = 96 h, fraction of precipitated iron and final ORP of experiments BB and BIO.

4.4.6 Implications for application

Results show that continuous magnetite formation from a ferrous iron solution with a feed concentration of 1 mM or higher is possible. Since iron concentrations in groundwater below this range occur, it should be considered to concentrate the groundwater stream by for instance membrane filtration, to elevate the iron concentration. Moreover, a higher iron feed concentration leads to a higher fraction of magnetite in the formed precipitates. The process takes place in a continuous reactor at circumneutral pH and does not call for temperature or pressure elevations or addition of chemicals. The main control parameter is the concentration of aqueous Fe^{2+} in the reactor vessel. Obviously, this depends on the iron feed concentration. Additionally, it can be influenced by the volume of O_2 that is added, which controls the oxidation rate.

The HRT is an important factor for reactor design. While magnetite is formed at an HRT of 8 h with an iron feed concentration of 2.25 mM, the fraction of side products increases compared to the experiments with longer HRTs. In these experiments, the optimal HRT for magnetite is around 34

h. Additional experiments are necessary to further elucidate the influence of the HRT on the iron phase formation.

The experiments in diluted tap water and growth medium show that the presence of ions other than iron inhibit magnetite formation in our CSTR. Since this was exploratory research and literature shows that magnetite formation in a growth medium is possible in batch experiments [51], additional research is recommended to evaluate technological feasibility in a continuous system.

Acknowledgements

We thank Loc Minh Tran for his contribution to the practical work that laid the basis for this chapter.

Chapter 5

Identification of redox potential and pH conditions for magnetite formation from hydrous ferric oxide by a mixed microbial culture

Yvonne M. Mos, Rick Idema, Cees J.N. Buisman, Jan Weijma

Sub-Department of Environmental Technology, Wageningen University & Research, P.O. Box 17, 6700 AA Wageningen, the Netherlands.

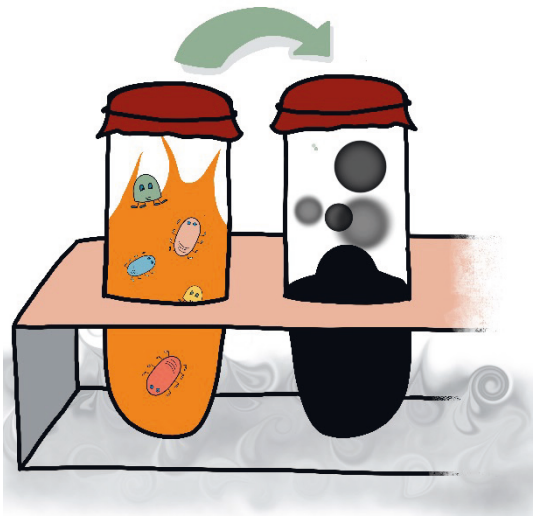

This chapter is submitted as:

Y.M. Mos, R. Idema, C.J.N. Buisman, J. Weijma, Identification of redox potential and pH conditions for magnetite formation from hydrous ferric oxide by a mixed microbial culture.

Abstract

Current practice in drinking water production from ferruginous groundwater yields Fe(III) rich sludge. Conversion of such sludge to magnetite increases the potential value of this residual stream. As a first step in the development of a biotechnological process for this conversion, we investigated the reduction of hydrous ferric oxide (HFO) by a mixed microbial culture, aiming to identify control parameters (pH, redox potential) for maximum selectivity for magnetite crystallization. Acetate, glucose, lactate or ethanol were electron donors for Fe(III) reduction at a starting concentration of 128 mg Fe L^{-1}. In the investigated pH range, iron oxide formation was controlled by the established pH and redox potential (ORP) rather than type of electron donor added. Magnetite was formed in a final pH and ORP region of 7.5 to 7.6 and -254 and -283 mV, respectively. A higher final pH and lower final ORP did not yield magnetite. The mixed microbial culture from a batch wherein magnetite was formed had a presence of iron reducers, while a mixed microbial culture from that did not yield magnetite predominantly contained methanogens. This paper demonstrates that microbial reduction of HFO from drinking water treatment sludge has potential to recover iron in the form of magnetite.

Keywords: biocrystallization; CSTR; groundwater; hydrous ferric oxide, iron removal; magnetite

5.1 Introduction

Most drinking water worldwide is produced from groundwater [1]. Ferrous iron is commonly present in anaerobic groundwater and needs to be removed to prevent the formation of precipitates and color in drinking water and to prevent clogging of pipes [2]. Iron removal from groundwater is usually accomplished by uncontrolled aeration to oxidize ferrous iron, followed by sand filtration [5]. This method yields large volumes of poorly dewaterable sludge with high concentrations of Fe(III) oxides [14]. The ferric iron sludge is used in low value applications, e.g. sulfur removal from gas streams [15]. Converting the Fe(III) oxides in iron sludge into magnetite would yield a valuable mineral with potentially high-end applications.

Magnetite ($Fe^{II}Fe^{III}_2O_4$) is a mixed-valent iron oxide with strong magnetic properties [3]. Due to these properties, magnetite can be used in magnetic data storage, contrast fluid for MRI, cell separation and site specific chemotherapy [29]. These applications require strict specifications for the morphology of the magnetite, because the strength of the magnetic properties depends on the size of the particles [20].

Several authors reported the induced crystallization of magnetite through reduction of Fe(III) oxides and hydroxides by dissimilatory iron reducing bacteria (DIRB) [29,39,41,42,51,54,55,57,60,61,86]. DIRB utilize many electron donors including pyruvate and H_2 [17]. Magnetite is formed through partial reduction of a ferric iron oxide by dissimilatory iron reducing bacteria (DIRB), followed by crystallization of magnetite:

$$Fe^{III}O_x \rightarrow Fe^{III}O_x + Fe^{2+} \quad \textit{(biological)} \tag{5.1}$$

$$Fe^{III}O_x + Fe^{2+} \rightarrow Fe_3O_4 \quad \textit{(chemical)} \tag{5.2}$$

The formation of magnetite by DIRB in batch cultures has been reported with a limited number of substrates; acetate, lactate, glucose and formate [39,54–56,58,59,61,64,87].

With the exception of Bell et al. [54], who used defined co-cultures, magnetite formation was found in pure Fe(III)-reducing cultures of *Geobacter metallireducens* (acetate), *Thermoanaerobacter ethanolicus* (acetate, glucose), *Shewanella putrefaciens* (lactate, formate), *S. oneidensis*, *S. pealeana* and *S. alga* (lactate) [17,39,54–56,58–61,64,87]. Initial concentrations of Fe(III) in the aforementioned literature range from 251 mg L^{-1} to 28 g L^{-1}.

Although both pH and redox potential (ORP) play an important role in magnetite formation, data on these parameters is rather fragmentary [29,57,61,64]. Bell et al. [54] pointed out the crucial role of pH in magnetite formation. Their batch cultures with glucose started at pH 7.4, which dropped to 5.5 during the experiment with no magnetite formation. Without glucose, the pH rose to 8.5 and magnetite formation took place. Fredrickson et al. [59] did not provide an initial pH value, but the final pH of the magnetite forming experiments were 7.1 and 7.3. Roh et al. (2003) [58] started their experiments within a pH range of 7.8 to 8.0 and found magnetite at a final pH

ranging from 7.5 to 8.5. Other researchers reported a pH drop of 7.2 to 7.1 [42] or a rise from pH 7.0 to 7.5 [41] in magnetite producing cultures. Zhang et al. [39] monitored the pH over time and found a sharp drop from initial pH 8.5 – 8.8 to 7.9, followed by a rise to 8.4, after which the pH slowly decreased again (not below 7.9). These fluctuations were attributed to the fast growth of the bacteria, producing organic acids and CO_2 through their metabolism. Behrends and Van Cappellen controlled the pH during their experiments and form magnetite at pH 7.5(±0.4) [60]. Phosphate or carbonate buffers were commonly used to stabilize the pH [39,54,58–61]. However, the presence of phosphate may lead to the formation of vivianite ($Fe^{II}_3(PO_4)_2{\cdot}2H_2O$) instead of magnetite, whereas the presence of carbonate may lead to siderite ($Fe^{II}CO_3$) formation [54,58,59,64]. Goethite (α-$Fe^{III}OOH$) [41,57,63], lepidocrocite (γ-$Fe^{III}OOH$) [42] and hematite (α-$Fe^{III}_2O_3$) [57] formation are also reported. Moreover, iron mineral formation depends strongly on the ORP. However, until now, literature on the relation between ORP and the formation of magnetite by DIRB has focused on thermodynamic models rather than experimental data. Literature that mentions measured ORP after magnetite formation from an Fe(III) phase, report a wide range of values between -200 and -450 mV [39,54,57,58,63].

While all aforementioned literature reported magnetite as the dominant phase, only Byrne et al. [57] and Zhang et al. [39] quantified their precipitates and reported 72 – 76% and >80% magnetite formation respectively, while Piepenbrock et al. [61] found 100% magnetite in their experiments.

In order to identify the proper range for pH and ORP for a biological process for the conversion of ferric sludge to magnetite, we investigated the relation between the iron phase formed after dissimilatory iron reduction, pH and redox, using HFO at a starting concentration of 128 mg Fe L^{-1}.

The effect of different electron donors, namely acetate, glucose, lactate and ethanol, on precipitate formation was evaluated. As our overall work pursues the development of a process to be applied in practice in open bioreactors, we used a mixed microbial culture enriched from primary sludge from a waste water treatment plant. The microbial cultures from two incubations of which only one yielded magnetite were analyzed with next generation sequencing.

5.2 Materials and methods

5.2.1 Mixed microbial culture and medium

The mixed microbial culture was enriched from primary sludge from the municipal waste water treatment plant in Bath, the Netherlands. Routine cultivation took place in a medium containing acetate as electron donor and Fe(III) as electron acceptor (batch series B0 to B10). A second series of enrichments, originating from an acetate-grown enrichment, was set up with ethanol as electron donor instead of acetate (batch series B11 to B13). The medium for microbial growth contained (mg L^{-1}): $FeCl_3.6H_2O$ (20), NH_4Cl (150), $NaH_2PO_4.H_2O$ (20), KCl (100), COD (1950) (as sodium acetate or ethanol), and 25 mL L^{-1} vitamin solution and 25 mL L^{-1} trace element solution [81]. Headspace composition was 100% N_2, at 0.5 bar overpressure. The pH of the acetate culture

medium was adjusted to 7.5 by the addition of 2500 mg L^{-1} $NaHCO_3$ and the pH of the ethanol culture medium to 7.0 by the addition of 2500 mg L^{-1} Na_2CO_3. All chemicals used were analytical grade. The cultures were incubated in a shaker (New Brunswick Scientific) at 30 °C and 120 rpm.

5.2.2 Batch experiments

The experiments aiming to identify pH and redox conditions for magnetite formation were conducted in closed bottles with 200 mL medium, 10 mL inoculum and 40 mL headspace. The medium contained (mg L^{-1}): $FeCl_3.6H_2O$ (811), NH_4Cl (150), Na_2CO_3 (481), NaH_2PO_4 (1), KCl (100), and 2 mL vitamin solution and 2 mL trace element solution. Additionally, 40, 27 or 13 mg L^{-1} COD (either as sodium acetate, sodium lactate, glucose or ethanol) was added to the batches. These concentrations were selected as an excess of electron donor (40 mg L^{-1}), meeting the stoichiometric ratio for the reduction of all Fe(III) (27 mg L^{-1}) and sufficient for the reduction of half of the Fe(III) (13 mg L^{-1}). The concentration of COD at the start of the batch experiments was up to 250% of the added COD, due to the acetate-COD present in the inoculum. The Fe(III) added as $FeCl_3$ formed an amorphous precipitate (confirmed by XRD analysis) immediately when the pH was adjusted (to either 7.5 or 7.0, see Table 5.1). The bottles were closed with rubber stoppers and aluminum caps. Headspace at the start of all batch experiments was 100% N_2 at 0.5 bar overpressure. The batches were inoculated with 10 mL mixed culture and incubated at 30 °C and shaken at 120 rpm. Batch experiments were conducted in duplicate or triplicate. Table 5.1 gives an overview of the conducted experiments. The varied parameters were electron donor, concentration of added electron donor, starting pH and type of inoculum.

5.2.3 Sampling and analysis

Before sampling, the bottles were put inside an anaerobic hood. The pH and (ORP) of samples were immediately measured in this anaerobic hood at the start as well as at the end of the batch experiments (QIS ORP electrode and MeterLAB PHM210 pH electrode). Substrate conversion was evaluated by analysis of dissolved COD and alcohols and volatile fatty acids (VFA). Samples were centrifuged (10 min at 10,000 rpm) prior to analysis. Alcohols and VFA were measured with gas chromatography (Agilent Technologies 7890B). For COD analysis (cuvette test Hach, Hach DR3900 spectrophotometer), an additional filtration step (0.2 µm cellulose-acetate filter, pre-washed to avoid COD contamination) was added after the centrifugation to exclude any interference by particles. Headspace composition was analyzed by gas chromatography (Shimadzu GC2010).

As an indicator test during the runtime of the experiment, a magnet was held up to the wall of the batch bottles to assess magnetic affinity of the precipitates. The precipitates were collected from the batch bottles, separated from the medium by settling and then air-dried (B4-II, B5-III, B6-III, B8 and B10) or dried under a N_2 atmosphere inside an anaerobic hood, in both cases at room temperature. The precipitate samples were manually grinded before being analyzed by X-Ray Diffraction (XRD) with a Bruker D8 Advance equipped with Cu radiation (1600 W). A Lynxeye XE-T detector was used with a position sensitive detection window set at 2.91°. The sample was spun at a speed of 5.0 rpm to ensure statistically optimal results. The scanning range was 10° to 90°

2θ and the step size was 0.02°. Phase identification and quantification was done with Diffrac.EVA (version 4.1.1, Bruker) and the PDF database (2004).

5.2.4 Biomass analysis

At the end of the incubation of batch series B8, 10 mL from B8-I and 10 mL from B8-II were added to 200 mL enrichment medium containing ethanol. The same was done for batches B10-I and B10-II. These cultures were incubated at 30 °C and shaken at 120 rpm. After 47 days, the biomass was harvested by centrifugation and submerged in liquid nitrogen and stored at -20 °C for next generation sequencing.

DNA was extracted from both cultures with the PowerSoil DNA isolation Kit (Mo Bio Laboratories Inc.) with some modifications (see Appendix). DNA concentrations were 9.3 $ng.\mu L^{-1}$ (B8) and 4.7 $ng.\mu L^{-1}$ (B10). Quantification was done with Q-bit (ThermoFisher Scientific). Amplification of the V3-V4 region of the 16S rDNA was done using the Illumina library generation method as described by Takahashi et al. [88] . Taxonomic analysis was performed using QIIME software (version 1.9.1) and OTU picking was performed using the SILVA 16S reference database (version 128) and Uclust.

5.2.5 Modeling

Modeling was done with OLI Studio 9.2 (OLI Systems, Inc.). The input parameters were the initial concentrations of the batch medium (disregarding trace elements and vitamins).

5.3 Results and discussion

5.3.1 Formed solid phase

Batch B0 with acetate as substrate but without the mixed microbial culture served as control experiment. The acetate concentration did not decrease within 63 days of incubation. There was no visible color change of the precipitates and no indication of magnetism. XRD analysis revealed the presence of hematite as sole mineral in the solids after 63 days, which implies that no iron reduction took place.

Batch code	*Substrate*	*Inoculum culture*	*Added COD [mg L^{-1}]*	*Initial pH [-]*	*Final pH [-]*	*Initial ORP [mV]*	*Final ORP [mV]*	*Precipitate composition*
B0	Lactate	none	40	7.5	7.5	-70	32	H (100%)
B4-I	Acetate	Acetate	40	7.5	7.7	-32	-195	L (100%)
B4-II	Acetate	Acetate	40	7.5	7.8	-47	-213	L (100%)
B5-I	Lactate	Acetate	40	7.4	7.7	-57	-266	M (100%)
B5-II	Lactate	Acetate	40	7.5	7.8	-76	-293	L (91%), Mh (9%)
B5-III	Lactate	Acetate	40	7.5	7.8	-67	-273	Mh (89%), L (11%)
B6-I	Glucose	Acetate	40	7.5	7.6	-60	-283	M (73%), L (27%)
B6-II	Glucose	Acetate	40	7.6	7.5	-69	-273	M (100%)
B6-III	Glucose	Acetate	40	7.5	7.8	-62	-307	L (100%)
B8-I	Ethanol	Acetate	40	7.4	7.5	-77	-254	M (100%)
B8-II	Ethanol	Acetate	40	7.5	7.5	-83	-267	M (100%)
B9-I	Ethanol	Acetate	40	6.9	7.6	-11	-280	L (100%)
B9-II	Ethanol	Acetate	40	7.0	7.7	-13	-284	L (100%)
B10-I	Ethanol	Acetate	40	6.9	7.7	-15	-283	L (100%)
B10-II	Ethanol	Acetate	40	7.0	7.7	-20	-288	L (100%)

Table 5.1a Overview of conducted batch experiments, initial and final conditions and formed precipitates. H = hematite, L = lepidocrocite, M = magnetite, Mh = maghemite, G = goethite.

Batch code	*Substrate*	*Inoculum culture*	*Added COD [mg L^{-1}]*	*Initial pH [-]*	*Final pH [-]*	*Initial ORP [mV]*	*Final ORP [mV]*	*Precipitate composition*
B11-I	Ethanol	Ethanol	27	7.0	7.6	-40	-269	M (92%), L (8%)
B11-II	Ethanol	Ethanol	27	7.1	7.6	-47	-265	L (100%)
B12-I	Ethanol	Ethanol	13	7.1	7.6	-39	-275	M (100%)
B12-II	Ethanol	Ethanol	13	7.0	7.5	-35	-273	M (96%), G (4%)
B13-I	Ethanol	Batch B8	40	6.9	7.5	-45	-277	M (100%)
B13-II	Ethanol	Batch B10	40	7.1	7.5	-39	-279	M (100%)

Table 5.1b Overview of conducted batch experiments, initial and final conditions and formed precipitates. H = hematite, L = lepidocrocite, M = magnetite, Mh = maghemite, G = goethite.

While the COD concentration decreased in all acetate batches (B1 to B4), none of these showed any visible color change of the precipitate within 13 days and none of the precipitates displayed magnetic affinity as defined in paragraph 5.2.3. XRD analysis of the precipitates present showed that lepidocrocite was formed in all these batches. The XRD results in combination with no visual color change indicate that ferric iron was not reduced.

In the batch series with lactate (B5) and glucose (B6), a color change of the precipitates from orange to dark green/black was visible within 5 days. After 21 days, magnetite was found in B5-I. However, both B5-II and B5-III contained a mixture of lepidocrocite and maghemite (γ-$Fe^{III}_2O_3$) (see Table 5.1). The batches with glucose yielded either magnetite (B6-I), lepidocrocite (B6-III) or a mixture of both (B6-II).

Batch series B8 to B13 were conducted with ethanol as electron donor. Batch series B9 and B10 yielded lepidocrocite while in all other batches magnetite was formed, occasionally with by-product lepidocrocite (B11) or goethite (B12) (Table 5.1). The fastest change in precipitate color from orange to dark brown was observed on day 4, gradually proceeding to black precipitates with magnetic properties on day 8. Batch series B9 and B10 were inoculated with a culture grown on acetate, whereas batch series B11 to B13 were inoculated with a culture grown on ethanol. It is therefore likely that the culture was less active in batch series B9 and B10. However, since the precipitates changed color during incubation, ferric iron reduction has taken place.

In some of the duplicates and triplicates the final solid phase differed in composition (i.e. in series B5, B6 and B11). In such cases the final pH and/or ORP are different, probably as a result of a difference in lag phase and subsequent biological activity. This supports the finding that pH and ORP are affecting the formed precipitate.

5.3.2 Electron donor pathway

The initial concentration of added electron donor in all batches except for B11 and B12 was 40 mg COD L^{-1}. Stoichiometrically, this was sufficient electron donor to reduce all Fe(III) present. Taking into consideration that only $^1/_3$ of the Fe(III) has to be reduced to form magnetite, there was an excess of electron donor present.

The headspace composition of the batches with acetate, glucose and lactate was analyzed after 11 days of incubation. The batches with added acetate showed a higher methane content (5.6% ± 0.3%) than batches with added glucose (3.2% ± 0.4%) and lactate (3.3% ± 0.4%). These percentages correspond with 4.3 mg COD for the acetate batches and 2.5 mg COD for the glucose and lactate batches. This means that a maximum of 27% of the added substrate was used for methanogenesis. The headspace composition of batches B13 was measured on days 6, 12 and 20 of the incubation. No methane was found.

The concentrations of volatile fatty acids were monitored over time in batch series B13 (Fig. 5.1). The production of acetate indicates that ethanol was oxidized via;

$$C_2H_5OH + H_2O \rightarrow CH_3COOH + 2\,H_2 \qquad (5.3)$$

In this scenario, both ethanol and H_2 may serve as an electron donor for Fe(III) reduction via;

$$12\ Fe^{3+} + C_2H_5OH + 3H_2O \rightarrow 12\ Fe^{2+} + 2\ CO_2 + 12\ H^+ \quad (5.4)$$

$$2\ Fe^{3+} + H_2 \rightarrow 2\ Fe^{2+} + 2\ H^+ \quad (5.5)$$

Headspace composition measurements with a detection limit of 0.5% did not confirm the presence of H_2. However, 0.5% of H_2 in the headspace equals 0.3 mmol L^{-1}, which is thermodynamically sufficient for reaction 5.5 to occur (calculations in Appendix). Therefore, neither iron reduction by ethanol directly nor via H_2 can be excluded. This also applies for the batches with glucose and lactate; iron reduction can have occurred via H_2.

Since there were no indications for iron reduction in the batches containing solely acetate as electron donor and acetate is not reduced in batch B13-II, we do not consider it an important electron donor for iron reduction by the mixed microbial culture. There is less acetate produced from ethanol then expected from stoichiometry (Fig. 5.1 and eq. 5.3). Bacterial growth and CO_2 formation (not measured) can account for this gap.

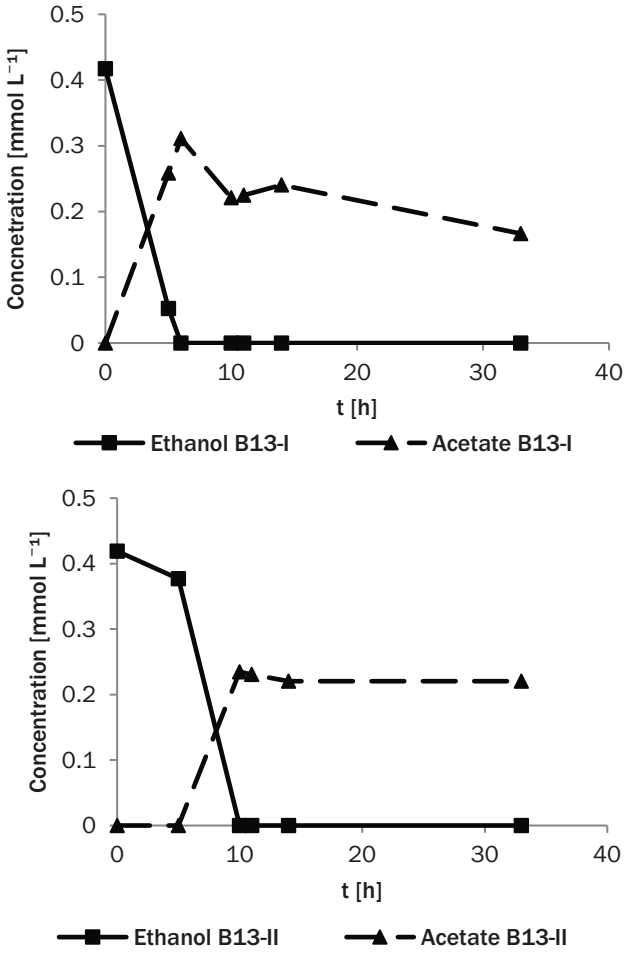

Figure 5.1 Concentrations of ethanol and acetate over time in batch series B13-I and B13-II

5.3.3 Solid phase formation as a function of pH and ORP

The starting precipitate was a hydrous ferric oxide (HFO) as was expected from the medium composition and was confirmed by XRD analysis [59,63,89]. Table 5.1 shows the pH and ORP at t=0 and the end of the experiments.

The precipitates in abiotic batch B0 remained orange throughout the incubation period while the pH remained stable at 7.5. XRD analysis showed the presence of hematite after 63 days. The formation thereof takes place through crystallization of HFO [3]. The ORP in B0 increased from -

70 mV to +32 mV. This indicates that the reducing conditions in the other batches are induced by the present microorganisms, which is consistent with literature [90].

A Pourbaix diagram created with OLI studio 9.2 (Fig. 5.2) shows that hematite and siderite are expected to be the most stable iron precipitate in the final pH and ORP range of our experiments. While the abiotic control experiment B0 conforms to this model, the biological experiments do not. This illustrates the influence of the microorganisms on the formation process of the precipitates. The formation of siderite is likely hindered by the decrease of available carbonate due to microbial metabolism.

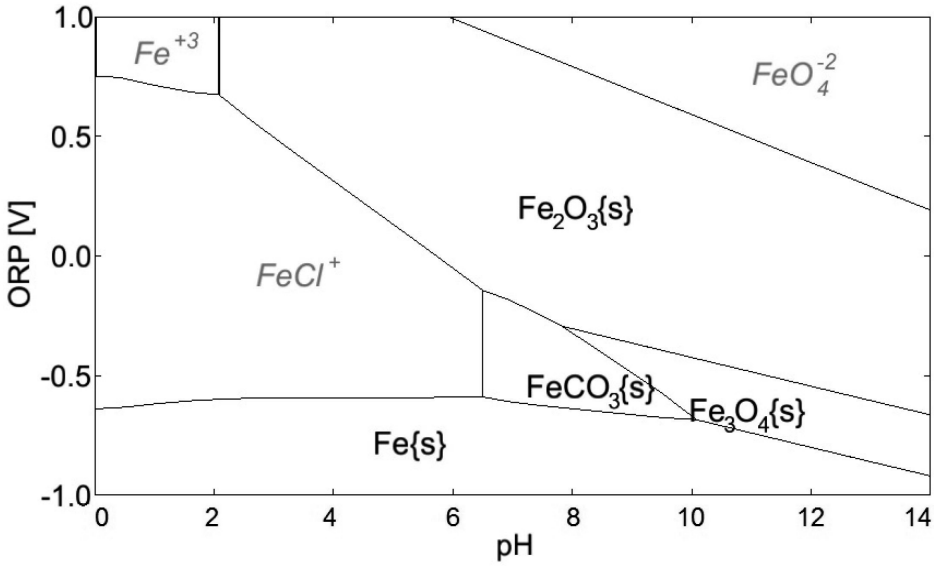

Figure 5.2 Pourbaix diagram created with OLI Studio 9.2.

Lepidocrocite was formed in batch series B4 (acetate). The pH is these batches increased to 7.7 - 7.8, while the ORP decreased to -195 or -215 mV for B4-I and B4-II respectively. No color changes were observed in these batches, which, in combination with the final precipitate being lepidocrocite (γ-$Fe^{III}OOH$), indicates that no iron reduction took place.

Batch series B5 to B8 had a starting pH of 7.5±0.1, which was stable or slightly elevated to a maximum of pH 7.8. Batch series B9 to B13 were started at pH 7.0±0.1 and had final pH values ranging from 7.5 to 7.7. Final ORP values ranged from -254 mV to -307 mV. Values per batch are given in Table 5.1. These batch series yield various precipitates; magnetite, lepidocrocite and maghemite (Table 5.1). Whether magnetite formation takes place or not is determined by the final pH and ORP in the batch. This becomes apparent when the values for final pH and ORP are grouped by the dominant precipitates formed (Fig. 5.3, see Table 5.1 for percentages). Note that

hematite from the control experiment is not included in Fig. 5.3 as it would lead to a visual clustering due to the high redox potential of that experiment.

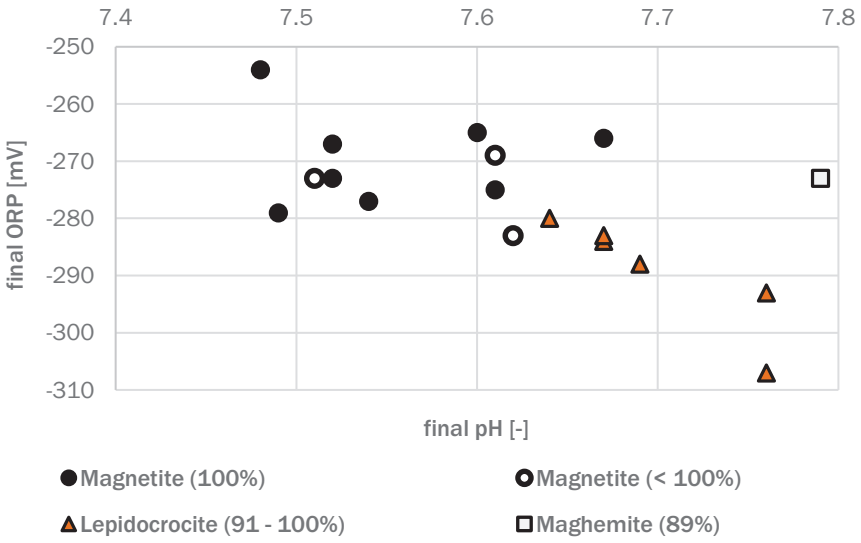

Figure 5.3 The dominant precipitates formed due to biological reduction of HFO in batch series B5 to B12 as a function of final pH and ORP values.

The detection of lepidocrocite can be explained from oxidation of green rust (GR) after opening the batch bottles. This is primarily based on the observation that the solids in all batches that yielded lepidocrocite became dark green during incubation and turned orange-brown after exposure to air (Fig. 5.4). These are indications for the formation of GR, and therefore iron reduction, in the batches from which the precipitates (mainly) consisted of lepidocrocite. The oxidation of GR to lepidocrocite by ambient air is very rapid and could not be prevented [3,91].

The precipitate in the batches that yielded magnetite (100% or less) turned black during incubation with no apparent color change after opening. Magnetite can be formed from HFO and aqueous Fe^{2+} without the need for a precursor phase [83]. However, GR formation is favored over magnetite formation at higher Fe^{2+} concentrations [59];

$$2\ Fe(OH)_3 + Fe^{2+} \rightarrow Fe_3O_4 + 2\ H_2O + 2\ H^+ \qquad (5.6)$$

$$2\ Fe(OH)_3 + 4\ Fe^{2+} + A^{2-}(CO_3^{2-}, SO_4^{2-}) + 9\ H_2O \rightarrow [Fe_4^{II} Fe_2^{III}(OH)_{12}][A^{2-} * 3\ H_2O] + 6\ H^+ \qquad (5.7)$$

Where $Fe(OH)_3$ represents HFO and $A^{2-}(CO_3^{2-}, SO_4^{2-})$ represents the anion that is incorporated into the GR, represented as $[Fe_4^{II}Fe_2^{III}(OH)_{12}][A^{2-} * 3\ H_2O]$.

Figure 5.4 End stage of batch series B9. Most likely GR was formed, that oxidized into lepidocrocite during sample preparation for XRD analysis.

Maghemite was formed in batches B5-II and B5-III, both containing lactate as electron donor. B5-III contained mainly maghemite, whereas it was a minor phase next to lepidocrocite in B5-II. Maghemite can form through oxidation of magnetite or dehydration of lepidocrocite [3]. However, the latter does not occur when iron is added as a chloride phase [36,92] and the batches have a reducing environment. Formation must have occurred during incubation, since formed magnetite that was dried in ambient air (B8) proved to be stable. Moreover, the magnetite samples were analyzed by XRD again after 2.5 months, yielding the same results. Maghemite formation is promoted by a relatively high pH (7.8) and average ORP (-273, -293) compared to the other experiments.

5.3.4 Composition of the mixed microbial culture

Two batch series yielding different precipitates were selected for biomass analysis; B8, in which magnetite was produced, and B10, that yielded lepidocrocite. These cultures were later used to inoculate batches B13-I (from B8) and B13-II (from B10). Magnetite was produced in both these batches.

Figure 5.5 shows the composition of the microbial community (> 1% abundance). The most dominant family in both samples is *Pseudomonadaceae* (23 to 42%), which is known to harbor iron reducing species [93,94]. *Geobacteraceae* represents 5 – 7% of the microbial community and

also includes members that induce magnetite formation [55,56]. The bacterial families of *Thermoanaerobacteraceae* and *Shewanellaceae* have been used for induced biomagnetite formation but were not found in our cultures [17,39,54,59–61,64,87].

The families *Rhodocyclaceae, Peptococcaceae, Desulfobulbaceae* are known to have iron reducing members, but have not been reported to play a role in magnetite formation [95–98]. *Synergistaceae* have been found in anaerobic digestion experiments where magnetite was seeded, but is not reported to be formed [99]. Both *Synergistaceae* and *Porphyromonadaceae* have been found in an iron reducing environment, but are only carefully linked to iron reduction [99,100].

Both samples also show a presence of methanogens, namely *Methanosaetaceae* and *Methanosarcinaceae*. [101–103]. *Anaerolineaceae* is known to live symbiotically with methanogens, supplying them with acetate [101]. *Syntrophomonadaceae* is known to play the same role, but has also member that can act as methanogen directly [103].

The microbial mixed culture from batch series B8 shows a higher abundance for known iron reducing bacteria, while the culture from batch series B10 shows a higher abundance of families related to methanogenesis. This reflects the final batch conditions, since batch series B8 had an average final ORP of -261 mV while batch series B10 had an average final ORP of -286 mV, favoring methanogenesis [104]. Both cultures were able to form magnetite when used for the inoculation of batch B13-I (from batch series B8) and batch B13-II (from batch series B10).

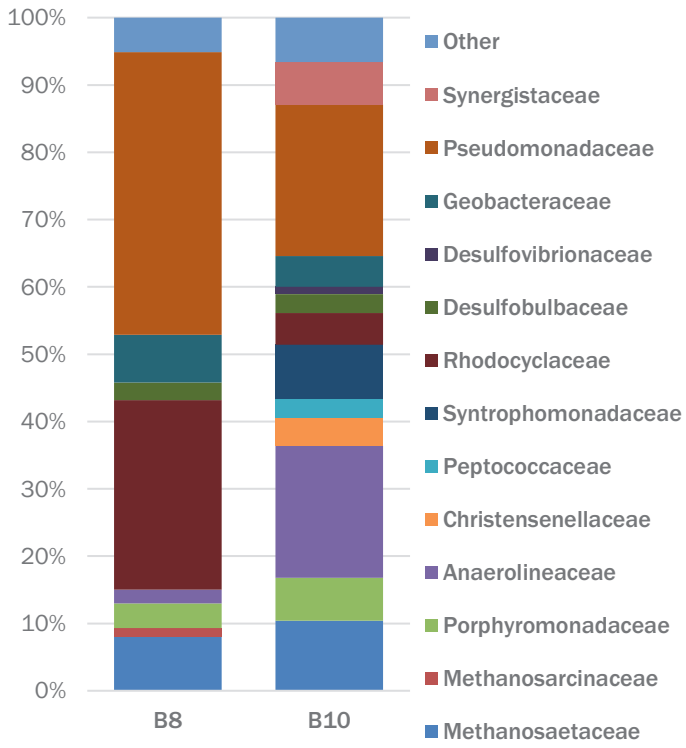

Figure 5.5 Composition of microbial communities (>1% abundance) in samples cultured from batch series B8 (magnetite formation) and B10 (lepidocrocite formation).

5.3.5 Implications for application

The application of biological magnetite formation from drinking water production sludge, as described in this paper, will recover the iron in the form of a valuable product with a range of possible applications. The discovery of a specific pH/ORP region for magnetite formation is essential input for efficient process design. The experiments described in this paper were conducted in a biological growth medium. Ions present in this medium did not inhibit the process of magnetite formation. However, actual sludge from drinking water production could contain many other (metal) ions that could prevent magnetite formation to take place or be incorporated into the formed magnetite [3,13]. This would negatively influence the application potential of magnetite in other processes. This should be investigated in future research. If the process proves not to be influenced by a more complex medium, this process could be applied to other iron containing streams, e.g. mining waste streams.

5.4 Appendix to Chapter 5

S5.1 Modifications Power soil kit DNA

S5.2 Thermodynamic calculations H_2 pathway

S5.1 Modifications Power soil kit DNA

Some modifications have been done and they are described by steps.

3- After this step put samples in heat block at 55 ° C for 15 min.
6 – Tubes were centrifuged per 1 min instead of 30 s.
14 – Solution C4 was added twice (600 µL first time and 500 µL second time) and vortexed twice as well.
15 – Spin filter was loaded with 650 µL instead of 675 µL to leave space on the tube for centrifugation.
20 – 30 µL of solution C6 were added instead of 100 µL. This was done to avoid dilution of the DNA, since concentrations were unknown.
23- Put in heat block for 15 min 55 ° C just before spinning C6 down.

S5.2 Thermodynamic calculations H_2 pathway

0.5% of H_2 in 40 mL headspace at 1.5 bar equals $1.2.10^{-2}$ mmol, calculated through;

$$PV = nRT \quad \text{(S5.1)}$$

With:

T = 303 K
P = 151325 Pa

Iron reduction takes place through:

$$2\ Fe^{3+} + H_2 \rightarrow 2\ Fe^{2+} + 2\ H^+ \quad \text{(S5.2)}$$

ΔG_f Fe^{3+}: -4.6024
ΔG_f Fe^{2+}: -78.8684
At pH 7.0

This leads to a ΔG^0r of -148.53

RTlnQ = 34.8 kJ
ΔG_r = -148.53 + 34.8 = -113.73
lnQ = 13.82

Leading to a minimum pH_2 necessary for the reaction to occur of 0.10 Pa.

This is equal to $1.59.10^{-6}$ mmol and is less than the $1.2.10^{-2}$ mmol that is maximally present in the headspace. The reaction can therefore take place

Chapter 6

Biological reduction of hydrous ferric oxide in a continuous stirred tank reactor

Yvonne M. Mos, Cees J.N. Buisman, Jan Weijma

Sub-Department of Environmental Technology, Wageningen University & Research, P.O. Box 17, 6700 AA Wageningen, the Netherlands

Abstract

Drinking water production from ferruginous groundwater yields iron rich sludge. This can be used as a source for production of valuable materials like magnetite. Magnetite is a mixed valence iron oxide with strong magnetic properties and therefore has high end potential. Previous research has shown that magnetite can be formed through biological partial reduction of hydrous ferric oxide in batch experiments. Here we attempt to reproduce partial iron reduction to magnetite in a continuous 2 L reactor. Experiments however, yielded green rust. The formation of magnetite was achieved by switching the reactor to batch mode and spiking it with aqueous $FeCl_3$.

Keywords: CSTR; green rust; hydrous ferric oxide; iron reduction; magnetite; mixed microbial culture

6.1 Introduction

The production of drinking water yields large volumes of sludge that is rich in ferric iron oxides [14]. This iron could potentially be used for the production of magnetite ($Fe^{II}Fe^{III}_2O_4$); a mixed-valence iron oxide that has strong magnetic properties [3]. Therefore, it has applications ranging from magnetic data storage to high-end in vivo applications like site-specific chemotherapy [29].

In chapter 5 we report the formation of magnetite from hydrous ferric oxide (HFO) through partial reduction by a mixed microbial culture;

$$Fe^{III}O_x \rightarrow Fe^{III}O_x + Fe^{2+} \quad \textit{(biological)} \tag{6.1}$$

$$Fe^{III}O_x + Fe^{2+} \rightarrow Fe_3O_4 \quad \textit{(chemical)} \tag{6.2}$$

Experiments were conducted in 200 mL batch reactors that yielded either green rust (GR) or magnetite, depending on the final pH and redox potential (ORP) in the batch. Observations over time led to the conclusion that GR served as a precursor for magnetite crystallization.

Here, we detail our attempt to scale up this process to a 2 L continuous CSTR. The bioreduction of HFO herein led to the formation of GR, whereas magnetite was not formed. Spiking the reactor containing the previously formed GR with 0.5 M aqueous $FeCl_3$ while in batch mode led to the formation of magnetite.

6.2 Materials & methods

6.2.1 Mixed microbial culture

The mixed microbial culture was enriched from primary sludge from the municipal waste water treatment plan in Bath, the Netherlands. Routine cultivation took place in a medium containing ethanol as electron donor and Fe(III) as electron acceptor. The medium and cultivation methods are described in chapter 5.

6.2.2 Continuous CSTR

A CSTR with a working volume of 2 L was continuously fed with growth medium, $FeCl_3$ solution and an ethanol solution. The medium was refrigerated and supplied with a flow of 138 mL h^{-1} and concentrations of (mg L^{-1}): NH_4Cl (150), Na_2CO_3 (481), NaH_2PO_4 (1), KCl (100), and 10 mL L^{-1} vitamin solution and 10 mL L^{-1} trace element solution [81]. A $FeCl_3$ solution (1.16 g Fe L^{-1}, 24 mL h^{-1}) was supplied with a loading rate of 28 mg Fe h^{-1}. The flow rate of the 20 vol% ethanol (98%) solution was varied in three stages of the experiment, leading to loading rates of; 1) 74 mg h^{-1}, 2) 46 mg h^{-1}, and 3) 4.1 mg h^{-1}. The HRT was 12.3 h in all three stages.

Mixing was accomplished with a stainless steel rotor with a diameter of 4 cm at 160 rpm and a 4-cm magnetic bead placed centrally on the reactor bottom. The reactor was connected to a pH electrode (QIS) and controller, which dispensed HCl (0.5 M) or KOH (0.5 M) when the absolute deviation from the pH set point value of 7.5 became more than 0.1. The $FeCl_3$ solution, HCl and KOH were constantly sparged with N_2. Sparging in the liquid phase was avoided in case of the medium and CSTR to minimize stripping of carbon dioxide. Instead, the headspace of the medium vessel and the CSTR were constantly flushed with N_2. Overpressures were released through water locks. Liquid samples were taken through a fixated tube situated between the rotor and CSTR wall and reaching halfway the depth of the liquid phase.

6.2.3 $FeCl_3$ spike

The reactor was set to batch mode by stopping all flows (pH control remained functional) and spiked with 32 mL of 81 g L^{-1} $FeCl_3$. The ferric iron solution had a pH of 0.9 which was not adjusted. ORP was logged with an electrode (QIS) and Fieldpoint (National Instruments).

6.2.4 Analysis

Alcohols and volatile fatty acids were analyzed by gas chromatography (Agilent Technologies 7890B). Samples were filtered (Chromafil Xtra, 0.2 µm) prior to analysis.

Precipitates from the CSTR were collected from the effluent vessel every 2 to 2.5 days. Precipitates of the experiment spiking with $FeCl_3$ were collected directly from the CSTR through the sampling tube. All precipitates were dried to ambient air at room temperature.

The precipitate samples were grinded manually before being analyzed by XRD with a Bruker D8 Advance equipped with Cu radiation (1600 W). A Lynxeye XE-T detector was used with a position sensitive detection window set at 2.91°. Samples were spun at a speed of 5 rpm to ensure statistically optimal results. The scanning range was 10° to 80° 2θ and the step size was 0.02°. Phase identification and quantification were done with Diffrac.EVA (version 4.1.1, Bruker) and the PDF database (2004).

6.3 Results & discussion

6.3.1 Green rust formation in continuous mode

The reactor was run in continuous mode with three different ethanol loads and therefore molar iron to ethanol ratios;

Day 0 - 28: 1 : 3.2 (74 mg ethanol h^{-1});
Day 29 - 48: 1 : 2.0 (46 mg ethanol h^{-1}), and;
Day 43 - 53: 1 : 0.2 (4.1 mg ethanol h^{-1}).

A steady state regarding ethanol and acetate concentrations was reached in all stages. The provided $FeCl_3$ was reduced while ethanol was converted to acetate that was not further oxidized as shown in Figure 6.1 for stage 1. A similar trend was visible in stages 2 and 3 (data not shown).

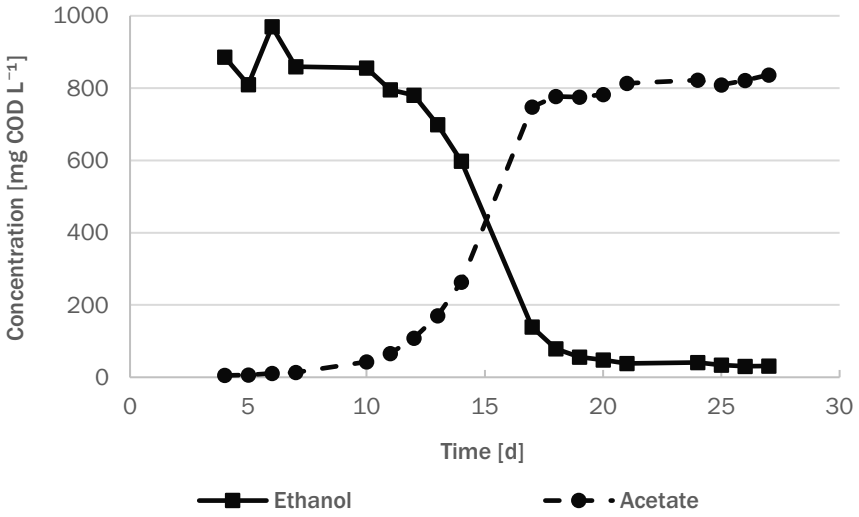

Figure 6.1 Concentrations of ethanol and acetate in the reactor (expressed in mg COD L^{-1}) during stage 1

The reaction equation shows that an excess of ethanol was provided in all three stages;

$$4\,Fe^{3+} + C_2H_5OH + H_2O \rightarrow 4\,Fe^{2+} + CH_3COOH + 4\,H^+ \qquad (6.3)$$

Figure 6.2 shows the diffractograms of precipitates sampled on day 1, day 15 and the final day of each stage, as well as the diffraction patterns of lepidocrocite (f) and goethite (g). The diffractogram of the solids on day 1 (Fig. 6.2a) shows that an amorphous precipitate (hydrous ferric oxide, HFO) is formed in the reactor environment at pH 7.5. Some small peaks that match the lepidocrocite pattern were identified. At this time, the reactor fluid had a red color. Within 11 days, the color of the reactor fluid changed to dark green, and more crystalline solids were formed as is evident from the peaks in the diffractogram (Fig 6.2b). Since samples had a dark green color that turned orange when being dried to ambient air, we assume that GR was formed in the reactor and oxidized when brought into contact with ambient air [3,105]. The product of this oxidation depends on the type of GR; chloride-GR ($[Fe_3^{II}Fe^{III}(OH)_8][Cl^- * nH_2O]$) [84] oxidizes to lepidocrocite, whereas carbonate-GR ($[Fe_4^{II}Fe_2^{III}(OH)_{12}][CO_3^{2-} * nH_2O]$) [84] oxidizes to goethite [3]. The type of GR that is formed depends on the presence of chloride and carbonate, but since the ratio between Fe^{II} and Fe^{III} varies between the different types, the relative presence of these iron ions in solution also influences the formation [106].

Figure 6.2c and d show that the decrease in ethanol load from 74 mg h^{-1} to 46 mg h^{-1} in stage 1 and 2, respectively, did not lead to any detectable change in iron oxide formation. In these stages, both lepidocrocite and goethite were detected in the same percentages; 90% lepidocrocite, 10% goethite. The further decrease of the ethanol load in stage 3 (4.1 mg h^{-1}) led to an increase in amorphous precipitates (Fig. 6.2e). The formation of chloride-GR continued during this stage. Carbonate-GR formation however, did no longer take place. The higher fraction of amorphous solids can be explained by the lower ethanol load leading to incomplete transformation of HFO. This indicates that a lower fraction of the initial iron phase is reduced. Moreover, a lower concentration of Fe^{2+} relative to the presence of a ferric iron phase is known to favor the formation of chloride-GR over carbonate-GR [107], explaining the absence of goethite formation in stage 3.

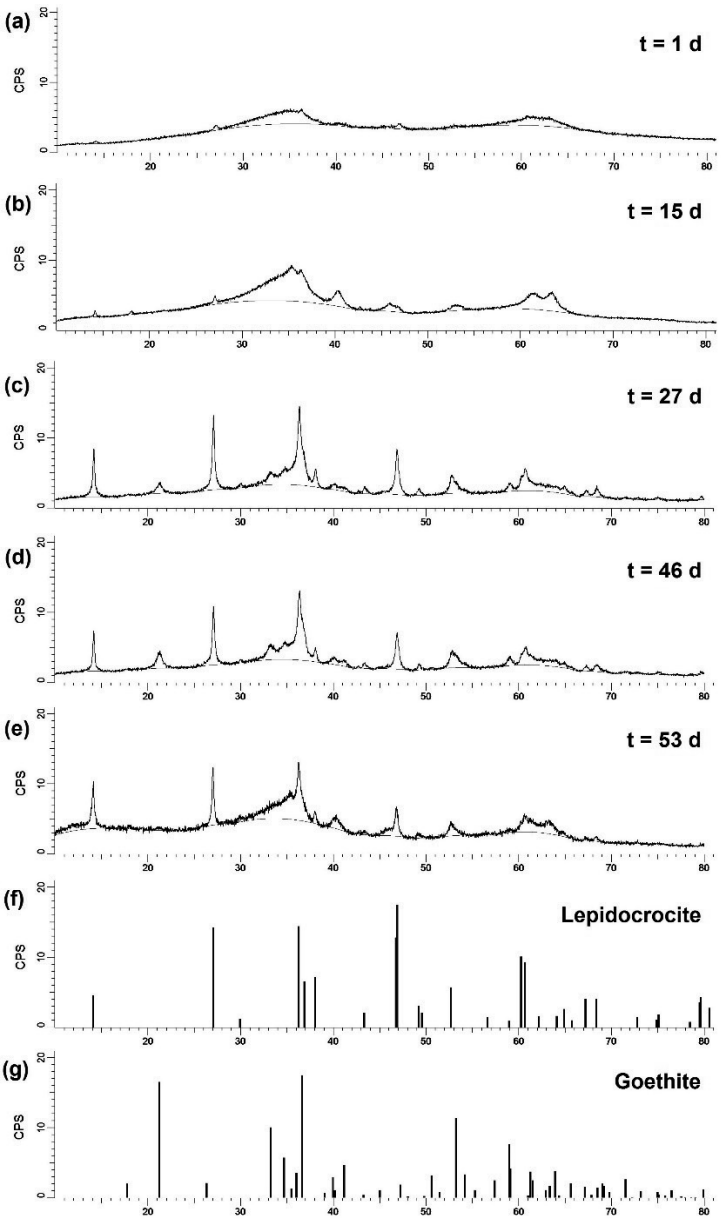

Figure 6.2 Precipitates collected from the continuous reactor experiments at the start of the experiment (a), directly after observed change in color of reactor medium from orange to dark green (b), and at the end of stage 1 (c), stage 2 (d) and stage 3 (e), as well as the diffraction patterns for lepidocrocite (f) and goethite (g).

After stage 3, the reactor operation was continued. The ethanol load was decreased further to a minimum of 1.1 mg h^{-1} on a trial-and-error basis, attempting to find the conditions for magnetite formation. However, the reactor fluid remained either dark green, indicating formation of green rust, or turned completely orange, indicating insufficient reduction. Omitting HCO_3^- from the medium aiming to reduce the stability of carbonate-GR [108] also did not lead to the formation of magnetite (data not shown).

6.3.2 $FeCl_3$ spike

On day 103, the reactor was switched to batch mode. Dark green precipitates, presumably GR, were suspended in the reactor medium. The reactor was then spiked with 32 mL of 0.5 M $FeCl_3$ solution. Figure 6.3 shows the trends of the pH and ORP from 10 min before the spike until 15 min thereafter. Since the addition of the $FeCl_3$ was rapid (< 1 min) and the solution had a pH of 0.9, the pH control could not keep up with the sudden change and the pH of the reactor dropped to 3.4. The pH controller then overdosed the reactor with base, leading to pH 9.4. Consequently, the ORP temporarily increased to +440 mV, before decreasing quickly to -430 mV and slowly decreasing further to -475 mV.

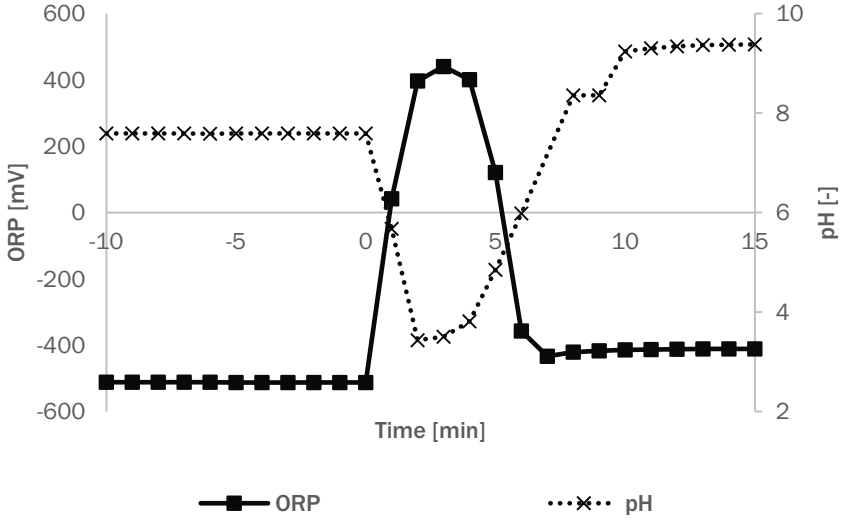

Figure 6.3 ORP and pH over time from 10 min before the spike with aqueous $FeCl_3$ to 15 min thereafter.

The added $FeCl_3$ reacted with the GR present in the reactor to form magnetite within seconds. Figure 6.4 presents the diffractogram of the formed precipitates and the matching iron oxide patterns. The sample was taken directly from the reactor. Consequently, the precipitate sample was small, leading to a relatively high background in the diffractogram (Fig. 6.4a). Next to magnetite, the sample also contained lepidocrocite, likely from oxidized chloride-GR. Other minor

peaks fit the diffractogram of akaganéite (β-FeOOH, Fig. 6.4d). Akaganéite is a known precursor in the formation of magnetite through coprecipitation of ferrous and ferric iron chloride salts [28].

6.4 Implications for application

The biological reduction of HFO in our continuous CSTR led to the formation of GR. Attempts to form magnetite in a continuous reactor system failed. Magnetite formation was achieved by the addition of aqueous $FeCl_3$ to the CSTR in batch mode containing previously biologically formed GR. Magnetite formation might therefore be achieved in a two-reactor system, in which the first reactor produces biological GR and that is transformed into magnetite through co-precipitation with aqueous $FeCl_3$ in a second reactor. The iron rich sludge formed in the production of drinking water could serve as a starting material for the formation of GR. The addition of solid phase ferric iron to the formed GR will likely not lead to magnetite formation like the spike with aqueous $FeCl_3$ did, since the Fe(III) ions in the sludge are present in the form of stable hydroxide complexes. Dissolving the sludge with acid is therefore necessary. Another possibility for the transformation of GR to magnetite is through partial oxidation with oxygen or nitrate as described in chapters 3 and 4 of this thesis. Hansen et al. [109] proposed to use this pathway for transformation of GR to magnetite as a tool for soil and sediment remediation with respect to nitrate.

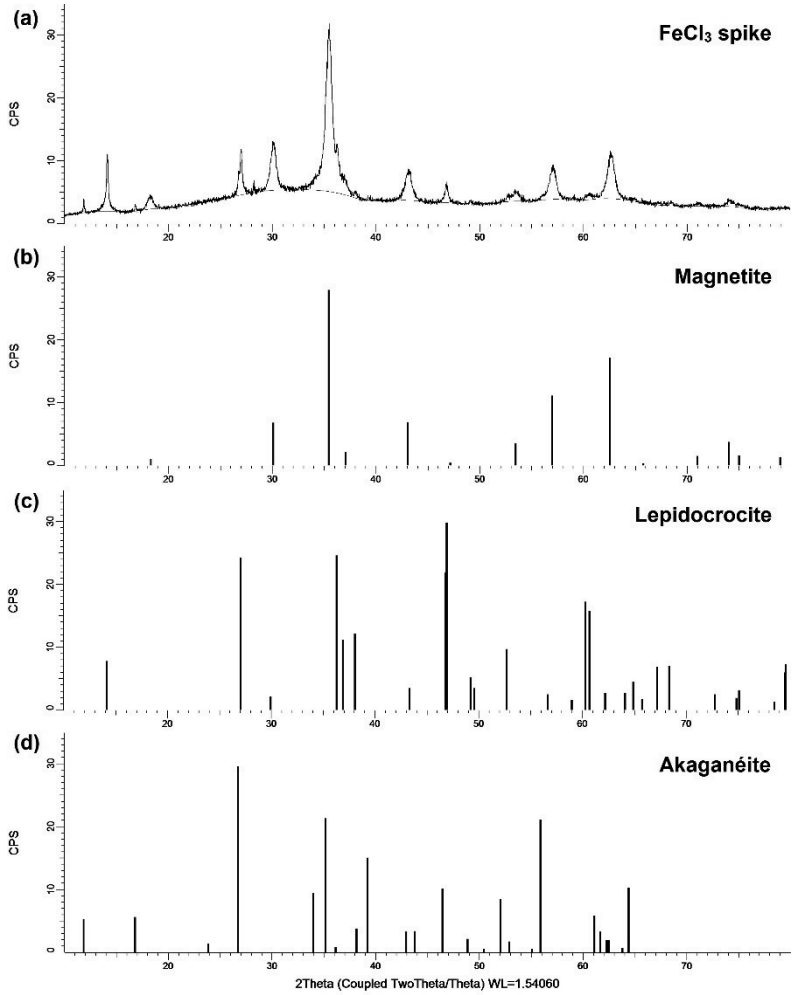

Figure 6.4 Formed precipitates during the spike with aqueous $FeCl_3$ (a), as well as the diffraction patterns for magnetite (b), lepidocrocite (c) and akaganéite (d).

Acknowledgements

We thank Rick Idema and Jin Huang for their contribution to the practical work that laid the basis for this chapter.

Chapter 7

General discussion

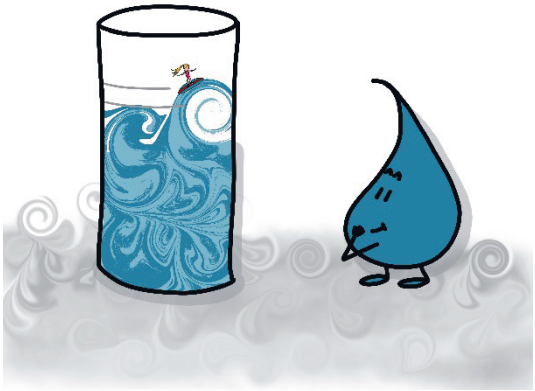

7.1 Introduction

The Dutch drinking water companies extracted a total volume of 758.10^9 L of groundwater for the production of drinking water in 2014 [110]. Current common practice of iron removal for the production of drinking water (i.e. rapid sand filtration) leads to 11,000 ton dry weight of iron sludge per year in the Netherlands [15]. While this drinking water treatment sludge has several applications e.g. in gas and water treatment [15], the recovery of iron in the form of magnetite could increase revenue. Magnetite ($Fe^{II}Fe^{III}_2O_4$) is a mixed valence iron oxide with strong magnetic properties and therefore high-tech applications. This thesis explored two pathways for magnetite crystallization in drinking water production: partial oxidation and partial biological reduction.

Chapter 3 and 4 focus on magnetite formation through the partial oxidation of aqueous $FeCl_2$ in a continuous reactor. Magnetite was formed in a medium of 50% tap water and 50% Milli-Q water (Ch. 3). Reactor operation included a start-up phase at pH 5.5 or 6.0, followed by a forced pH raise to 6.8 – 7.5 that initiated magnetite formation. Alternatively, magnetite formation was achieved when the reactor was seeded with previously formed magnetite particles and operated at a stable pH of 7. Initially, nitrate was supplied as the intended electron acceptor for the iron oxidation. However, diffusion of O_2 into the system could not be prevented and was sufficient to render the added nitrate redundant. To gain control over the O_2 influx, the reactor system was placed inside a glovebox filled with N_2 under minimal overpressure (Ch. 4). A small flow of compressed air was supplied to the headspace of the reactor to facilitate controlled iron oxidation. Magnetite formation was achieved at an iron feed concentration of 1 mM or higher. Decreasing the hydraulic retention time (HRT) from 34 to 8 hours reduced the efficiency for magnetite formation. Under these conditions, magnetite formation did not occur in a medium containing ≥ 50% tap water or in growth medium. While in the experiments described in Chapter 3, the only crystalline iron phases that were formed are magnetite and lepidocrocite (γ-FeOOH), the experiments in Milli-Q water with controlled O_2 addition (Ch. 4) also yielded goethite (α-FeOOH) and maghemite (γ-Fe_2O_3). The main parameter determining the iron phase formation with controlled O_2 addition was the Fe^{2+} concentration in the reactor; magnetite formation did not take place at a concentration below 0.4 mM Fe^{2+}. Lepidocrocite formation increased with an increasing Fe^{2+} concentration, while lower concentrations of Fe^{2+} yielded a large fraction of amorphous precipitates and a small fraction of maghemite. The maximum efficiency for magnetite formation with controlled O_2 addition was 27%.

Chapter 5 and 6 focus on partial bioreduction of hydrous ferric oxide (HFO). Batch experiments showed that magnetite formation can be achieved with a mixed microbial culture and either lactate, glucose or ethanol as electron donor (Ch. 5). Based on the observation of the color changes, a green rust (GR) precursor phase was formed in all batch bottles. When the final pH and ORP were in the range of 7.5 to 7.6 and -254 and -283 mV, transformation of GR to magnetite took place. At a higher pH and lower ORP however, GR remained stable until it was exposed to air. Oxidation by ambient air yielded the orange iron phase lepidocrocite. Bioreduction of HFO in a continuous reactor setup was failed to result in magnetite formation (Ch. 6). Reactor operation with various ethanol loads and therefore various ORP conditions led to the formation of GR, but

the transformation to magnetite did not take place. Rapidly adding 0.5 M aqueous $FeCl_3$ to the reactor in batch mode that was containing GR did yield magnetite.

7.2 The partial oxidation process

7.2.1 The magnetite crystallization pathway

The crystallization of magnetite through the partial oxidation pathway is initiated by either a forced pH raise from 5.5 – 6.0 to 6.8 – 7.5 or by seeding with previously formed magnetite. Starting the reactor experiment at pH 7.0, without any further adjustment and without magnetite seeds did not yield magnetite (Ch. 3). At the start of the experiments, the reactor contained medium without iron. Therefore, the iron concentration gradually increased during the first experimental phase at pH 5.5 – 6.0. At the end of this phase, the reactor medium showed an orange discoloration and a slight turbidity. This indicates the presence of Fe^{3+} phases in suspension, which apparently are crucial for the magnetite crystallization process in the absence of magnetite seeds. The formation of Fe^{3+} phases is expected from the constant influx of O_2 (either via uncontrolled diffusion to the setup or by controlled addition to the headspace) and the poor solubility of Fe^{3+} at pH 6.8 and higher [3]. The distinct orange discoloration in combination with a slight turbidity in the initial experimental phase indicates that a significant fraction of the iron was oxidized. During the second experimental phase at pH 6.8 or higher, the formation of GR was visible. Since GR is a mixed-valence complex, this indicates that the solubility of Fe^{2+} was so low that the precipitation was faster than the oxidation thereof. This caused the Fe^{2+} to precipitate with the already present ferric iron complexes, leading to a mixed-valence precipitate. The formed GR then proceeded to react with the supplied Fe^{2+} to form magnetite (Ch. 3) [20]. Once this state in the reactor was reached, the situation was equal to a reactor run at the constant pH of 7 containing a magnetite seed. Seeding is known to benefit formation of crystals with a similar structure as the seed by reducing the energy barrier for nucleation [105]. Crystallization of magnetite in the reactor setup was continuous (Ch. 3 and 4) and therefore has potential for application to large and continuous streams.

7.2.2 The challenge of a complex medium

The application of the partial oxidation process to a medium other than Milli-Q water is troublesome. Tap water was used in the experiments as a step towards the complexity of a groundwater medium. Magnetite crystallization was achieved in a medium of 50% tap water with nitrate and an uncontrolled O_2 influx (Ch. 3). However, the attempt to reproduce this with controlled O_2 addition (Ch. 4, TW-A) failed and the experiment yielded mainly amorphous precipitates and maghemite. Comparison of experiments (e) (Ch. 3) and TW-A (Ch. 4), that have the same pH regime, shows higher concentrations of both Fe^{2+} and Fe^{3+} in solution for the latter, indicating that less precipitation took place as well as explaining the high fraction of amorphous precipitates, since these were formed from aqueous iron complexes during sample preparation for XRD analysis.

The main differences between the experiments were the means and location of the oxidant addition; while O_2 addition in TW-A was limited to dosing to the headspace of the reactor, in experiment (e), O_2 diffusion took place through the tubing, connections and reactor lid and nitrate was present in the reactor medium. The iron feed tubing in experiment (e) showed an orange discoloration for its entire length from the iron feed solution bottle to the reactor (approximately 1 m). This indicates that iron oxidation took place before the solution entered the reactor. Therefore, the feed contained both Fe^{2+} and Fe^{3+} at the moment that it entered the reactor. There, the pH of the solution was elevated to 7.5. This led to fast precipitation of the iron ions in the form of GR. In experiment TW-A in the other hand, the solution entering the reactor contained only Fe^{2+} and oxidation only took place in the reactor and therefore at pH 7.5. Presumably, the rate of oxidation of Fe^{2+} in this case was higher than the precipitation thereof, leading to the crystallization of the ferric iron mineral maghemite. Reducing the O_2 flow to the headspace would reduce the overall rate of oxidation of Fe^{2+}, therefore favoring the precipitation of mixed-valence phases like GR and magnetite.

The experiment in 90% tap water with controlled O_2 (Ch. 4, TW-B) yielded predominantly goethite. Likely, this was caused by the elevated concentration of carbonates (from the tap water) in the medium, leading to the formation of carbonate-GR instead of chloride-GR. Carbonate-GR oxidizes to goethite when exposed to ambient air, which occurred during sample preparation for XRD analysis [84]. The high fraction of goethite and lack of magnetite crystallization indicate that the carbonate concentration was sufficiently high to stabilize the GR during the experiment [108]. The Wageningen tap water contains 1.6 mM HCO_3^- on average [80], which is low compared to the average concentration in groundwater in the Netherlands [110,111], but apparently sufficiently high to disrupt the magnetite crystallization process (Ch. 3 and 4). However, experiments described in literature with a pure culture of *Dechlorosoma suillum* showed that magnetite crystallization is possible in a medium containing 30 mM HCO_3^- [51,52], indicating that the presence of microorganisms can help overcome carbonate inhibition at groundwater concentrations.

7.2.3 Vivianite crystallization induced by inoculation with activated sludge

Biological experiments were conducted using a growth medium from which carbonate was omitted (Ch. 4). Carbon was added solely to the headspace in the form of CO_2 in air, staying well below the concentration of 1.6 mM. As expected due to the low concentration, the experiments did not yield goethite. The chemical control experiment yielded predominantly lepidocrocite, indicating that chloride-GR was formed and stabilized in the reactor environment [84]. Chloride-GR is stabilized by a high Fe^{2+} concentration [59], but measurements show that the Fe^{2+} concentration in this experiment was average compared to concentrations found in experiments that did yield magnetite. There must therefore be another factor present in the medium that controls GR stability. However, none of the added ions are known to affect this.

The inoculation with microorganisms in a growth medium (Ch. 4) did not aid the transformation of GR to magnetite. Instead, the predominant formation of the ferrous iron mineral vivianite ($Fe_3(PO_4)_2$) indicates that the formation of GR did not take place. The phosphate concentration in the medium was deliberately kept low ($7.3.10^{-3}$ mM), aiming to avoid vivianite crystallization.

However, by inoculation through the addition of (washed and diluted) primary sludge from a waste water treatment plant, phosphate and possibly even vivianite was added to the system, stimulating the (additional) crystallization of the latter. The addition of a microbial culture in a different form may yield a different iron phase and therefore offers chances for magnetite crystallization.

7.2.4 Challenges for the application to groundwater

The partial oxidation process as presented in this thesis, takes place at a circumneutral pH, which concurs with the natural pH of groundwater in the Netherlands [5]. The maximum Fe^{2+} concentration in Dutch groundwater is around 0.5 mM [5]. The partial oxidation experiment with an iron feed concentration equal to or below this did not yield magnetite. Treating groundwater with the partial oxidation process would therefore require concentrating the feed stream (e.g. by membrane filtration) to elevate the iron concentration. This however, would also increase the concentration of the other ions like carbonate, leading to inhibition of magnetite crystallization. Additional research is therefore required to investigate if biological partial oxidation for magnetite crystallization in growth medium in batch is technologically feasible in a continuous reactor setup.

7.3 The partial bioreduction process

7.3.1 Determining factors for iron phase formation

The product of HFO bioreduction depends on the final pH and ORP of the medium (Ch. 5). Observation of the batch experiments over time, indicated that HFO was partially reduced to GR that subsequently crystallized to magnetite. This transformation to magnetite occurred within a defined window of a final pH of 7.5 to 7.6 and final ORP of -254 to -283 mV. A lower ORP refers to a higher concentration of aqueous Fe^{2+} in the medium, which stabilizes GR and thereby inhibits the transformation to magnetite [59]. This stabilization is likely due to the Fe^{2+}/Fe^{3+} ratio in the GR, as this is known to vary [84]. When the formed GR consists of Fe^{2+}/Fe^{3+} in the ratio of 1 : 2, like in magnetite, transformation into magnetite is straightforward. When the ratio is higher, this transformation would require the loss of Fe^{2+} through either partial oxidation or a dissolution-reprecipitation mechanism. The first is unlikely in the batch experiments, since the environment is anaerobic and reductive. The latter needs a provocation, like a sudden change in pH, ORP or Fe^{2+} concentration, which also does not occur in the batch experiments [3], resulting in GR as stable precipitate.

Additional batch experiments with H_2 as electron donor show that magnetite crystallization through partial bioreduction of HFO is also possible with a final pH of 8.1 to 8.2 and final ORP of -370 to -460 mV (own unpublished data). Figure 7.1 shows the values for final pH and ORP grouped by the dominant precipitates formed including the batch experiments with added H_2 (adjusted from Fig. 5.3). It is clear that more factors than solely the ORP and therefore the Fe^{2+} concentration affect the iron phase that is formed when a broader pH range is considered. As derived above, the ratio of Fe^{2+}/Fe^{3+} in the GR precursor phase determines whether or not magnetite crystallization takes place. This ratio depends on the relative presence of the two ions, which in these experiments is

determined by the rate of the HFO bioreduction and the rate of precipitation. Since the solubility of both Fe^{2+} and Fe^{3+} decreases with increasing pH, driving force for precipitation increases with increasing pH. This means that at a lower pH, a larger concentration of Fe^{2+} can remain in solution, leading to a higher Fe^{2+}/Fe^{3+} ratio in the formed GR that is therefore relatively stable. In contrast, at a higher pH, the formed Fe^{2+} has an increased tendency for the adsorption to the surface of the HFO (compared to remaining in solution). Here, it will form the mixed-valence GR with a low Fe^{2+}/Fe^{3+} ratio. Due to this low ratio, the GR is less stable and an ideal precursor for magnetite.

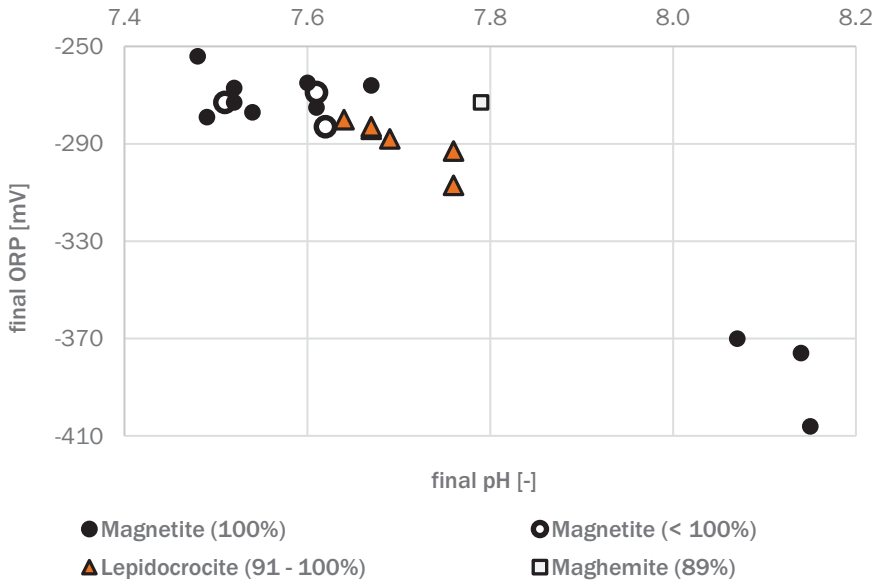

Figure 7.1 The dominant precipitates formed due to biological reduction of HFO in the batch experiments described in Ch. 5 plus the additional batch experiments with H_2 as electron donor.

In conclusion, the determining factors for iron phase formation through bioreduction of HFO are not only pH and ORP, but likely also the reduction rate. This indicates that the amount of biological activity is an important parameter.

7.3.2 The stability of green rust in a continuous reactor setup

The attempt to produce magnetite through the partial bioreduction of HFO at pH 7.5 in a continuous reactor setup was unsuccessful (Ch. 6). The predominant iron phases that were produced were lepidocrocite and goethite. The fraction of the latter consistently increased with an increasing (i.e. less negative) ORP. Since samples of the reactor were green at the moment of extraction form the reaction at all instances, it is assumed that lepidocrocite and goethite respectively represent chloride-GR and carbonate-GR. The formation of one or the other depends

on the presence of chloride and carbonate as well as the Fe^{2+}/Fe^{3+} ratio (and thus the ORP), as follows from the general formulas of chloride-GR ($[Fe_3^{II}Fe^{III}(OH)_8][Cl^- * nH_2O]$) and carbonate-GR ($[Fe_4^{II}Fe_2^{III}(OH)_{12}][CO_3^{2-} * nH_2O]$) [84]. The ethanol load to the reactor was varied during various stages of operation, leading to ORP values between approximately -200 to -500 mV. Based on batch experiments (Ch. 5), the transformation of the GR that was present in the reactor to magnetite was expected to occur in the ORP range of -250 to -290 mV (Fig. 7.1). However, in the continuous reactor setup, the GR remained stable.

The factors that determine the formation of either magnetite of GR through (bio)reduction of a ferric iron phase are not well understood. Influential parameters suggested by literature are medium composition, pH and ORP values, Fe(III) reduction rate and ratio between bacterial cells and Fe(III) [112]. The medium composition was the same in the batch and reactor experiments. In contrast to the batch environment, there is a continuous supply of medium, Fe(III) and ethanol to the reactor, leading to a steady state situation. The most important difference ensuing from this is the Fe^{2+}/Fe^{3+} ratio. This ratio determines the ORP, which has been varied in the reactor by different ethanol load settings during experimental stages. The initial pH in the batch experiments was set to 7.0 or 7.5 without adjustment thereafter, while the pH in the reactor was controlled at 7.5±0.1. However, while the pH is allowed to deviate in the batch experiments, magnetite crystallization was successful at a final pH in the range of 7.4 to 7.6.

A possible explanation for the difference in GR stability between the batch experiments and the continuous reactor is a variation in the ratio of the Fe(III) phase to the microbial cells present in the reactor. This was identified as the determining factor for the eventual formation of either GR or magnetite by Zegeye et al. [112] who studied the formation of iron minerals through the bioreduction of lepidocrocite. They showed that a cell density higher than $1.3.10^{10}$ cells mmol iron^{-1} leads to aggregates that more densely packed and hypothesize that the released Fe^{2+} is physically trapped in the microenvironment within the aggregate, leading to a high Fe^{2+} concentration near the Fe(III) mineral surface and consequently to the formation of GR. The batch bottles and the reactor were inoculated with respectively 20 mL and 200 mL of microbial culture, which was 10% of their respected volumes. Although these inoculations originated from the same initial culture, the composition of the microbial inoculation was different, since the experiments were conducted several months apart and the culture was regularly transferred to new medium to promote growth. The density of the microbial culture is therefore expected to be higher in the reactor. Moreover, the reactor was run in the continuous mode for 103 days, allowing for biomass growth during the experiment. Following the hypothesis of Zegeye et al. [112], this favored the stability of GR over the transformation to magnetite in the reactor setup. Since neither the microbial activity nor the number of microbial cells were determined in our experiments, this hypothesis can unfortunately not be substantiated further.

7.3.3 Challenges for the application to drinking water treatment sludge

Magnetite crystallization through partial bioreduction of HFO was achieved with various electron donors. Moreover, the presence of ions other than iron did not inhibit the process. It should be noted however, that the concentrations of carbonates and phosphate were deliberately kept to a minimum to decrease the possibility of siderite and vivianite crystallization. Application of this

process to actual drinking water treatment sludge however, would introduce other (metal) ions into the system [13]. The crystallization of magnetite is not expected to be inhibited by the presence of these ions, but it is known that ions like Co, Ni, Zn, Cu, Mn and Cd can be incorporated into magnetite [3,27], which possibly leads to a reduction of the value and applicability of the product.

7.4 A process for magnetite crystallization from groundwater

The aim of this thesis was to develop a process for the recovery of iron from groundwater in the form of magnetite, with the production of drinking water as intended field of application. Since the production of drinking water deals with large volumes of groundwater, the developed process should be applicable to a continuous stream. Moreover, both groundwater and drinking water treatment sludge contain components like carbonates and metal ions other than iron [5,113,114]. The addition of chemicals that are necessary for the process should not endanger the drinking water quality and should be kept to a minimum in order to avoid the production of chemical waste as well as high costs.

The explorative research presented in this thesis shows that magnetite crystallization from groundwater has potential. For the first time, magnetite was produced continuously. This was achieved through the partial oxidation process. The partial bioreduction process showed that magnetite crystallization is possible in the presence of 'foreign' ions. Moreover, magnetite formation took place at circumneutral pH and requires only small volumes of added chemicals (for pH control, electron donor). However, additional research is required to develop a process that is both continuous and applicable in a complex matrix and that is suitable for low iron concentrations.

7.4.1 A two-reactor setup

In both processes, magnetite crystallization proceeded through a GR precursor. In the partial oxidation process, GR transformed into maghemite instead of magnetite at iron concentrations below 1 mM. In the partial bioreduction process, the transformation of GR to magnetite was not achieved in a continuous system. Combining the two pathways in a two-reactor system could remove the inhibitions and facilitate the crystallization of magnetite from drinking water treatment sludge in a continuous system.

Figure 7.2 shows the proposed reactor setup. Drinking water treatment sludge is fed to reactor 1, where a mixed microbial community partially reduces the iron in the sludge to form GR. The suspension containing the GR that is formed in reactor 1 is then pumped to reactor 2. Here, the controlled addition of O_2 will partially oxidize the GR, leading to magnetite crystallization. The precipitates that are collected from reactor 2 will likely by a mixture of magnetite, lepidocrocite and possibly minor fractions of goethite and maghemite. Magnetite can be extracted from this mixture through magnetic separation. The remainder of the products can added to the feed of reactor 1 for optimal efficiency. If necessary, an additional step in which the product is treated

with a mixture of citrate-bicarbonate-dithionite (CBD) can eliminate the presence of other iron minerals further [115].

This combined process intended for application to drinking water treatment sludge, removing the complicating factor of a low iron concentration. The partial bioreduction in reactor 1 will likely not be inhibited by the presence of foreign ions, although the effects of other metal ions present in the sludge on the formation of GR are not known. This, as well as the effects on the subsequent magnetite crystallization, requires additional research.

Since the chemical oxidation of iron by O_2 is very rapid at a circumneutral pH, both processes are sensitive to the presence thereof. The presence of O_2 will reduce the efficiency of partial reduction process in reactor 1. An excess of O_2 in reactor 2 will lead to the crystallization of lepidocrocite, goethite or maghemite instead of magnetite. Strict control over the O_2 concentration is therefore crucial.

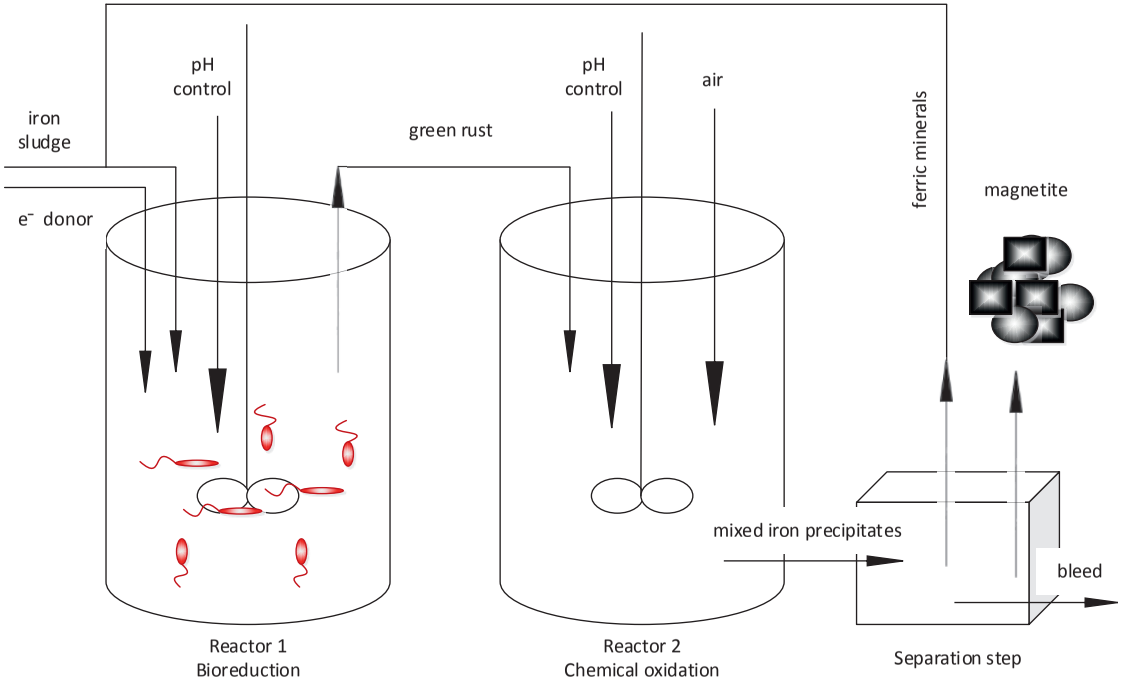

Figure 7.2 Proposed two-reactor setup in which drinking water treatment sludge is partially bioreduced to GR in reactor 1, followed by partial chemical oxidation to form magnetite in reactor 2. The formed iron precipitates are magnetically separated and magnetite is harvested, while ferric iron phases like lepidocrocite are led back to reactor 1.

7.4.2 *Reactor design*

The HRT and therefore the size of reactor 1 should be determined by the reduction rate and the biological growth in the system, ensuring a steady biomass concentration. The bioreactor setup discussed in Chapter 6 had an HRT of 12.3 h. The treatment of all iron sludge produced in the production of drinking water in the Netherlands would require a reactor volume of 74 m^3 for reactor 1 (calculations in Appendix). The reactor setup for partial oxidation as discussed in chapters 3 and 4 had an HRT of 34 h. Reducing the HRT to 8 h led to a decrease of the fraction of magnetite from 69% to 18% (Ch. 4). While it should be noted that in these experiments the reactor was started without any iron present and GR formation had to take place before magnetite could be formed, the results do indicate that the HRT should be longer than 8 h to facilitate an efficient process. Additional research is required for optimization of both processes, possibly leading to lower optimal HRTs.

7.4.3 *Operating the two-reactor setup*

Both the partial oxidation and the partial bioreduction process require a circumneutral pH. The simplified half-reaction equations show that pH control is necessary in both reactors;

$$4\ Fe^{III}OOH + Cl^- + \ 4\ H^+ + H_2O \ \rightarrow \ Fe_3^{II}Fe^{III}(OH)_8.[Cl^-.H_2O] \qquad \text{(reactor 1)}$$

$$3\ Fe_3^{II}Fe^{III}(OH)_8.[Cl^-.H_2O] \rightarrow 4\ Fe^{II}Fe_2^{III}O_4 + 9\ H_2O + 8\ H^+ \qquad \text{(reactor 2)}$$

The drinking water treatment sludge is expected to have a location-dependent buffering capacity due to the presence of carbonate species [5]. The volumes of acid and base that are necessary for maintaining a circumneutral pH in the reactors will therefore be site specific.

The partial bioreduction of iron requires the presence of an electron donor. This is not naturally present in drinking water treatment sludge and should therefore be added continuously. Several electron donors like lactate, glucose, ethanol and H_2 can facilitate the process (Ch. 5 and 6).

The partial oxidation process in reactor 2 requires the controlled addition of O_2, which can simply be in the form of air.

7.5 General conclusions

The focus of this study was the development of a process for the crystallization of magnetite from groundwater. The results show that the partial oxidation of $FeCl_2$ can lead to the continuous crystallization of magnetite. The formation of the iron phase in pure water was dictated by the aqueous ferrous iron concentration in the reactor. The magnetite crystallization process can be inhibited by the presence of foreign ions. Additionally, this thesis showed that the production of magnetite through the partial bioreduction of HFO can be facilitated by a mixed microbial culture

using several electron donors. The iron phase formation was dictated by the pH/ORP range, the bioreduction rate and possibly the ratio between microbial cells and the ferric iron phase concentration.

Combining the two processes presented in this thesis in a two-reactor setup offers chances to produce magnetite in a continuous system under mild conditions, without the extensive addition of chemicals and in the presence of foreign ions. Additional research is required to test the technological feasibility of the two-reactor setup and to optimize both processes.

7.6 Appendix to Chapter 7

S7.1 HRT calculations reactor 1

S7.1 HRT calculations reactor 1

Iron sludge streams per year [15]:

- $5.08.10^{10}$ g watery iron sludge, density $1.05.10^{6}$ – $1.2.10^{6}$ g $(m^3)^{-1}$
- $2.04.10^{10}$ g iron sludge, density $5.2.10^{6}$ g $(m^3)^{-1}$

Total volume: $5.2.10^{4}$ m^3 y^{-1} (ass. density of watery sludge of $1.05.10^{6}$ g $(m^3)^{-1}$)

Flow = 6.0 m^3 h^{-1}
With HRT = 12.3 h
V = 73 m^3

References

[1] WWAP, The United Nations world water development report 2015: Water for a sustainable world, 2015. doi:978-92-3-100071-3.
[2] WHO, Guidelines for drinking-water quality, 2011.
[3] R.M. Cornell, U. Schwertmann, The iron oxides: Structure, properties, reactions, occurences and uses, 2nd ed., WILEY-VCH Verlag GMBH & Co., Weinheim, 2003.
[4] S. Laurent, D. Forge, M. Port, A. Roch, C. Robic, L. Vander Elst, R.N. Muller, Magnetic iron oxide nanoparticles: Synthesis, stabilization, vectorization, physicochemical characterizations, and biological applications, Chem. Rev. 108 (2008) 2064–2110. doi:10.1021/cr068445e.
[5] C.G.E.M. Van Beek, J. Dusseldorp, K. Joris, K. Huysman, H. Leijssen, F. Schoonenberg Kegel, W.W.J.M. De Vet, S. Van de Wetering, B. Hofs, Contributions of homogeneous, heterogeneous and biological iron(II) oxidation in aeration and rapid sand filtration (RSF) in field sites, J. Water Supply Res. Technol. — AQUA. 65 (2016) 195–207. doi:10.1017/CBO9781107415324.004.
[6] K.R. Arturi, C.B. Koch, E.G. Sogard, Characterization and comparison of iron oxyhydroxide precipitates form biotic and abiotic groundwater treatments, J. Water Supply Res. Technol. — AQUA. 67 (2017) 96–104.
[7] D. Vries, C. Bertelkamp, F. Schoonenberg Kegel, B. Hofs, J. Dusseldorp, J.H. Bruins, W. de Vet, B. van den Akker, Iron and manganese removal: Recent advances in modelling treatment efficiency by rapid sand filtration, Water Res. 109 (2017) 35–45. doi:10.1016/j.watres.2016.11.032.
[8] W. Davison, G. Seed, The kinetics of the oxidation of ferrous iron in synthetic and natural waters, Geochim. Cosmochim. Acta. 47 (1983) 67–79. doi:10.1016/0016-7037(83)90091-1.
[9] D. Ellis, C. Bouchard, G. Lantagne, Removal of iron and manganese from groundwater by oxidation and microfiltration, Desalination. 130 (2000) 255–264. doi:10.1016/S0011-9164(00)00090-4.
[10] X. Du, G. Liu, F. Qu, K. Li, S. Shao, G. Li, H. Liang, Removal of iron, manganese and ammonia from groundwater using a PAC-MBR system: The anti-pollution ability, microbial population and membrane fouling, Desalination. 403 (2017) 97–106. doi:10.1016/j.desal.2016.03.002.
[11] K.H. Choo, H. Lee, S.J. Choi, Iron and manganese removal and membrane fouling during UF in conjunction with prechlorination for drinking water treatment, J. Memb. Sci. 267 (2005) 18–26. doi:10.1016/j.memsci.2005.05.021.
[12] N. Khatri, S. Tyagi, D. Rawtani, Recent strategies for the removal of iron from water: A review, J. Water Process Eng. 19 (2017) 291–304. doi:10.1016/j.jwpe.2017.08.015.
[13] A.O. Babatunde, Y.Q. Zhao, Constructive approaches toward water treatment works sludge management: An international review of beneficial reuses, Crit. Rev. Environ. Sci. Technol. 37 (2007) 129–164. doi:10.1080/10643380600776239.
[14] M. Razali, Y.Q. Zhao, M. Bruen, Effectiveness of a drinking-water treatment sludge in removing different phosphorus species from aqueous solution, Sep. Purif. Technol. 55 (2007) 300–306. doi:10.1016/j.seppur.2006.12.004.
[15] O. Van der Kolk, personal communication, Aquaminerals. (2018) 1.
[16] L. Feenstra, J.G. ten Wolde, C.M. Eenstroom, Reusing water treatment plant sludge as secondary raw material in brick manufacturing, in: J.J.J.M. Goumans, G.J. Senden, H.A. Van der Sloot (Eds.), Waste Mater. Constr. Putt. Theory into Pract., 1st ed., Elsevier B.V., 1997: pp. 641–645. doi:10.1016/S0166-1116(97)80247-6.
[17] K.A. Weber, L.A. Achenbach, J.D. Coates, Microorganisms pumping iron: Anaerobic microbial iron oxidation and reduction, Nat. Rev. Microbiol. 4 (2006) 752–764. doi:10.1038/nrmicro1490.
[18] M. Etique, F.P.A. Jorand, C. Ruby, Magnetite as a precursor for green rust through the

hydrogenotrophic activity of the iron-reducing bacteria Shewanella putrefaciens, Geobiology. (2015). doi:10.1111/gbi.12170.
[19] V. Lambinet, M.E. Hayden, K. Reigl, S. Gomis, G. Gries, Linking magnetite in the abdomen of honey bees to a magnetoreceptive function, Proc. R. Soc. B. 284 (2017). doi:10.1098/rspb.2016.2873.
[20] G. Mirabello, J.J.M. Lenders, N.A.J.M. Sommerdijk, Bioinspired synthesis of magnetite nanoparticles, Chem Soc Rev. 45 (2016) 5085–5106. doi:10.1039/C6CS00432F.
[21] D. Faivre, Biomimetic formation of magnetite nanoparticles, in: P. Behrens, E. Bäuerlein (Eds.), Handb. Biominer., 1st ed., WILEY-VCH, 2007: pp. 159–171. doi:10.1002/9783527619443.ch33.
[22] C.T. Lefevre, D.A. Bazylinski, Ecology, diversity, and evolution of magnetotactic bacteria, Microbiol. Mol. Biol. Rev. 77 (2013) 497–526. doi:10.1128/MMBR.00021-13.
[23] V. Reichel, D. Faivre, Magnetite nucleation and growth, in: A. van Driessche, M. Kellermeier, L.G. Benning, D. Gebauer (Eds.), New Perspect. Miner. Nucleation Growth, 1st ed., Springer International Publishing, Cham, Zwitserland, 2017: pp. 275–291. doi:10.1007/978-3-319-45669-0.
[24] MagNet, Magnetite facts & figures, Magn. Netw. (2011). http://www.magnetitenetwork.com.au/who-we-are/magnetite/ (accessed April 2, 2018).
[25] N. Joshi, F. Liu, M.P. Watts, H. Williams, V.S. Coker, D. Schmid, T. Hofmann, J.R. Lloyd, Optimising the transport properties and reactivity of microbially-synthesised magnetite for in situ remediation, Sci. Rep. 8 (2018) 1–12. doi:10.1038/s41598-018-21733-y.
[26] W. Wu, Z. Wu, T. Yu, C. Jiang, W.S. Kim, Recent progress on magnetic iron oxide nanoparticles: Synthesis, surface functional strategies and biomedical applications, Sci. Technol. Adv. Mater. 16 (2015) 23501. doi:10.1088/1468-6996/16/2/023501.
[27] P.S. Sidhu, R.J. Gilkes, A.M. Posner, The synthesis and some properties of Co, Ni, Zn, Cu, Mn and Cd substituted magnetites, J. Inorg. Nucleation Chem. 40 (1978) 429–435. doi:10.1016/0022-1902(78)80418-7.
[28] T. Ahn, J.H. Kim, H.M. Yang, J.W. Lee, J.D. Kim, Formation pathways of magnetite nanoparticles by coprecipitation method, J. Phys. Chem. 116 (2012) 6069–6076. doi:10.1021/jp211843g.
[29] Y. Amemiya, A. Arakaki, S.S. Staniland, T. Tanaka, T. Matsunaga, Controlled formation of magnetite crystal by partial oxidation of ferrous hydroxide in the presence of recombinant magnetotactic bacterial protein Mms6, Biomaterials. 28 (2007) 5381–5389. doi:10.1016/j.biomaterials.2007.07.051.
[30] J.S. Salazar, L. Perez, O. De Abril, L.T. Phuoc, D. Ihiawakrim, M. Vazquez, J.-M. Greneche, S. Begin-Colin, G. Pourroy, Magnetic iron oxide nanoparticles in 10 - 40 nm range: Composition in terms of magnetite/maghemite ratio and effect on the magnetic properties, Chem. Mater. 23 (2011) 1379–1386. doi:10.1021/cm103188a.
[31] C. Pereira, A.M. Pereira, M. Rocha, C. Freire, C.F.G.C. Geraldes, Architectured design of superparamagnetic Fe3O4 nanoparticles for application as MRI contrast agents: mastering size and magnetism for enhanced relaxivity, J. Mater. Chem. B. 3 (2015) 6261–6273. doi:10.1039/C5TB00789E.
[32] J. Baumgartner, L. Bertinetti, M. Widdrat, A.M. Hirt, D. Faivre, Formation of magnetite nanoparticles at low temperature: From superparamagnetic to stable single domain particles, PLoS One. 8 (2013). doi:10.1371/journal.pone.0057070.
[33] Y. Tamaura, K. Ito, T. Katsura, Transformation of y-FeO(OH) to Fe3O4 by adsorption of iron-II ion on y-FeO(OH), J. Chem. Soc. Dalt. Trans. 2 (1983) 189–194. doi:10.1039/DT9830000189.
[34] J.J.M. Lenders, G. Mirabello, N.A.J.M. Sommerdijk, Bioinspired magnetite synthesis via solid precursor phases, Chem. Sci. 7 (2016) 5624–5634. doi:10.1039/C6SC00523C.
[35] T. Misawa, K. Hashimoto, S. Shimodaira, The mechanism of formation of iron oxide and

oxyhydroxides in aqueous solutions at room temperature, Corros. Sci. 14 (1974) 131–149. doi:10.1016/S0010-938X(74)80051-X.

[36] H. Guo, A.S. Barnard, Naturally occurring iron oxide nanoparticles: Morphology, surface chemistry and environmental stability, J. Mater. Chem. A. 1 (2013) 27–42. doi:10.1039/C2TA00523A.

[37] B. Morgan, O. Lahav, The effect of pH on the kinetics of spontaneous Fe(II) oxidation by O2 in aqueous solution–basic principles and a simple heuristic description., Chemosphere. 68 (2007) 2080–4. doi:10.1016/j.chemosphere.2007.02.015.

[38] L. Babes, B. Denizot, G. Tanguy, J.J. Le Jeune, P. Jallet, Synthesis of iron oxide nanoparticles used as MRI contrast agents: A parametric study, J. Colloid Interface Sci. 212 (1999) 474–482. doi:0021-9797/99.

[39] C. Zhang, H. Vali, C.S. Romanek, T.J. Phelps, S. V. Liu, Formation of single-domain magnetite by a thermophilic bacterium, Am. Mineral. 83 (1998) 1409–1418. doi:10.2138/am-1998-11-1230.

[40] D.A. Bazylinski, R.B. Frankel, K.O. Konhauser, Modes of biomineralization of magnetite by microbes, Geomicrobiol. J. 24 (2007) 465–475. doi:10.1080/01490450701572259.

[41] D.C. Cooper, F. Picardal, J. Rivera, C. Talbot, Zinc immobilization and magnetite formation via ferric oxide reduction by Shewanella putrefaciens 200, Environ. Sci. Technol. 34 (2000) 100–106. doi:10.1021/es990510x.

[42] H. Vali, B. Weiss, Y.-L. Li, S.K. Sears, S.S. Kim, J.L. Kirschvink, C.L. Zhang, Formation of tabular single-domain magnetite induced by Geobacter metallireducens GS-15, Proc. Natl. Acad. Sci. U. S. A. 101 (2004) 16121–6. doi:10.1073/pnas.0404040101.

[43] A. Bharde, A. Wani, Y. Shouche, P. a Joy, B.L. V Prasad, M. Sastry, Bacterial aerobic synthesis of nanocrystalline magnetite, J. Am. Chem. Soc. 127 (2005) 9326–9327. doi:10.1021/ja0508469.

[44] A. Bharde, D. Rautaray, V. Bansal, A. Ahmad, I. Sarkar, S.M. Yusuf, M. Sanyal, M. Sastry, Extracellular biosynthesis of magnetite using fungi, Small. 2 (2006) 135–141. doi:10.1002/smll.200500180.

[45] C.M. Hansel, S.G. Benner, S. Fendorf, Competing Fe(II)-induced mineralization pathways of ferrihydrite, Environ. Sci. Technol. 39 (2005) 7147–7153. doi:10.1021/es050666z.

[46] T. Sugimoto, E. Matijević, Formation of uniform spherical magnetite particles by crystallization from ferrous hydroxide gels, J. Colloid Interface Sci. 74 (1980) 227–243. doi:10.1016/0021-9797(80)90187-3.

[47] L.H.G. Chaves, The role of green rust in the environment: A review, Rev. Bras. Eng. Agrícola e Ambient. 9 (2005) 284–288. doi:10.1590/S1415-43662005000200021.

[48] C.J. Matocha, P. Dhakal, S.M. Pyzola, The role of abiotic and coupled biotic/abiotic mineral controlled redox processes in nitrate reduction, in: D. Sparks (Ed.), Adv. Agron., 1st ed., Elsevier Inc., San Diego, 2012: pp. 181–214. doi:10.1016/B978-0-12-394276-0.00004-4.

[49] M. Etique, A. Zegeye, B. Grégoire, C. Carteret, C. Ruby, Nitrate reduction by mixed iron(II-III) hydroxycarbonate green rust in the presence of phosphate anions: The key parameters influencing the ammonium selectivity, Water Res. 62 (2014) 29–39. doi:10.1016/j.watres.2014.05.028.

[50] S.B. Couling, S. Mann, The influence of inorganic phosphate on the crystallization of magnetite (Fe3O4) from aqueous solution, J. Chem. Soc. Chem. Commun. 1 (1985) 1713–1715. doi:10.1039/C39850001713.

[51] S.K. Chaudhuri, J.G. Lack, J.D. Coates, Biogenic magnetite formation through anaerobic biooxidation of Fe(II), Appl. Environ. Microbiol. 67 (2001) 2844–2848. doi:10.1128/AEM.67.6.2844.

[52] R.A. Bruce, L.A. Achenbach, J.D. Coates, Reduction of (per)chlorate by a novel organism isolated from paper mill waste, Environ. Microbiol. 1 (1999) 319–329.

doi:10.1046/j.1462-2920.1999.00042.x.
[53] J. Miot, J. Li, K. Benzerara, M.T. Sougrati, G. Ona-Nguema, S. Bernard, J.C. Jumas, F. Guyot, Formation of single domain magnetite by green rust oxidation promoted by microbial anaerobic nitrate-dependent iron oxidation, Geochim. Cosmochim. Acta. 139 (2014) 327–343. doi:10.1016/j.gca.2014.04.047.
[54] P.E. Bell, A.L. Mills, J.S. Herman, Biogeochemical conditions favoring magnetite formation during anaerobic iron reduction, Appl. Environ. Microbiol. 53 (1987) 2610–6. http://www.pubmedcentral.nih.gov/articlerender.fcgi?artid=204161&tool=pmcentrez&rendertype=abstract.
[55] D.R. Lovley, J.F. Stolz, G.L.J. Nord, E.J.P. Phillips, Anaerobic production of magnetite by a dissimilatory iron-reducing microorganism, Nature. 330 (1987). doi:10.1038/330252a0.
[56] D.R. Lovley, E.J.P. Phillips, Novel mode of microbial energy metabolism: Organic carbon oxidation coupled to dissimilatory reduction of iron or manganese, Appl. Environ. Microbiol. 54 (1988) 1472–1480. doi:10.1103/PhysRevLett.50.1998.
[57] J.M. Byrne, H. Muhamadali, V.S. Coker, J. Cooper, J.R. Lloyd, Scale-up of the production of highly reactive biogenic magnetite nanoparticles using Geobacter sulfurreducens, J. R. Soc. Interface. 12 (2015). doi:10.1098/rsif.2015.0240.
[58] Y. Roh, C.L. Zhang, H. Vali, R.J. Lauf, J. Zhou, T.J. Phelps, Biogeochemical and environmental factors in Fe biomineralization: Magnetite and siderite formation, Clays Clay Miner. 51 (2003) 83–95. doi:10.1346/CCMN.2003.510110.
[59] J.K. Fredrickson, J.M. Zachara, D.W. Kennedy, H. Dong, T.C. Onstott, N.W. Hinman, S.M. Li, Biogenic iron mineralization accompanying the dissimilatory reduction of hydrous ferric oxide by a groundwater bacterium, Geochim. Cosmochim. Acta. 62 (1998) 3239–3257. doi:10.1016/S0016-7037(98)00243-9.
[60] T. Behrends, P. Van Cappellen, Transformation of hematite into magnetite during dissimilatory iron reduction: Conditions and mechanisms, Geomicrobiol. J. 24 (2007) 403–416. doi:10.1080/01490450701436497.
[61] A. Piepenbrock, U. Dippon, K. Porsch, E. Appel, A. Kappler, Dependence of microbial magnetite formation on humic substance and ferrihydrite concentrations, Geochim. Cosmochim. Acta. 75 (2011) 6844–6858. doi:10.1016/j.gca.2011.09.007.
[62] W.F. Wu, F.P. Wang, J.H. Li, X.W. Yang, X. Xiao, Y.X. Pan, Iron reduction and mineralization of deep-sea iron reducing bacterium Shewanella piezotolerans WP3 at elevated hydrostatic pressures., Geobiology. 11 (2013) 593–601. doi:10.1111/gbi.12061.
[63] S. Glasauer, P.G. Weidler, S. Langley, T.J. Beveridge, Controls on Fe reduction and mineral formation by a subsurface bacterium, Geochim. Cosmochim. Acta. 67 (2003) 1277–1288. doi:10.1016/S0016-7037(00)01199-7.
[64] E.J. O'Loughlin, C.A. Gorski, M.M. Scherer, M.I. Boyanov, K.M. Kemner, Effects of oxyanions, natural organic matter, and bacterial cell numbers on the bioreduction lepidocrocite (γ-FeOOH) and the formation of secondary mineralization products, Environ. Sci. Technol. 44 (2008) GEOC-022. doi:10.1021/es100294w.
[65] L.K. Adams, J.M. Harrison, J.R. Lloyd, S. Langley, D. Fortin, Activity and diversity of Fe(III)-reducing bacteria in a 3000-year-old acid mine drainage site analogue, Geomicrobiol. J. 24 (2007) 295–305. doi:10.1080/01490450701456974.
[66] K. Amstaetter, T. Borch, A. Kappler, Influence of humic acid imposed changes of ferrihydrite aggregation on microbial Fe(III) reduction, Geochim. Cosmochim. Acta. 85 (2012) 326–341. doi:10.1016/j.gca.2012.02.003.
[67] A. Dey, J.J.M. Lenders, N.A.J.M. Sommerdijk, Bioinspired magnetite formation from a disordered ferrihydrite-derived precursor, Faraday Discuss. 179 (2015) 215–225. doi:10.1039/C4FD00227J.
[68] X. Châtellier, M.M. West, J. Rose, D. Fortin, G.G. Leppard, F.G. Ferris, Characterization of iron-oxides formed by oxidation of ferrous ions in the presence of various bacterial species

and inorganic ligands, Geomicrobiol. J. 21 (2004) 99–112. doi:10.1080/01490450490266343.
[69] B.D. Cullity, Elements of X-ray diffraction, in: Elem. X-Ray Diffr., Second, Addison-Wesley Publishing Company, Inc., 1978. doi:10.1021/ed034pA178.
[70] H.P. Klug, L.E. Alexander, Special scattering and diffraction effects, in: X-Ray Diffr. Proced. Polycryst. Amorph. Mater., 2nd ed., 1954: pp. 493, 494.
[71] M.J. Fransen, 1- and 2-dimensional detection systems and the problem of sample fluorescence in X-ray diffractometry, Adv. X-Ray Anal. 47 (2004) 224–231. doi:10.1154/1.1706962.
[72] F. Vereda, J. de Vicente, R. Hidalgo-Alvarez, Oxidation of ferrous hydroxides with nitrate: A versatile method for the preparation of magnetic colloidal particles, J. Colloid Interface Sci. 392 (2013) 50–56. doi:10.1016/j.jcis.2012.09.064.
[73] J.J.M. Lenders, Biomimetic macromolecule-mediated magnetite mineralization, Technische Universiteit Eindhoven, 2015.
[74] C.L. Altan, J.J.M. Lenders, P.H.H. Bomans, G. De With, H. Friedrich, S. Bucak, N.A.J.M. Sommerdijk, Partial oxidation as a rational approach to kinetic control in bioinspired magnetite synthesis, Chem. - A Eur. J. 21 (2015) 6150–6156. doi:10.1002/chem.201405973.
[75] G.C.C. Yang, H.-L. Lee, Chemical reduction of nitrate by nanosized iron: kinetics and pathways, Water Res. 39 (2005) 884–894. doi:10.1016/j.watres.2004.11.030.
[76] M. Kiyama, Conditions for the formation of Fe3O4 by the air oxidation of Fe(OH)2 suspensions, Bull. Chem. Soc. Jpn. 47 (1974) 1646–1650. doi:10.1246/bcsj.47.1646.
[77] J. Baumgartner, A. Dey, P.H.H. Bomans, C. Le Coadou, P. Fratzl, N. a J.M. Sommerdijk, D. Faivre, Nucleation and growth of magnetite from solution, Nat. Mater. 12 (2013) 310–4. doi:10.1038/nmat3558.
[78] M.A. Blesa, E. Matijevic, Phase transformations of iron oxides, oxohydroxides, and hydrous oxides in aqueous media, Adv. Colloid Interface Sci. 29 (1989) 173–221. doi:10.1016/0001-8686(89)80009-0.
[79] G. Ona-Nguema, G. Morin, Y. Wang, N. Menguy, F. Juillot, L. Olivi, G. Aquilanti, M. Abdelmoula, C. Ruby, J.R. Bargar, F. Guyot, G. Calas, G.E. Brown, Arsenite sequestration at the surface of nano-Fe(OH)2, ferrous-carbonate hydroxide, and green-rust after bioreduction of arsenic-sorbed lepidocrocite by Shewanella putrefaciens, Geochim. Cosmochim. Acta. 73 (2009) 1359–1381. doi:10.1016/j.gca.2008.12.005.
[80] Personal communication, Vitens N.V. (2014).
[81] DSMZ, 141. Methanogenium Medium (H2/CO2), 2017.
[82] OLI Systems, OLI - Scaling Tendencies - wiki, OLI Syst. Wiki. (2016) 1. http://wiki.olisystems.com/wiki/Scaling_Tendencies (accessed May 25, 2018).
[83] F. Jorand, A. Zegeye, J. Ghanbaja, M. Abdelmoula, The formation of green rust induced by tropical river biofilm components., Sci. Total Environ. 409 (2011) 2586–96. doi:10.1016/j.scitotenv.2011.03.030.
[84] M. Abdelmoula, P. Refait, S.H. Drissi, J.P. Mihe, J.M. Génin, Conversion Electron Mössbauer Spectroscopy and X-ray Diffraction Studies of the Formation of Carbonate-containing Green Rust one by Corrosion of Metallic Iran in NaHCO3 and (NaHCO3 + NaCl) solutions, Corros. Sci. 38 (1996) 623–633. doi:10.1016/0010-938X(95)00153-B.
[85] J. Liu, X. Cheng, X. Qi, N. Li, J. Tian, B. Qiu, K. Xu, D. Qu, Recovery of phosphate from aqueous solutions via vivianite crystallization: Thermodynamics and influence of pH, Chem. Eng. J. 349 (2018) 37–46. doi:10.1016/j.cej.2018.05.064.
[86] M. Vainshtein, N. Belova, T. Kulakovskaya, N. Suzina, V. Sorokin, Synthesis of magneto-sensitive iron-containing nanoparticles by yeasts, J. Ind. Microbiol. Biotechnol. 41 (2014) 657–63. doi:10.1007/s10295-014-1417-4.
[87] E.E. Roden, J.M. Zachara, Microbial reduction of crystalline iron(III) oxides: Influence of

oxide surface area and potential for cell growth, Environ. Sci. Technol. 30 (1996) 1618–1628. doi:10.1021/es9506216.

[88] S. Takahashi, J. Tomita, K. Nishioka, T. Hisada, M. Nishijima, Development of a prokaryotic universal primer for simultaneous analysis of bacteria and archaea using next-generation sequencing, PLoS One. 9 (2014). doi:10.1371/journal.pone.0105592.

[89] D.R. Lovley, D.J. Lonergan, Anaerobic oxidation of toluene, phenol, and para-cresol by the dissimilatorty iron-reducing organism, GS-15, Appl. Environ. Microbiol. 56 (1990) 1858–1864.

[90] D.R. Lovley, E.J.P. Phillips, D.J. Lonergan, Enzymatic versus nonenzymatic mechanisms for Fe(III) reduction in aquatic sediments, Environ. Sci. Technol. 25 (1991) 1062–1067. doi:10.1021/es00018a007.

[91] U. Schwertmann, The formation of green rust and its transformation to lepidocrocite, Clay Miner. 29 (1994) 87–92. doi:10.1180/claymin.1994.029.1.10.

[92] T. Hanslik, M. Ghodsi, A. Solcova, J. Subrt, Reduction dehydration of iron oxide hydroxide by iron metal in aqueous medium, Zeitschrift Für Anorgische Und Allgeinie Chemie. 477 (1981) 210–216. doi:10.1002/zaac.19814770628.

[93] J.C.G. Ottow, H. Glathe, Isolation and identification of iron-reducing bacteria from gley soils, Soil Biol. Biochem. 3 (1971) 43–55. doi:10.1016/0038-0717(71)90030-7.

[94] Q. an Peng, M. Shaaban, Y. Wu, R. Hu, B. Wang, J. Wang, The diversity of iron reducing bacteria communities in subtropical paddy soils of China, Appl. Soil Ecol. 101 (2016) 20–27. doi:10.1016/j.apsoil.2016.01.012.

[95] E. Rosenberg, E.F. DeLong, S. Lory, E. Stackebrandt, F. Thompson, The prokaryotes: Alphaproteobacteria and betaproteobacteria, 4th ed., Springer Reference, 2006. doi:10.1007/0-387-30745-1.

[96] U. Kunapuli, M.K. Jahn, T. Lueders, R. Geyer, H.J. Heipieper, R.U. Meckenstock, Desulfitobacterium aromaticivorans sp. nov. and Geobacter toluenoxydans sp. nov., iron-reducing bacteria capable of anaerobic degradation of monoaromatic hydrocarbons, Int. J. Syst. Evol. Microbiol. 60 (2010) 686–695. doi:10.1099/ijs.0.003525-0.

[97] G.T. Kim, G. Webster, J.W.T. Wimpenny, B.H. Kim, H.J. Kim, A.J. Weightman, Bacterial community structure, compartmentalization and activity in a microbial fuel cell, J. Appl. Microbiol. 101 (2006) 698–710. doi:10.1111/j.1365-2672.2006.02923.x.

[98] J. Wang, M. Sickinger, V. Ciobota, M. Herrmann, H. Rasch, P. Rösch, J. Popp, K. Küsel, Revealing the microbial community structure of clogging materials in dewatering wells differing in physico-chemical parameters in an open-cast mining area, Water Res. 63 (2014) 222–233. doi:10.1016/j.watres.2014.06.021.

[99] H. Peng, Y. Zhang, D. Tan, Z. Zhao, H. Zhao, X. Quan, Roles of magnetite and granular activated carbon in improvement of anaerobic sludge digestion, Bioresour. Technol. 249 (2018) 666–672. doi:10.1016/j.biortech.2017.10.047.

[100] A. Wang, L. Liu, D. Sun, N. Ren, D.J. Lee, Isolation of Fe(III)-reducing fermentative bacterium Bacteroides sp. W7 in the anode suspension of a microbial electrolysis cell (MEC), Int. J. Hydrogen Energy. 35 (2010) 3178–3182. doi:10.1016/j.ijhydene.2009.12.154.

[101] B. Liang, L.Y. Wang, S.M. Mbadinga, J.F. Liu, S.Z. Yang, J.D. Gu, B.Z. Mu, Anaerolineaceae and Methanosaeta turned to be the dominant microorganisms in alkanes-dependent methanogenic culture after long-term of incubation, AMB Express. 5 (2015). doi:10.1186/s13568-015-0117-4.

[102] H. Li, J. Chang, P. Liu, L. Fu, D. Ding, Y. Lu, Direct interspecies electron transfer accelerates syntrophic oxidation of butyrate in paddy soil enrichments, Environ. Microbiol. 17 (2015) 1533–1547. doi:10.1111/1462-2920.12576.

[103] E. Rosenberg, E.F. DeLong, S. Lory, E. Stackebrandt, F. Thompson, The prokaryotes: Firmicutes and tenericutes, 4th ed., Springer Reference, 2006. doi:10.1007/0-387-

30743-5.
[104] C.M. Bethke, R.A. Sanford, M.F. Kirk, Q. Jin, T.M. Flynn, The thermodynamic ladder in geomicrobiology, Am. J. Sci. 311 (2011) 183–210. doi:10.2475/03.2011.01.
[105] U. Schwertmann, R.M. Cornell, Iron oxides in the laboratory: Preparation and characterization, 2nd ed., WILEY-VCH, Weinheim, 1993. doi:10.1097/00010694-199311000-00012.
[106] P. Refait, S.H. Drissi, J. Pytkiewicz, J.M.R. Génin, The anionic species competition in iron aqueous corrosion: Role of various green rust compounds, Corros. Sci. 39 (1997) 1699–1710. doi:10.1016/S0010-938X(97)00076-0.
[107] J.M.R. Génin, C. Ruby, A. Géhin, P. Refait, Synthesis of green rusts by oxidation of Fe(OH)2, their products of oxidation and reduction of ferric oxyhydroxides; Eh-pH Pourbaix diagrams, Comptes Rendus - Geosci. 338 (2006) 433–446. doi:10.1016/j.crte.2006.04.004.
[108] S.H. Drissi, P. Refait, M. Abdelmoula, J.M.R. Génin, The preparation and thermodynamic properties of Fe(II)-Fe(III) hydroxide-carbonate (green rust 1); Pourbaix diagram of iron in carbonate-containing aqueous media, Corros. Sci. 37 (1995) 2025–2041. doi:10.1016/0010-938X(95)00096-3.
[109] H.C.B. Hansen, C.B. Koch, H. Nancke-Krogh, O.K. Borggaard, J. Sørensen, Abiotic nitrate reduction to ammonium: Key role of green rust, Environ. Sci. Technol. 30 (1996) 2053–2056. doi:10.1021/es950844w.
[110] Vewin, Drinkwaterstatistieken 2017, 2017.
[111] M.P.C.P. Paulissen, R.C. Nijboer, P.F.M. Verdonschot, Grondwater in perspectief, Wageningen, 2007.
[112] A. Zegeye, C. Mustin, F. Jorand, Bacterial and iron oxide aggregates mediate secondary iron mineral formation: Green rust versus magnetite, Geobiology. 8 (2010) 209–22. doi:10.1111/j.1472-4669.2010.00238.x.
[113] Personal communication, Vitens N.V. (2016).
[114] Personal communication, Oasen N.V. (2016).
[115] M.D.F.F. Lelis, C.M. Gonçalves, J.D. Fabris, W.N. Mussel, W.A. Pacheco Serrano, Effectiveness of selective chemical treatments on concentrating magnetic minerals of samples from a nickel-ore peridotite mantle, J. Braz. Chem. Soc. 15 (2004) 884–889. doi:10.1590/S0103-50532004000600015.
[116] Oxford, Lodestone, Oxford Ref. (2018) 1. http://www.oxfordreference.com/view/10.1093/oi/authority.20110803100112476 (accessed April 2, 2018).

Summary

Most drinking water worldwide is produced from groundwater which contains up to 0.9 mM aqueous ferrous iron. Since the recommended maximum iron concentration in drinking water is 5.10^{-3} mM (World Health Organization), iron is removed in the purification process. The most common method for this is uncontrolled chemical iron oxidation, leading to precipitation of ferric iron oxides, followed by rapid sand filtration. This is an effective method, but produces large volumes of poorly dewaterable sludge with a low value. By recovering this iron in the form of magnetite, the value and application potential could be increased. Magnetite ($Fe^{II}Fe^{III}_2O_4$) is a crystalline and compact mixed valence iron oxide with strong magnetic properties and therefore a multitude of high-end applications including magnetic data storage and site-specific chemotherapy. This thesis describes two processes for the crystallization of magnetite from aqueous ferrous iron and hydrous ferric oxide.

Research on crystalline materials often uses X-Ray Diffraction for phase identification. In this analytical technique, the sample is hit with X-rays that are scattered when they hit an electron. There are two types of scattering; elastic scattering yields a phase specific diffraction pattern, while inelastic scattering leads to a background noise. The use of copper radiation for the analysis of samples containing iron generally leads to a high background signal. Many examples exist in literature where diffractograms with a high background noise lead to ambiguous phase identification. This can be prevented by using cobalt radiation or take physical measures to decrease the detected level of background noise.

Crystallization of magnetite was achieved through the partial chemical oxidation of aqueous Fe^{2+} in a continuous stirred tank reactor. The reactor was fed with a medium of 50% tap water and 50% Milli-Q water. The reactor was operated at pH 5.5 or 6.0 for 24 hours, after which the pH was increased to 6.8 – 7.5, initiating magnetite crystallization. Alternatively, seeding the reactor with previously formed magnetite and operating it at a constant pH of 7.0 also yielded magnetite. Magnetite formation did not take place at a pH below 6.8 or when the reactor was operated at a constant pH without seeding. Color changes of the medium in the reactor indicate that magnetite formation took place via a green rust (GR) precursor phase. During the aforementioned experiments, nitrate was added as electron acceptor. However, mass balance calculations revealed that O_2, diffused into the reactor setup, also served as electron acceptor. This was confirmed in an experiment in which nitrate was omitted from the medium, which yielded magnetite.

The reactor was moved to a glovebox with a N_2 atmosphere to eliminate the O_2 diffusion. A controlled O_2 flow was added to the reactor headspace in the form of compressed air. Magnetite crystallization was achieved in 100% Milli-Q water at an iron feed concentration equal to or above 1 mM. An iron feed concentration of 2.25 mM and a hydraulic retention time (HRT) of 34 h yielded 69% magnetite. Reducing the HRT to 8 h yielded 18% magnetite, while the fraction of side products, mainly lepidocrocite (γ-FeOOH), increased. This indicates an incomplete transformation of chloride-GR into magnetite at an HRT of 8 h. The main factor determining the iron phase formation however, was the Fe^{2+} concentration in the reactor. Magnetite crystallization took place at a concentration equal to or above 0.4 mM Fe^{2+} (aq) in the reactor.

Increasing medium complexity by using diluted tap water or growth medium, hindered magnetite crystallization. An experiment with medium consisting of 50% tap water and 50% Milli-Q water with the controlled addition of O_2 to the headspace yielded lepidocrocite instead of magnetite, indicating the inhibition of the transformation of chloride-GR into magnetite. Increasing the percentage of tap water to 90% (and 10% Milli-Q water) led to the formation of goethite (α-FeOOH). This indicates the formation of carbonate-GR that was oxidized by ambient air during sample preparation for XRD analysis. The formation of carbonate-GR was induced by the presence of carbonates in the tap water. The use of growth medium in an experiment without inoculation of microbial biomass led to the formation of lepidocrocite and goethite, while the experiment that was inoculated with activated sludge yielded vivianite ($Fe_3(PO4)_2$). The latter was likely induced by the presence of phosphate and possibly vivianite in the added sludge.

Magnetite crystallization was also achieved by partial biological reduction of hydrous ferric oxide (HFO). Batch experiments were conducted in growth medium with acetate, lactate, glucose or ethanol as electron donor. While experiments with acetate did not yield magnetite, the crystallization of magnetite in the remainder of the batch experiments was independent of the electron donor. The main factors determining the iron phase formation in these experiments were the final pH and redox potential (ORP). Magnetite was formed when the final pH and ORP were in the range of 7.5 to 7.6 and -254 to -283 mV. Like in the partial oxidation process, observation of medium color changes indicated that magnetite crystallization took place through a GR precursor phase. At an ORP below -283 mV, the increased Fe^{2+} concentration stabilized the formed GR, thereby inhibiting the transformation into magnetite. The GR was oxidized to lepidocrocite by ambient air during sample preparation for XRD analysis.

The attempt to reproduce magnetite crystallization through partial bioreduction of HFO in a continuous reactor setup was unsuccessful. The ethanol (electron donor) flow to the reactor was varied to induce various ORP conditions in the reactor, mimicking the final conditions in the batch experiments. However, all settings that induced reduction of HFO led to the formation of GR. Spiking the reactor containing the formed GR with a 0.5 M aqueous $FeCl_3$ solution did lead to the formation of magnetite.

Magnetite was produced continuously through the partial oxidation process. The partial bioreduction process shows that magnetite crystallization is possible in the presence of ‘foreign’ ions. Both processes take place at circumneutral pH and require only small volumes of added chemicals. However, additional research is required to develop a process that is both continuous and applicable in a complex matrix and that is suitable for low iron concentrations. Therefore, a combination of both processes is proposed. Here, drinking water treatment sludge is partially bioreduced to form GR in a continuous reactor. The GR is then moved to a second reactor, where the controlled addition of O_2 leads to the oxidation of GR to magnetite.

Samenvatting

Wereldwijd wordt het meeste drinkwater geproduceerd uit grondwater. Dit grondwater bevat tot 0.9 mM opgelost tweewaardig ijzer. Aangezien de aanbevolen maximum concentratie van ijzer in drinkwater 5.10^{-3} mM is (World Health Organization), behoort ijzerverwijdering tot het zuiveringsproces. De meest gebruikte methode hiervoor is ongecontroleerde ijzeroxidatie. Dit leidt tot precipitatie van driewaardige ijzeroxides, die vervolgens verwijderd worden door middel van snelle zandfiltratie. Dit is een effectieve methode, maar het produceert grote volumes moeilijk te ontwateren slib van lage waarde. Door het ijzer terug te winnen in de vorm van magnetiet kan de waarde en het toepassingspotentieel verhoogd worden. Magnetiet ($Fe^{II}Fe^{III}_2O_4$) is een kristallijn en compact ijzeroxide dat zowel twee- als driewaardig ijzer bevat. Hierdoor heeft magnetiet sterke magnetische eigenschappen en meerdere hoogwaardige toepassingen waaronder magnetische dataopslag en locatie-specifieke chemotherapie. Deze dissertatie beschrijft twee processen voor de kristallisatie van magnetiet uit opgelost tweewaardig ijzer en amorf driewaardig ijzer.

Onderzoek naar kristallijne materialen maakt vaak gebruik van röntgendiffractie (XRD) voor fasebepaling. In deze analysetechniek wordt een monster bestraald door röntgenstraling, die wordt verstrooid wanneer een elektron geraakt wordt. Er zijn twee soorten verstrooiing; elastische verstrooiing levert het fase-specifieke patroon op, terwijl inelastische verstrooiing zorgt voor ruis. Het gebruik van koperstraling voor de analyse van een monster dat ijzer bevat leidt over het algemeen tot veel ruis. Er zijn veel voorbeelden te vinden in de literatuur waar de aanwezigheid van veel ruis leidt tot twijfelachtige fase-identificatie. Dit kan worden voorkomen door het gebruik van kobaltstraling of door het nemen van fysieke maatregelen om de detectie van ruis te beperken.

Kristallisatie van magnetiet is bereikt door middel van chemische partiële oxidatie van opgelost Fe^{2+} in een continureactor. De reactor was gevuld met een medium van 50% kraanwater en 50% Milli-Q water. De reactor werd de eerste 24 uur bedreven bij een pH van 5.5 of 6.0, waarna de pH verhoogd werd tot 6.8 – 7.5, leidend tot de kristallisatie van magnetiet. Het bedrijven van de reactor bij een constante pH van 7.0 terwijl er eerder gevormd magnetiet aanwezig was, leidde ook tot magnetiet vorming. De kristallisatie van magnetiet vond niet plaats bij een pH lager dan 6.8 of bij een constante pH van 7.0 wanneer er geen eerder gevormd magnetiet toegevoegd was. Kleurveranderingen van het reactormedium gaven de indicatie dat magnetiet werd gevormd via de voorloper groene roest (GR). Tijdens de voorgenoemde experimenten werd nitraat toegevoegd als elektronenacceptor. Uit de massabalansen bleek echter dat O_2, dat via diffusie de reactor binnen kwam, ook de functie van elektronenacceptor vervulde. Dit werd bevestigd door een experiment waarbij geen nitraat werd toegevoegd, waarin ook magnetiet gevormd werd.

De reactor werd verplaatst naar een gasdichte kast met een N_2 atmosfeer om de diffusie van O_2 uit te sluiten. Een gecontroleerde hoeveelheid O_2 in de vorm van perslucht werd toegevoegd aan de gasfase van de reactor. Magnetiet werd gevormd in 100% Milli-Q water met een ijzertoevoer met een concentratie gelijk aan of hoger dan 1 mM. Een ijzertoevoer met een concentratie van 2.25 mM en een vloeistof retentietijd (VRT) van 34 u leidde tot de vorming van 69% magnetiet. Het verkorten van de VRT naar 8 u leidde tot de vorming van 18% magnetiet, terwijl de fractie van bijproducten, voornamelijk lepidocrociet (γ-FeOOH), toenam. Dit duidt op de onvolledige omzetting van GR naar magnetiet bij een VRT van 8 u. De voornaamste factor die de vorming van ijzerfases

bepaalt, is de opgeloste Fe^{2+} concentratie in de reactor. Magnetiet werd gevormd bij een concentratie van 0.4 mM Fe^{2+} (aq) of hoger in de reactor.

Toenemende complexiteit van het medium door het gebruik van verdund kraanwater en groeimedium verhinderde de kristallisatie van magnetiet. Een experiment met medium van 50% kraanwater en 50% Milli-Q water en gecontroleerde toevoeging van O_2 aan de gasfase van de reactor leidde tot de vorming van lepidocrociet, duidend op verhindering van de omzetting van GR naar magnetiet. Het verhogen van het percentage kraanwater naar 90% (en 10% Milli-Q water) leidde tot de kristallizatie van goethiet (α-FeOOH). Dit duidt op vorming van carbonaat-GR dat geoxideerd is door omgevingslucht tijdens de monstervoorbereiding voor XRD. De vorming van carbonaat-GR werd gefaciliteerd door de aanwezigheid van carbonaten in het kraanwater. Het gebruik van groeimedium in een experiment zonder inoculatie met microben leidde tot de vorming van lepidocrociet en goethiet, terwijl vivianiet ($Fe_3(PO4)_2$) gevormd werd in het experiment dat geïnoculeerd werd met actief slib. De vorming van vivianiet werd waarschijnlijk veroorzaakt door de aanwezigheid van fosfaat en wellicht vivianiet in het slib.

Magnetietkristallisatie werd ook bereikt door partiële biologische reductie van een amorfe fase van driewaardig ijzer (HFO). Batchexperimenten werd uitgevoerd in groeimedium met acetaat, lactaat, glucose of ethanol as elektronendonor. Magnetiet werd niet gevormd in experimenten met acetaat, maar wel met de overige elektronendonoren. De voornaamste factoren die bepaalden welke ijzerfase er gevormd werd waren de pH en het redox potentiaal (ORP). Magnetiet werd gevormd wanneer de uiteindelijke pH en ORP in het gebied van 7.5 tot 7.6 en -254 tot -283 mV lagen. Evenals in het oxidatieve proces, wezen de kleurveranderingen in het medium op magnetietvorming via GR. Bij een uiteindelijke ORP lager dan -283 mV werd de gevormde GR gestabiliseerd door een hogere Fe^{2+} concentratie die de omzetting naar magnetiet verhinderde. De GR werd geoxideerd naar lepidocrociet door omgevingslucht tijdens de monstervoorbereiding voor XRD.

De poging om de kristallisatie van magnetiet door middel van bioreductie van HFO te realiseren in een continureactor was niet succesvol. De ethanoldosering (elektronendonor) werd gevarieerd om verschillende ORP condities in de reactor te veroorzaken, zodat deze vergelijkbaar waren met de uiteindelijke condities in de batchexperimenten. Alle doseringen die de reductie van HFO faciliteerden leidden echter tot GR vorming. Een snelle toevoeging van een 0.5 M $Fecl_3$ oplossing in de GR bevattende reactor leidde wel tot magnetietkristallisatie.

In het partiële oxidatieproces werd continu magnetiet geproduceerd. Het partiële reductieproces laat zien dat de kristallisatie van magnetiet in een complexer medium mogelijk is. Beide processen vinden plaats bij een neutrale pH en behoeven de toevoeging van slechts kleine volumes van chemicaliën. Echter, verder onderzoek is nodig om een proces te ontwikkelen dat zowel continu als in een complexer medium werkt en dat geschikt is voor lage ijzerconcentraties. Om die reden wordt een combinatie van beide processen voorgesteld. In dit voorstel wordt het slib dat vrijkomt bij drinkwaterproductie gereduceerd tot GR, waarna het verplaatst wordt naar een tweede reactor, alwaar de gecontroleerde toevoeging van O_2 leidt tot de oxidatie van GR naar magnetiet.

Acknowledgements

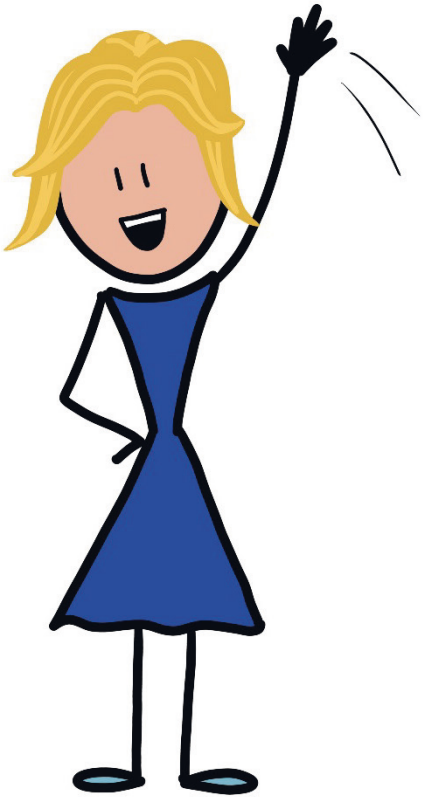

I remember that 8 years ago someone said to me *'who knows, maybe you'll do a PhD in the future'*, I laughed. *Me? Never going to happen*. So I'm not really sure how I got here and I can hardly believe that I did, but somehow you're reading the acknowledgements of my thesis. Maybe you're reading this because you read my thesis cover to cover or maybe this is the only part you'll read. Either way; thank you.

There are many people who have been essential the process of the past four years and I'm very grateful for all the help I received during my PhD. I always try to thank people in the moment itself and I hope I've managed to do that consistently. Still, I would like to use this opportunity to thank some people specifically.

Allereerst uiteraard mijn grote dank aan mijn promotor en co-promotor. Cees; jouw overzicht, frisse blik op resultaten en ideeën voor volgende stappen zorgden voor een never-ending to-do-lijst, maar ook en veel belangrijker, voor richting, visie en goede resultaten. Bedankt voor de suggesties en nodige bijsturingen. Jan W.; we hebben het elkaar niet altijd makkelijk gemaakt, maar we zijn er wel altijd samen uitgekomen en daar ben ik erg dankbaar voor. Je hebt me niet alleen veel geleerd over ijzer en wetenschap in het algemeen, maar ook over mezelf. Dankjewel voor alle wijze lessen en de goede samenwerking.

Even essentieel voor het halen van de eindstreep was Jan K. Elk PhD traject schijnt ups en downs te hebben en het mijne was geen uitzondering. Toen ik in een dip zat, was jij daar met een peptalk. Door jouw vertrouwen in mij kreeg ik mijn eigen vertrouwen weer terug. Bedankt dat je er toen precies op het juiste moment, en daarna nog zo veel vaker, was.

I've had the pleasure to work with several students during their master thesis. Zhenya, Wudi, Karin, Rick, Jin and Loc; I wouldn't have managed to get this result without you. Not only were you invaluable for the research, each of you has helped me grow as a person. Thank you.

My ETE colleagues made me feel at home for the past six years. Sometimes you're kind of a strange bunch, but that's what makes you awesome. I've always felt that I could be myself no matter what, a big thanks to all of you for that.

Of course, none of this work could have been done without the solid foundation that the secretary and lab teams provide. I cannot thank you enough for all the help and support throughout the years.

I want to specifically thank the 10:45h coffee break-crew for making these breaks so enjoyable that they sometimes extended to lunch time.

Rieks; thank you for making lab time more enjoyable, especially on Easter Monday. Your questions and suggestions helped shape my discussion. Two reactor systems for the win!

Miriam; you've always taken the time to help me or brainstorm with me. Thank you for the wise words, both work-related and personal, and of course for being my fellow commentator during the Olympics.

Veluweloop drill instructor Hans; thank you for being my friend. For sharing the good as well as the not-so-good times and of course the running accomplishments.

Leire; *'you is kind, you is smart, you is important'*. Don't go rolling in those *ortigas* chica, you've got this. Thank you for all the hugs and laughs.

To my former office mates; thank you for putting up with my incessant talking while procrastinating. Diego; thank you for being my buddy, not just in the ETE definition. Kasper; thank you for the office brainstorm sessions, Excel tips and tricks, your ability to shut out girl-talk conversations, endless supplies of bread, peanut butter and licorice and good company. Lucia, my dear, you are the sweetest and most sincere person I've ever met. Please don't ever change. Thank you for the previously mentioned girl-talk, hugs, dinners, breakfasts and most importantly; for just being there.

Proposition 8 is of course dedicated to my fellow *Stitch 'n Bitch* ladies. Thank you for lovely evenings, liters of tea and kilos of chocolate. Never stop stitching.

Ik ben wellicht de eerste die mijn fysiotherapeut bedankt in haar thesis, maar Sijmen: dankjewel! Je hebt me door een groot deel van de achtbaan van de schouderblessure gesleept. Hoe verregend, chagrijnig of hopeloos ik ook aan kwam, ik ging altijd weer vrolijk de deur uit. Ik ben blij dat ik nog steeds langs mag komen.

Diezelfde achtbaan was nog minder leuk geweest zonder de altijd meelevende teamgenootjes Suzanne, Lotte en Marjolein. Bedankt voor het zijn van mijn onvermoeibare cheerleaders. In de zandbak spelen doe ik het liefst met jullie.

Silke en de donderdagavonddames; dankjewel voor de gezelligheid en nodige ontspanning, de thee, het meedenken met projecten, de zelfspot als alles mis gaat en de enthousiaste reacties als iets goed gelukt is.

Utrecht zou een stuk saaier zijn zonder Tivoli-vriendjes. Stijn, Sander en Jouke; hoe vaak ik ook voor langere tijd onder een steen kruip, jullie zijn er altijd als ik weer boven kom. Dankjewel voor al jullie geduld, de goede gesprekken, leuke reisjes, slechte woordgrappen en late avonden.

Tom; ik ben blij dat ik niet alleen kennis over heb gehouden aan mijn tijd bij de UU. Je nuchtere blik en positieve insteek zijn heel waardevol voor mij, zowel voor mijn PhD als in het persoonlijke leven. Bedankt daarvoor en voor alle gezelligheid.

Christina; thank you for the joint adventures and for showing me that anything is possible. I look forward to many more holidays and meetups across the globe.

Er zijn twee dames die het al meer dan mijn halve leven met me uithouden. Marlous en Ansfrida; ik vind het bijzonder dat we de pubertijd, eerste liefdes, studies en eerste banen samen hebben beleefd. Bedankt voor alle jaren avonturen, vriendschap en onvoorwaardelijke steun.

Peter, ik weet dat jij vindt dat jouw naam hier niet hoort te staan, maar dat ben ik niet met je eens. Bedankt voor het stellen van kritische vragen op juiste momenten en het samen vieren van de successen.

Mama, bedankt voor de goede basis die je me mee hebt gegeven, voor alle uur-lange telefoongesprekken sindsdien en voor de vrijheid die je me altijd gegeven hebt.

'I don't know how people get by without a sister'. Eveline, ik weet niet waar ik moet beginnen je te bedanken. Het luisterend oor, de kritische vragen, de wijze woorden, de schouder, de wandelingen, de bemoedigende appjes, het delen van champagne-momenten. Jij vindt het kleine dingen, maar ik weet hoe belangrijk die dingen waren. Ze hielpen me enorm en maakten het promoveren leuker en makkelijker. Ik ben heel erg blij en trots dat jouw illustraties in mijn boekje staan. Je bent mijn Grote Zus waar ik altijd een beetje tegenop zal kijken en tegelijkertijd mijn beste vriendin.

Ik weet niet of ik de finishlijn gehaald had zonder mijn paranimfen Gea en Justine. Gea, dankjewel voor je openheid en de goede gesprekken en adviezen. En natuurlijk voor spontaan op mijn bureau verschijnende bonbons met wijze woorden en de reden om goede koffie te drinken op de campus. Justine, je voelde altijd feilloos aan wat ik op dat moment nodig had; een peptalk of juist een gesprek over iets heel anders, een picknick in het park, hulp bij het zoeken van een huisje voor een schrijfweek, een foto van een baby alpaca of gewoon meer chocolade. Dankjewel dat jullie er altijd waren.

Netherlands Research School for the
Socio-Economic and Natural Sciences of the Environment

D I P L O M A

For specialised PhD training

The Netherlands Research School for the
Socio-Economic and Natural Sciences of the Environment
(SENSE) declares that

Yvonne Maria Mos

born on 17 April 1985 in Weesp, the Netherlands

has successfully fulfilled all requirements of the
Educational Programme of SENSE.

Wageningen, 19 October 2018

On behalf of the SENSE board

Prof. dr. Huub Rijnaarts

the SENSE Director of Education

Dr. Ad van Dommelen

The SENSE Research School has been accredited by the Royal Netherlands Academy of Arts and Sciences (KNAW)

KONINKLIJKE NEDERLANDSE
AKADEMIE VAN WETENSCHAPPEN

The SENSE Research School declares that **Yvonne Maria Mos** has successfully fulfilled all requirements of the Educational PhD Programme of SENSE with a work load of 34.6 EC, including the following activities:

SENSE PhD Courses

- SENSE writing week (2014)
- Environmental research in context (2014)
- Research in context activity: 'Organizing and presenting expert course on X-ray powder diffraction (XRD), analytical technique in crystallography, 27-29 January 2015, Wageningen'

Other PhD and Advanced MSc Courses

- Radiation safety 5b, Boerhaave Nascholing, LUMC (2014)
- Teaching and supervising thesis students, Wageningen University (2015)
- Biological processes for resource recovery, Wageningen University (2015)
- Expert course on X-ray powder diffraction (XRD), analytical technique in crystallography, Wageningen University & Malvern Panalytical B.V. (2015)

Management and Didactic Skills Training

- Supervising six MSc student with theses (2015-2018)
- Teaching in the BSc course 'Introduction to Environmental Sciences' (2014-2016)
- Teaching in the MSc course 'Biological Processes for Resource Recovery' (2015-2018)
- Member of the Lab Committee at the Environmental Technology Group (2015-2018)
- Member of the Role Definition Committee at the Environmental Technology Group (2016-2017)

Oral Presentation

- *Strategies for Magnetite Formation.* Goldschmidt 2017, 13-18 August 2017, Paris, France

Poster Presentations

- *Production of Magnetite from Groundwater.* Environmental Technology for Impact (ETEI), 29-30 April 2015, Wageningen, The Netherlands
- *X-Ray Diffraction of Iron Containing Samples: the Importance of a Suitable Configuration*. 22nd International Biohydrometallurgy Symposium, 24-27 September 2017, Freiberg, Germany

SENSE Coordinator PhD Education

Dr. Peter Vermeulen

This work is part of the research program Watertech 2013 with project number 13344, which is (partly) financed by the Netherlands Organisation for Scientific Research (NWO). We thank WLN, Vitens N.V., AquaMinerals, Oasen N.V., NV Waterleiding Maatschappij Limburg, and A. Hak Beheer B.V. for their contributions to this project.

Financial support from Wageningen University & Research and NWO for printing this thesis is gratefully acknowledged.

Cover design and artwork by Eveline Mos, https://www.linkedin.com/in/evelinemos/

Printed by ProefschriftMaken, https://www.proefschriftmaken.nl

This thesis is printed on FSC certified paper.

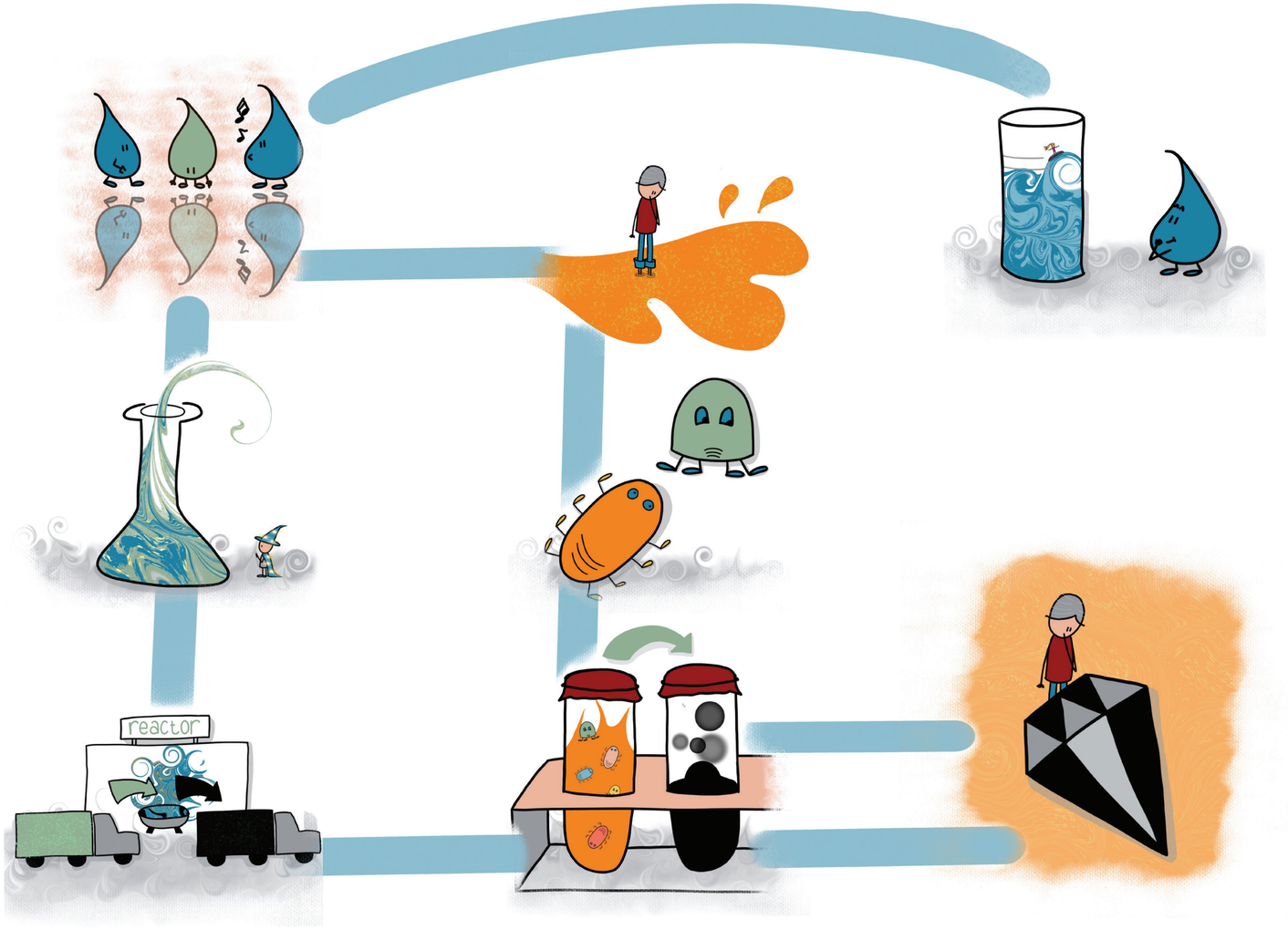
reactor